AD-A034 278 AIR FORCE INST OF TECH WRIGHT-PATTERSON AFB OHIO SCH--ETC F/G 17/7
COVARIANCE ANALYSIS OF KALMAN FILTERS PROPOSED FOR A RADIOMETRI--ETC(U)
DEC 76 C K FITSCHEN

UNCLASSIFIED GE/EE/76D-23 NL

1 OF 2
AD
A034278

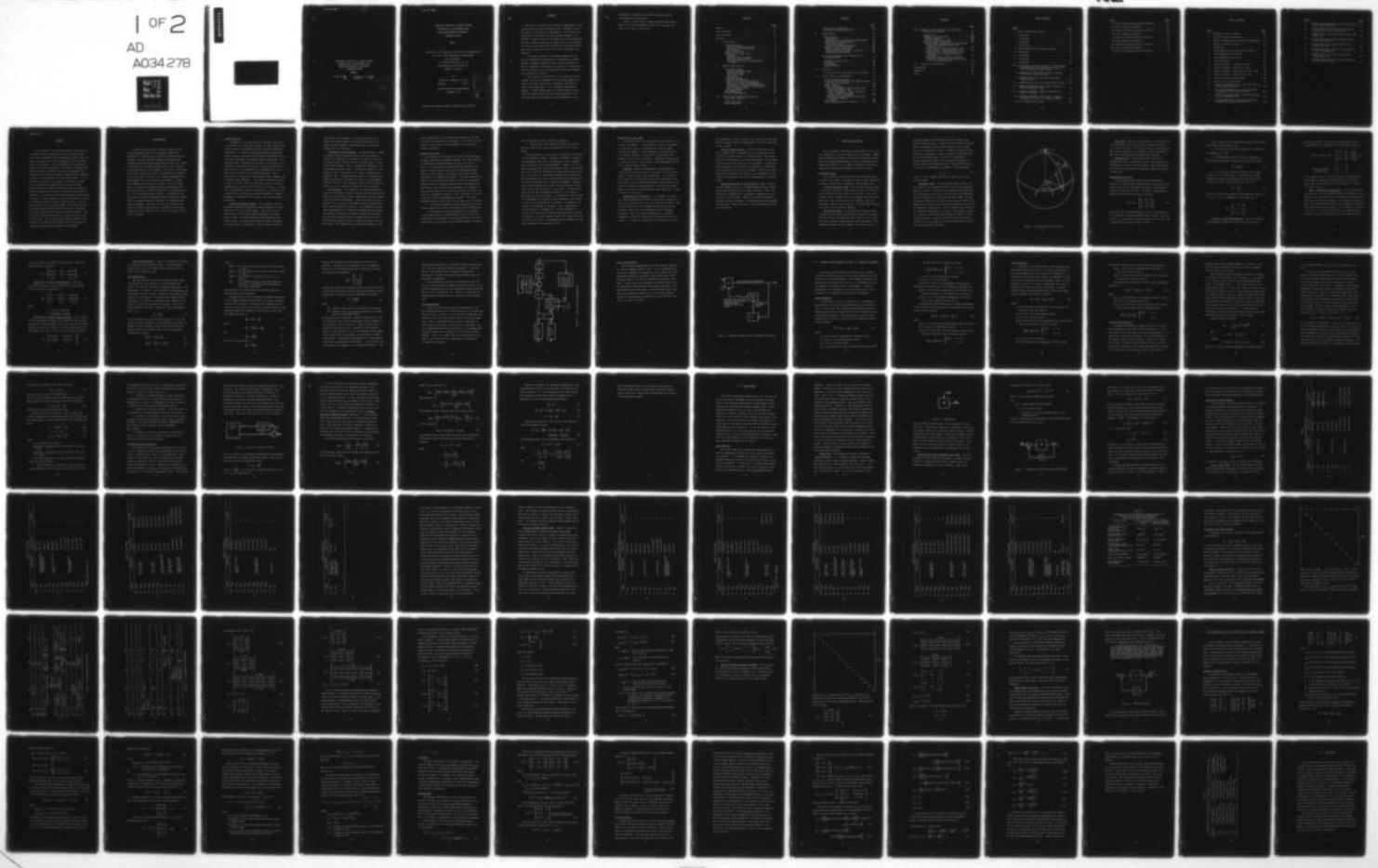

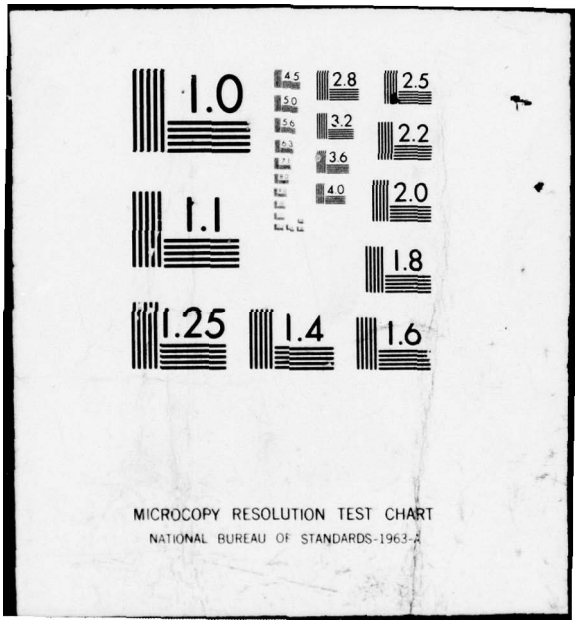
1.0
1.1
1.25
1.4
1.6
1.8
2.0
2.2
2.5
2.8
3.2
3.6
4.0
4.5
5.0
5.6
MICROCOPY RESOLUTION TEST CHART
NATIONAL BUREAU OF STANDARDS-1963-A

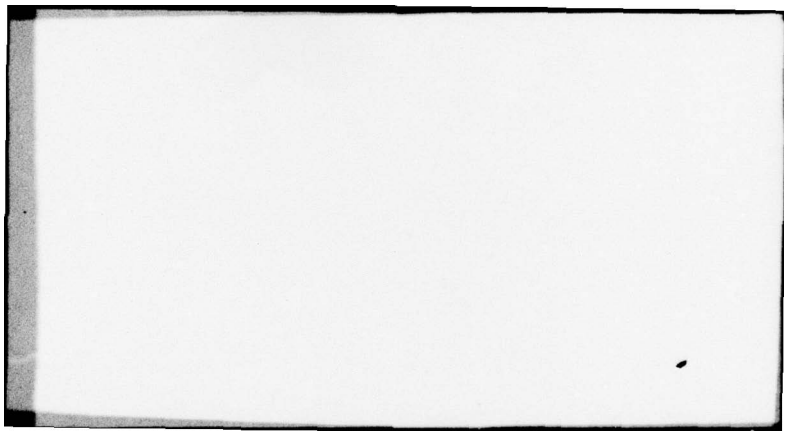

GE/EE/76D-23

(1)

COVARIANCE ANALYSIS OF KALMAN FILTERS PROPOSED FOR A RADIOMETRIC AREA CORRELATOR/INERTIAL NAVIGATION GUIDANCE SYSTEM

THESIS

GE/EE/76D-23

Charles K. Fitschen
Captain USAF

GE/EE/76D-23

COVARIANCE ANALYSIS OF KALMAN FILTERS PROPOSED FOR A RADIOMETRIC AREA CORRELATOR/INERTIAL NAVIGATION GUIDANCE SYSTEM

THESIS

Presented to the Faculty of the School of Engineering
of the Air Force Institute of Technology
Air University
in Partial Fulfillment of the
Requirements for the Degree of
Master of Science

by

Charles K. Fitschen, B.S.E.E.
Captain USAF

Graduate Electrical Engineering
December 1976

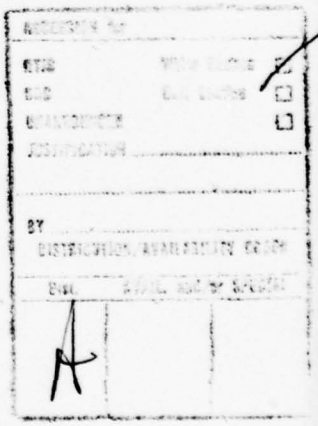

Approved for public release; distribution unlimited.

Preface

The entire foundation for the work accomplished on this thesis topic was set by Professor Peter S. Maybeck, a faculty member of the School of Engineering, in two reports he prepared for Eglin AFB on the RAC guidance system. I am indebted to him not only for the free use of his reports and the time he spent detailing the significance of his results, but also for the access he allowed me to his private working papers and computer programs, which were invaluable in my analysis.

I am further indebted to Professor Maybeck for the patient guidance and instruction he rendered as my thesis advisor. Although staggered under the heavy workload of author, consultant, instructor, and advisor, he always managed to find the time to evaluate my progress and meaningfully redirect my efforts.

I also thank Mr. Phil Richter of the AFATL, my thesis sponsor. His exact definition of the problem scope, criteria to be used, and suitable approaches saved me many hours of fruitless labor. Two classmates also deserve mention: Captain Robert Mann, and Captain Robert Lutter. Although burdened with their own research projects, the time they spent with me sharing their experience in the

application of Kalman filter theory greatly aided my understanding of the subject.

Lastly, I would like to thank my typist, Mrs. Donna M. Hadley, for the professional job she did in typing this report in so short a time span.

Contents

Contents

Contents

List of Tables

List of Figures

Abstract

In this report, a covariance analysis is performed on two Kalman filters proposed for use in a weapon system utilizing a strapdown inertial navigation system (INS), updated by position data from a radiometric area correlator (RAC), for guidance. Filter performance is analyzed when primary navigation information is provided by a Sperry INS, which uses laser gyroscopes, and when an INS employing conventional dry-tuned gyroscopes, manufactured by Hamilton-Standard, is incorporated into the weapon system. For the covariance analysis, truth models in the form of linear state equations are presented which reflect the best description of the weapon system when either the Sperry or Hamilton-Standard INS is used. The Sperry system model is composed of 46 states and the Hamilton-Standard system model 61 states. Primary emphasis in this investigation is placed on minimizing system terminal navigation error. This is done through a filter tuning process, and an optimization of six highly accurate RAC position fixes along a simulated trajectory which reflects the actual system dynamics. The two filters analyzed each employ a linear six state mathematical model. Due to the security classification of the trajectory and RAC characteristics, filter performance is conveyed through unscaled graphs and percentages.

I. Introduction

A lesson learned from the Vietnam conflict is that heavily defended tactical and strategic targets are destroyed at a severe price in terms of attacking men and aircraft. The fact that the highly sophisticated and extremely accurate weaponry developed to attack such targets in that conflict required delivery within their vicinity contributed greatly to the losses. The length of time spent by the pilot acquiring a target, delivering his ordinance, and in some cases "steering" it to impact, subjected him to considerable risk in that hostile environment. The Air Force Armament Test Laboratory (AFATL), Eglin Air Force Base, is currently developing weapons systems which will afford the pilot a "standoff capability" in ordinance delivery. One such weapon system utilizes a radiometric area correlator (RAC) and a strapdown inertial navigation system (INS) in conjunction with an estimator for midcourse and terminal guidance. The RAC, INS, and the estimator are housed in a glide vehicle which is capable of maneuvering through pitch and "skid to turn" along an extended trajectory to a target.

System Operation

In concept, the glide vehicle is released from a captive aircraft at a drop point, within its glide range to the target, which is determined using the existing atmospheric conditions. It "flies" a specified trajectory toward the target, relying on the INS for navigation information and on the RAC and estimator for updating the INS optimally. At a specified point, dependent on the range of the target, the radiometer "looks down" and takes a picture of the terrain. This "picture" is correlated with a preloaded map of the area, and a position fix is thereby generated. This position fix is supplied to the estimator, which updates its navigation error estimates. This process continues through a number of "fixes" until the vehicle is within a certain altitude-range "window" with respect to the target. At that time, the controlled glide of the vehicle is converted into a rapid dive by initiating a pitchover maneuver. Closely following the completion of pitchover, the vehicle impacts the ground.

Inertial Navigation Systems. Two strapdown inertial navigation systems are presently being considered for implementation in the RAC weapon system. The first INS is a Sperry model, which employs laser gyroscopes to measure angular rates. The second model is manufactured by Hamilton-Standard, and uses conventional dry-tuned gyroscopes to provide angular information. Both of these systems use

conventional accelerometers to measure specific force. Because the weapon system is designed for one-time use, these inertial navigation systems are being considered because they are "low cost."

Radiometric Area Correlator. The RAC provides a number of highly accurate position fixes as the glide vehicle "flies" the trajectory. The number of fixes is limited by the storage space allotted for the reference maps. In the present design phase, five or six maps are considered to be the maximum practical number. The RAC is mounted on a gimbaled platform, which allows it a limited capability for "looking" down. A design question still to be answered is whether the degree of freedom of movement of the gimbaled platform should be large enough to allow a RAC fix when the vehicle is in its steep dive during and after pitchover.

The Estimator. The estimator for the RAC system combines the information received from the INS and the RAC, and estimates the navigation errors committed by the INS through a set of recursion algorithms. These algorithms are programmed into a portion of the general purpose guidance computer located onboard the vehicle. The estimator presently under consideration is a Kalman filter designed by Lockheed. This design is deliberately simple, because the estimator was allocated a limited amount of memory space in the onboard guidance computer during preliminary planning for the RAC system. The Lockheed filter provides estimates of the

errors committed by the INS which are fed back to the INS to correct its navigation information. In this way, the INS errors are kept small, and the adequacy of linear error models is enhanced.

Scope of this Study

This report is an extension of the RAC Guidance System Analysis completed by Professor Maybeck, Air Force Institute of Technology, Wright-Patterson Air Force Base (Ref 1; Ref 2). He analyzed the navigation errors committed by a simple six-state Kalman filter and the Lockheed approximation to that filter as the weapon system flew a benign trajectory in a computer simulation. His study compared the filter error estimates when either the Sperry or Hamilton-Standard inertial navigation systems were implemented into the system. These filter error estimates were compared to the true navigation errors committed during the "flight" by means of a covariance analysis. Thus, a measure of how well the filter actually performed was obtained. The major extensions made to that study in this report are as follows:

1. The benign trajectory will be replaced by one that is more realistic for the glide vehicle under consideration.

2. The estimation errors committed by the Lockheed filter design and an alternate Kalman filter, which is in reality the correct Kalman filter formulation for the Lockheed design, as the system flies the more dynamic trajectory

will be analyzed through a covariance analysis.

3. The position fixes taken by the RAC will be optimized in time so that terminal navigation error is minimized.

The development of this report is presented by chapters in the following sequence. Possible integration of the various components (RAC, INS, and estimator) into a workable unit is outlined in the second chapter. Chapter III introduces the algorithms used by the Kalman filter in estimating INS errors, and also discusses the covariance analysis process. In Chapter IV, two models developed by Professor Maybeck describing the overall system when either the Sperry or the Hamilton-Standard INS is used are presented. Chapter V details the Lockheed filter model and the alternate filter model used as the estimators in this study. A mathematical model for the more realistic trajectory of this work is developed in the sixth chapter. In Chapter VII, the process for determining the values of system variables that yields the best filter performance is outlined. In addition, the resulting performance is analyzed. Filter performance is further analyzed in Chapter VIII, in which effects of varying the trajectory and the RAC position update schedule are explored. The last chapter details the results and conclusions of this study, and proposes system changes that may reduce overall system navigation error.

Limitations of this Study

An inherent step in any problem-solving technique is to "define the problem." In an attempt to define the problem for this work, certain assumptions were made and some restrictions imposed. These assumptions and restrictions are important factors in the work to be presented, and broadly fall into four categories: modeling, interpretation of results, security classification, and approximations made due to insufficiency of data.

Modeling. Extensive mathematical representation of "real world dynamics" is done in this work so that certain tools of linear analysis may be employed. It is realized that these real world dynamics defy exact mathematical representation, so the modeling performed in this study can at best be considered an approximation. Care has been taken, however, to model as completely and accurately as the "state of the art" will allow.

Interpretation of Results. It is tempting to equate the results presented in this work with overall system circular error probabilities, but this would not be valid. The results reflect only the probable navigation errors committed by the filter if the system flew the trajectory precisely. Thus, the errors committed by a controller attempting to keep the vehicle on flight path are not considered. In addition, the ability of the system to correct

the trajectory in order to impact the target when conditions such as adverse winds are encountered is in no way reflected in the results.

Security Classification. A major restriction on the work presented here is imposed due to the security classification of several aspects of the RAC system. The trajectory of the glide vehicle is classified Secret, so altitudes, distances, and flight times are not presented. In addition, several parameters of the RAC are classified, so their specific numerical values are not included. Whenever possible, classified information pertinent to the development is sanitized and presented in the form of percentages or unscaled graphs.

Approximations Due to Insufficiency of Data. Because the RAC system is still in the developmental stage, overall system specifications have not been finalized. Also, the performance capabilities of individual components have not yet been fully evaluated. Based on the known parameters, judgment has been exercised to approximate unknowns throughout this work. Where they occur, these approximations have been delineated.

II. System Mechanization

In this chapter, functional block diagrams of the various components of the RAC system will be developed. These block diagrams will then be integrated to form one possible scheme for system mechanization. Before developing these components, however, it is useful to define the coordinate frames and transformation matrices that will be used.

Coordinate Frames

Five different coordinate frames are described below for use in this study. The axes of each of these respective reference frames form an orthogonal right-handed triad.

Inertial Reference Frame. The inertial reference frame, I-frame, has its origin at the center of mass of the earth and is nonrotating with respect to the stars. The Z-axis extends through the North Pole in alignment with the earth's spin axis. The X and Y axes of the inertial frame are coincident with the X and Y axes of the earth-fixed frame at the start of the navigation problem.

Earth-Fixed Frame. The earth-fixed reference frame, E-frame, has its origin at the center of mass of the earth with its Z-axis coincident with the Z-axis of the I-frame. The X-axis extends outward through the intersection of the Greenwich meridian and the equator, while the Y-axis is

directed through the intersection of the 90 degree east meridian and the equator. Since this frame rotates with the earth, its angular velocity with respect to the I-frame, ω_{IE}, is one revolution per day. Points on the earth's surface can be expressed in terms of two Euler angle rotations in the earth-fixed frame. The first is longitude, a rotation about the Z-axis, and the second is latitude, a rotation about the displaced X-axis. Inertial longitude, λ, is related to geographical longitude, ℓ, by the equation

$$\lambda = \omega_{IE} \Delta t + \ell \qquad (1)$$

where Δt is the elapsed time from the start of the navigation problem.

Navigation Frame. The navigation frame, N-frame, for this study is the coordinate system in which the navigation problem is solved. INS errors as computed by the estimator are expressed in this frame. For this work, the navigation frame is defined as an east-north-up (ENU) triad. The ENU navigation frame has its origin at the center of mass of the glide vehicle with its axes pointing in the east, north, and up directions respectively. "Up" is defined to be normal to the reference ellipsoid at all times. The geometry relating the inertial, earth-fixed, and navigation frames is illustrated in Figure 1, where the X_I-Y_I-Z_I axes represent the inertial triad, X_E-Y_E-Z_E are the earth-fixed axes, and E-N-U are the navigation frame axes.

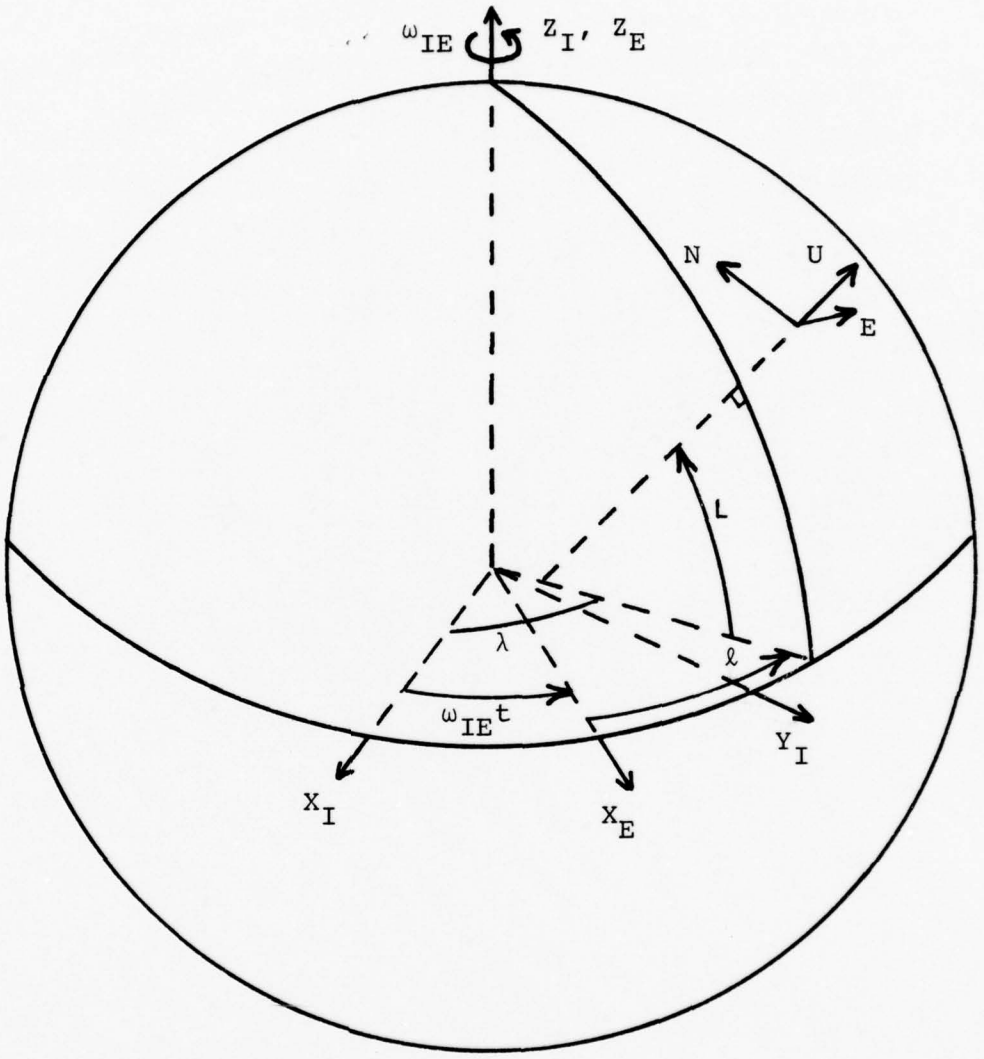

Figure 1. Coordinate Frame Orientation

Body Frame. The body frame, B-frame, is fixed relative to the glide vehicle with its origin located at the vehicle's center of mass. The B-frame's X and Y axis extend out the nose and right wing of the glide vehicle respectively, while the Z-axis points down through the fuselage.

Platform Frame. The platform frame, P-frame, is aligned with the X-Y-Z sensitive axes of the gyroscope and accelerometer triads of the INS system. This frame differs for each of the two inertial navigation systems considered in this study.

Transformation Matrices

Vectors representing quantities such as position, velocity, or angular rate coordinatized in a particular reference frame can be transformed to another frame through a direction cosine matrix (DCM). The DCM or transformation matrix is defined for this work as follows:

$$\text{DCM} = C_i^j = \begin{bmatrix} C_{11} & C_{12} & C_{13} \\ C_{21} & C_{22} & C_{23} \\ C_{31} & C_{32} & C_{33} \end{bmatrix} \tag{2}$$

where C_i^j is the DCM transforming a vector coordinatized in the i-frame to a vector expressed in the j-frame. The element $C_{k\ell}$ is the direction cosine between the kth axis in the j-frame and the ℓth axis in the i-frame.

Useful properties of the DCM which apply to the orthogonal frames outlined above are:

1. The inverse of the DCM is equal to its transpose, for example $C_i^j = (C_j^i)^T$

2. Transformation matrices relating frames can be found using intermediate frames in the following manner:

$$C_i^j = C_\ell^j C_k^\ell C_i^k \tag{3}$$

3. If the angular velocity vector of the j-frame relative to the i-frame ($\underline{\omega}_{ij}$) is expressed in j-frame coordinates as $\underline{\omega}_{ij}^j$, an expression for the time rate of change of the DCM C_j^i can be written as (Ref 3:17)

$$\dot{C}_j^i = C_j^i \Omega_{ij}^j \tag{4}$$

where Ω_{ij}^j is the skew symmetric matrix defined in terms of the ω_X, ω_Y, and ω_Z components of the vector $\underline{\omega}_{ij}^j$ as

$$\Omega_{ij}^j = \begin{bmatrix} 0 & -\omega_Z & \omega_Y \\ \omega_Z & 0 & -\omega_X \\ -\omega_Y & \omega_X & 0 \end{bmatrix} \tag{5}$$

Platform to Body Transformation. The time invariant transformation matrices for each of the two inertial

navigation systems, relating the platform triad of the accelerometers and gyroscopes to the fixed body frame are

$$C_P^B \text{ of the Sperry INS} = \begin{bmatrix} 1/\sqrt{3} & 1/\sqrt{3} & 1/\sqrt{3} \\ 0 & 1/\sqrt{2} & -1/\sqrt{2} \\ -2/\sqrt{6} & 1/\sqrt{6} & 1/\sqrt{6} \end{bmatrix} \quad (6)$$

$$C_P^B \text{ of the Hamilton-Standard INS} = \begin{bmatrix} -1 & 0 & 0 \\ 0 & -1 & 0 \\ 0 & 0 & 1 \end{bmatrix} \quad (7)$$

in the Sperry design, the sensitive axes of the measuring instruments are skewed from the body axes to avoid subjecting any one instrument to the full input of a vehicle yaw, pitch, or roll.

Body to Navigation Transformation. The transformation from the body to the navigation frame is time-varying, as it depends on the time history of the vehicle's orientation in space as it flies the trajectory. At a specific instant of time, this transformation matrix can be determined using the three Euler angles of the vehicle, i.e., heading, ψ, pitch, Θ, and roll, Φ. Because the vehicle under consideration maneuvers through pitch and skid, the roll angle for this

study will always be considered zero degrees. With this simplification, the DCM is

$$C_B^N = \begin{bmatrix} \sin\psi\cos\Theta & \cos\psi & \sin\psi\cos\Theta \\ \cos\psi\cos\Theta & -\sin\psi & \cos\psi\sin\Theta \\ \sin\Theta & 0 & -\cos\Theta \end{bmatrix} \tag{8}$$

Navigation to Inertial Transformation. The time-varying DCM relating a vector expressed in the ENU frame to one in inertial coordinates is

$$C_N^I = \begin{bmatrix} -\sin\lambda & -\sin L\cos\lambda & \cos L\cos\lambda \\ \cos\lambda & -\sin L\sin\lambda & \cos L\sin\lambda \\ 0 & \cos L & \sin L \end{bmatrix} \tag{9}$$

where

λ = inertial longitude

L = geographic latitude

Earth-Fixed to Inertial Transformation. The following is the transformation between the earth-fixed and inertial coordinate reference frames, where again, ω_{IE} is the earth's angular velocity with respect to inertial space and Δt is the elapsed time from the start of the navigation problem:

$$C_E^I = \begin{bmatrix} \cos(\omega_{IE}\Delta t) & -\sin(\omega_{IE}\Delta t) & 0 \\ \sin(\omega_{IE}\Delta t) & \cos(\omega_{IE}\Delta t) & 0 \\ 0 & 0 & 1 \end{bmatrix} \tag{10}$$

Other Transformations. Using the properties of orthogonal reference frames outlined above, the relationships between any of the five frames used in this work may be found at any instant of time.

INS Mechanization

The two strapdown inertial navigation systems under consideration differ radically in the gyroscopes they employ, but they both generate navigation information in the same manner. In general, the strapdown INS experiences the same specific forces, angular velocities, and angular accelerations as the vehicle. To resolve these dynamic inputs accurately, the vehicle's orientation with respect to some reference frame must constantly be tracked. This can be accomplished by utilizing a property of the DCM presented above, i.e.,

$$\dot{C}_j^i = C_j^i \Omega_{ij}^j \tag{4}$$

if the navigation and body reference frames are used, the onboard guidance computer can be programmed to estimate the C_B^N DCM cursively through an approximate first-order integration routine, in discrete time, using the following equations as a basis:

$$\dot{C}_B^N(\Delta t) = C_B^N(t_1)\Omega_{NB}^B \tag{11}$$

$$C_B^N(t_2) = C_B^N(t_1) + \dot{C}_B^N(\Delta t) \tag{12}$$

where

$C_B^N(t_1)$ = the DCM relating the inertial and body frames at time t_1

$C_B^N(t_2)$ = the DCM relating the inertial and body frames at time t_2

$\dot{C}_B^N(\Delta t)$ = the change in the C_B^N DCM from time t_1 to time t_2

Ω_{NB}^B = the angular velocity of the body frame relative to the navigation frame expressed in body frame coordinates

The recursion is initiated with the estimated C_B^N matrix after system initial alignment.

The $\underline{\omega}_{NB}^B$ vector for this integration scheme is generated by the onboard guidance computer using the angular velocity vector of the platform in inertial space estimated by the rate gyro triad, $\underline{\omega}_{IP}^P$, and the angular velocity vector of the navigation frame with respect to the inertial frame, $\underline{\omega}_{IN}^N$. The computation made is

$$\underline{\omega}_{NB}^B = \underline{\omega}_{IB}^B - \underline{\omega}_{IN}^B \tag{13}$$

where

$$\underline{\omega}_{IB}^B = C_P^B(\underline{\omega}_{IP}^P + \underline{\omega}_{PB}^P) \tag{14}$$

and

$$\underline{\omega}_{IN}^B = C_N^B\underline{\omega}_{IN}^N \tag{15}$$

Equation (14) simplifies to

$$\underline{\omega}_{IB}^B = C_P^B\underline{\omega}_{IP}^P \tag{16}$$

because the platform and body frames are mutually non-rotating. The $\underline{\omega}_{IN}^{N}$ vector of Equation (14) is computed in discrete time by using navigational information to update the following relationship:

$$\underline{\omega}_{IN}^{N} = \begin{bmatrix} \dot{} \\ -L \\ \dot{\lambda}\cos L \\ \dot{\lambda}\sin L \end{bmatrix} \tag{17}$$

Through the recursively generated C_B^N DCM, the specific force in platform coordinates sensed by the accelerometers can be transformed to navigation frame coordinates as follows:

$$\underline{f}^N = C_B^N C_P^B \underline{f}^P \tag{18}$$

where

$\underline{f}^N$ = specific force vector in navigation coordinates

$\underline{f}^P$ = specific force in platform coordinates as sensed by the accelerometer triad

By subtracting the navigation frame referenced gravity vector $\underline{G}^N$ from $\underline{f}^N$, the vehicle acceleration vector relative to the navigation frame is obtained. There are many ways to estimate this gravity vector, dependent on the sophistication of earth modeling, the use of external altitude measuring devices such as altimeters, and inclusion of higher order effects. An excellent development of a gravitational field model is presented in Reference 3. For this work, the gravity vector is assumed to be calculated discretely. The

calculations are based on a reference ellipsoid earth model with altimeter supplied altitude information. Irregularities to the surface of the reference ellipsoid are accounted for indirectly through noise processes that are described in Chapter IV.

The acceleration vector in the navigation frame, $\ddot{\underline{r}}^N$, formed by differencing the specific force and gravity vector can be integrated twice to yield navigation frame referenced velocity, $\dot{\underline{r}}^N$, and position, $\underline{r}^N$. Figure 2 illustrates the mechanization outlined above for the INS in block diagram form.

RAC Mechanization

Using the filter-aided navigation information, the RAC's gimbaled platform is leveled relative to the reference ellipsoid, and a "picture" of the terrain is taken when the vehicle is over the area recorded on one of the pre-loaded maps. After a processing delay in which the picture is correlated with the map, a position fix is generated. One of the approximations made in this work is to disregard the processing delay, and to assume the fix is made instantaneously. Thus, at an update time, an instantaneous fix is made by the RAC which can be expressed in geographical latitude and longitude.

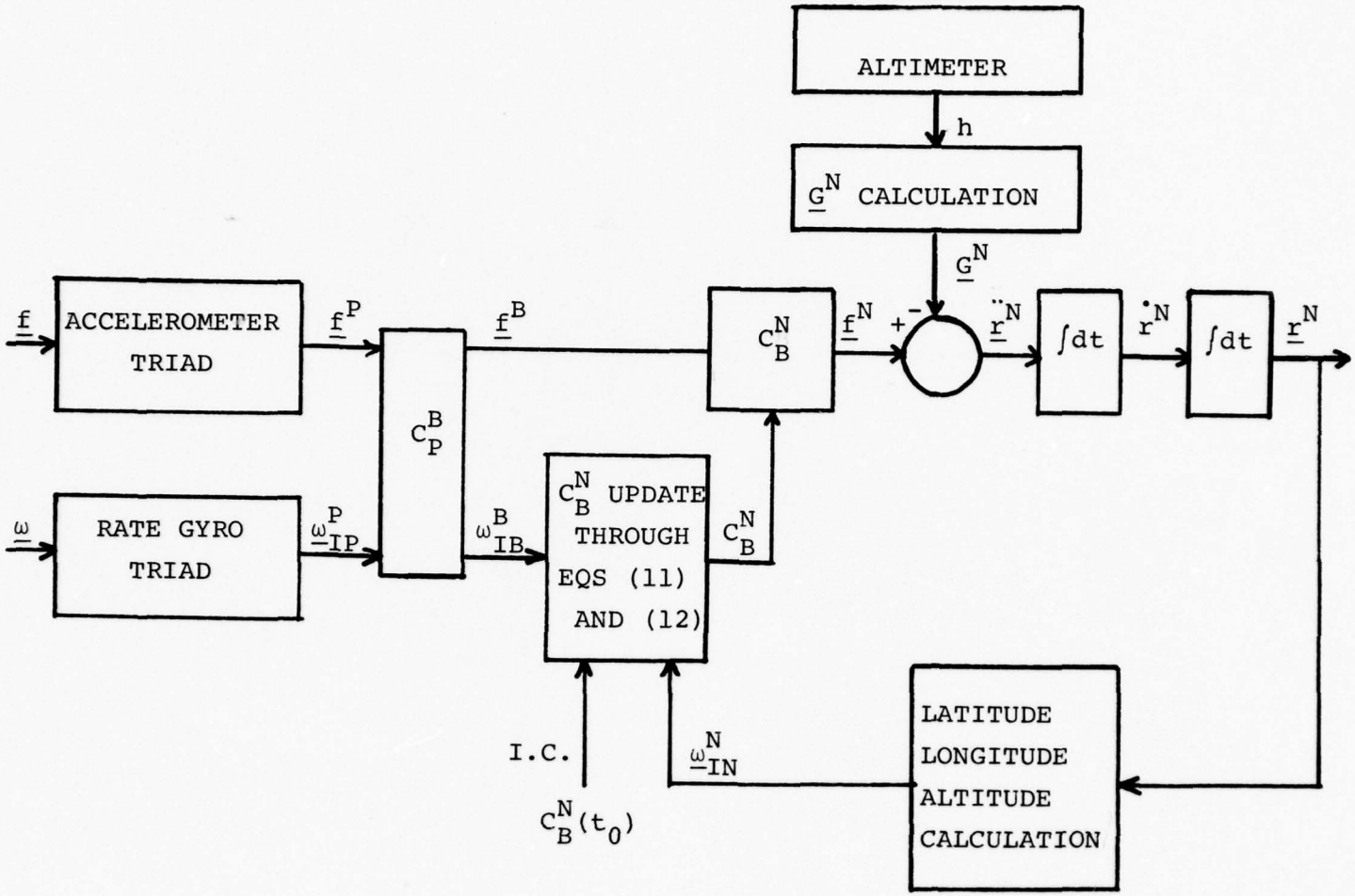

Figure 2. Inertial System Mechanization

Filter Mechanization

The estimator implemented in the RAC guidance system is an indirect feedback Kalman filter. In this configuration, the filter estimates INS navigation errors rather than total navigation parameters (indirect), and directs these error estimates back to the INS for navigation correction (feedback). These errors are estimated in discrete-time and can be calculated as RAC position fixes become available. The algorithms used by the filter to generate these error estimates are detailed in Chapter III. An overall representation of the information channeling for the INS, RAC, and filter is shown in Figure 3.

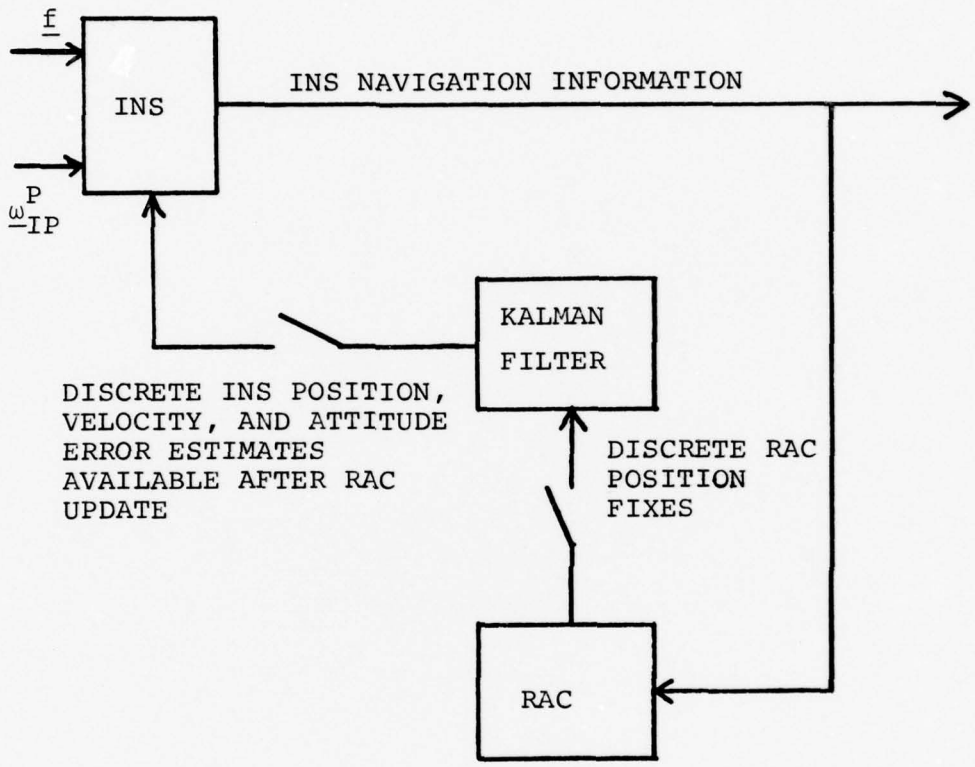

Figure 3. RAC/INS Guidance System Information Channeling

III. Kalman Filter Equations as Used in a Covariance Analysis

Analyzing the performance of a Kalman filter through a covariance analysis requires a state-space formulation of the filter and its driving dynamics. This chapter introduces the computations performed by the filter as it propagates in time and updates its estimates after a measurement. With this background, the incorporation of the equations into a form suitable for a covariance analysis will be discussed.

System Equations

In designing the optimal Kalman filter, a mathematical description of the entire system dynamics is made through a set of linear first order stochastic differential equations. These equations should describe the system as completely and accurately as possible. This formulation is known as the "system model," with the following vector stochastic differential equation:

$$\dot{\underline{X}}_S = F_S\underline{X}_S + G_S\underline{W}_S + B_S\underline{U}_S \qquad (19)$$

where

$\underline{X}_S$ is an N1-vector representing the system state

F_S is an N1 x N1 system dynamics matrix

G_S is an N1 x M1 gain matrix

$\underline{W}_S$ is an M1-vector of white Gaussian noise inputs which

are zero mean and of strength Q_S where

$$E[\underline{W}_S(t_1)\underline{W}_S^T(t_2)] = \begin{cases} Q_S(t_1) & t_1 = t_2 \\ 0 & t_1 \neq t_2 \end{cases}$$

and $E[\cdot]$ is the expectation operator

B_S is an N1 x P1 gain matrix

$\underline{U}_S$ is an P1 vector of deterministic control inputs.

The initial conditions for this differential equation are

$\hat{\underline{X}}_S(t_0)$ - an N1-vector representing the estimate (the $\hat{}$ denotes estimate) of the system state at time t_0

$P_S(t_0)$ - an N1 x N1 matrix representing the covariance of the system state at time t_0.

Discrete-time measurements made of linear combinations of the system's state variables are represented by the following vector equation:

$$\underline{Z}_S(t_i) = H_S\underline{X}_S(t_i) + \underline{V}_S(t_i) \qquad (20)$$

where

$\underline{Z}_S(t_i)$ is an R1-vector of measurements taken at time t_i

H_S is an R1 x N1 measurement matrix

$\underline{V}_S(t_i)$ is an R1-vector of white Gaussian noise inputs which are zero mean and of strength R_S where

$$E[\underline{V}_S(t_1)\underline{V}_S^T(t_2)] = \begin{cases} R_S(t_1) & t_1 = t_2 \\ 0 & t_1 \neq t_2 \end{cases}$$

Filter Equations

In practice, the optimal Kalman filter based upon the high-dimensioned "system model" is seldom used because of the heavy computational load required to implement it. A sub-optimal filter with fewer states, yet designed to have many of the characteristics of the optimal filter, is used instead, resulting in a loss in performance for a gain in computational ease and storage requirements. The sub-optimal filter can be described by the linear first order vector stochastic differential equation

$$\dot{\underline{X}}_F = F_F \underline{X}_F + G_F \underline{W}_F + B_F \underline{U}_F \qquad (21)$$

where

$\underline{X}_F$ is an N2-vector representing the filter state (N2 typically much less than N1)

F_F is an N2 x N2 filter dynamics matrix

G_F is an N2 x M2 gain matrix

$\underline{W}_F$ is an M2-vector of white Gaussian noise inputs which are zero mean and of strength Q_F where

$$E\left[\underline{W}_F(t_1)\underline{W}_F^T(t_2)\right] = \begin{cases} Q_F(t_1) & t_1 = t_2 \\ 0 & t_1 \neq t_2 \end{cases}$$

B_F is an N2 x P2 gain matrix

$\underline{U}_F$ is an P2-vector of deterministic control inputs.

The initial conditions for this differential equation are

$\hat{\underline{X}}_F(t_0)$ - an N2-vector representing the estimate of the filter state at time t_0

$P_F(t_0)$ - an N2 x N2 matrix representing the covariance of the filter state at time t_0.

The associated discrete-time linear vector measurement equation is

$$\underline{Z}_F(t_i) = H_F\underline{X}_F(t_i) + \underline{V}_F(t_i) \tag{22}$$

where

$\underline{Z}_F(t_i)$ is an R1-vector of measurements taken at time t_1

H_F is an R1 x N2 measurement matrix

$\underline{V}_F(t_i)$ is an R2-vector of white Gaussian noise inputs which are zero mean and of strength R_F where

$$E\left[\underline{V}_F(t_1)\underline{V}_F^T(t_2)\right] = \begin{cases} R_F(t_1) & t_1 = t_2 \\ 0 & t_1 \neq t_2 \end{cases}$$

Kalman Filter Equations

The Gaussian probability density function is an integral assumption in the Kalman filter formulation. If the statistics of both the states and the driving noises of the system can be modeled as Gaussian, then the mathematics of the optimal filter become tractable. Modeling the states and noises as Gaussian random variables is not a limiting restriction, because it can be shown mathematically (through use of the Central Limit Theorem) that a large number of

random variables when added together have statistics that are very nearly Gaussian regardless of their individual density function (Ref 4:96).

The Gaussian probability density function is a normal bell-shaped curve centered about its mean, μ. The measure of the spread of this curve is called the standard deviation, or one-sigma value, σ. The region under the curve and one-sigma value to the left and right of the mean covers 68.3% of the function's area. Thus, a sharply peaked Gaussian density function will have a smaller standard deviation than a flatly peaked Gaussian density function. Since the Gaussian density function of a variable relates probability of occurrence, 68.3% of the time the estimate of the variable will be within the bounds $\mu \pm \sigma$. The equations describing the Gaussian density function and its associated mean and variance are given below (Ref 4:78-86).

Gaussian density function

$$F_x(\varepsilon) = \frac{1}{(2\pi)^{\frac{3}{2}}\sigma} \exp \frac{-(\varepsilon-\mu)^2}{2\sigma^2} \tag{23}$$

Mean

$$\mu = E[X] = \int_{-\infty}^{\infty} \varepsilon F_x(\varepsilon) d\varepsilon \tag{24}$$

Variance

$$\sigma^2 = E[X^2] = \int_{-\infty}^{\infty} (\varepsilon-\mu)^2 F_x(\varepsilon) d\varepsilon \tag{25}$$

where ε is a dummy variable representing possible values of

X, the random variable, and $E[\cdot]$ is the expectation operator.

If the states and associated driving noises of the system are modeled as Gaussian, then it can be shown that one joint Gaussian density function of the same dimension as the state vector can be used to describe the state-vectors probability (Ref 4:49). The Kalman filter provides estimates of individual states by propagating this joint density function in time and altering its shape when "new information" is obtained at a measurement time. The initial conditions for this propagation are provided to the filter in the $\hat{\underline{X}}(t_0)$ vector, this vector contains the initial mean of each state, and the initial covariance matrix, $P(t_0)$, this matrix is formed by finding the covariance kernel of the state vector at time t_0 (Ref 4:48), i.e.,

$$P(t_0) = E\{[\underline{X}(t_0) - \hat{\underline{X}}(t_0)][\underline{X}(t_0) - \hat{\underline{X}}(t_0)]^T\} \quad (26)$$

If the states are independent, this matrix is diagonal with its ii^{th} element equal to the variance of the i^{th} state. As the joint density function at any instant of time represents total knowledge of the state and its associated covariance, the conditional mean and the conditional covariance of this function form the best estimates of system performance. The conditional mean of the state is propagated in time through

the following continuous time matrix equation:

$$\dot{\underline{X}} = F\,\hat{\underline{X}} + B\,\underline{U} \tag{27}$$

starting from the initial condition $\hat{\underline{X}}(t_0)$.

The conditional covariance of this state vector is propagated through a similar continuous time matrix equation,

$$\dot{P} = FP + PF^T + GQG^T \tag{28}$$

starting from the initial condition $P(t_0)$.

When an external measurement is used to update the filter's estimate of the conditional mean and its associated covariance matrix, the following Kalman filter equations are used:

$$K = P^- H^T\left[HP^-H^T + R\right]^{-1} \tag{29}$$

$$P^+ = P^- - KHP^- \tag{30}$$

$$\hat{\underline{X}}+ = \hat{\underline{X}}^- + K\left[\underline{Z} - H\hat{\underline{X}}^-\right] \tag{31}$$

where

K is the Kalman gain matrix

superscript$^+$ represents the best estimate just after update

superscript$^-$ represents the best estimate just prior to update.

From these equations, it can be seen that the Kalman filter does the following:

1. Takes estimates of the initial state vector and its corresponding error covariance matrix, $\hat{\underline{X}}(t_0)$ and $P(t_0)$,

and propagates them in time until a measurement is supplied. The filter's best estimates before incorporating the measurement at time t_1 are $\hat{\underline{X}}(t_1^-)$ and $P(t_1^-)$.

2. Computes a weighting matrix, K, based upon $P(t_1^-)$, the measurement matrix H (which indicates the states or combination of states to be measured), and the variance of the white noise corrupting the measurement vector.

3. Updates the covariance matrix. (Note that there is no dependence on the measurement value for this update.)

4. Provides a new estimate of the state vector, $\hat{\underline{X}}(t_1^+)$, by updating its previous estimate, $\hat{\underline{X}}(t_1^-)$, with a weighted estimate of the error between the actual measurement and the filters a priori estimate of the measurement, $K\left[\underline{Z} - H\hat{\underline{X}}(t_1^-)\right]$.

5. Iterates on the above procedure to step along in time; i.e., $\hat{\underline{X}}(t_1^+)$ and $P(t_1^+)$ become the new initial conditions, and the recursion continues.

Covariance Analysis Equations

The Kalman filter equations presented above are sufficient to completely evaluate the performance of the optimal filter, or system model, along a given trajectory. This filter's state vector, $\underline{X}_S$, and its associated covariance matrix P_S, represent the true statistics of the entire system at any point in time. Although the optimal filter is seldom implemented, it can be very useful in evaluating the performance of a particular sub-optimal filter. The process

by which this is done is called a covariance analysis. Conceptually, the system model provides measurements, $\underline{Z}_S$, to the sub-optimal filter, which uses this information to provide an estimate of the state vector, $\hat{\underline{X}}_F$, through the propagation and update equations presented above. The difference between the filter's state estimate and the true state is the error vector. The principal concepts involved in obtaining the error vector are characterized in Figure 4 (Ref 1:18). Note that the difference in vector dimension

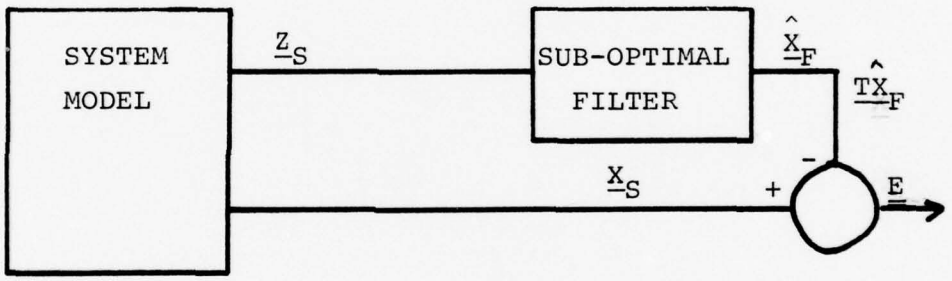

Figure 4. Concept of the Error Vector

can be corrected by the following mathematical manipulation, provided that the states of the sub-optimal filter are the same as the first N2 components of $\underline{X}_S$:

$$\underline{E} = \underline{X}_S - T\hat{\underline{X}}_F$$

where $T = \left[\frac{I}{0}\right]$ with I an N2 x N2 identity matrix and 0 an (N1 - N2) x N2 null matrix.

It is the statistics of the error vector, especially the upper N2 partition, that determine how well a sub-optimal filter will perform, because the error vector is the best description of the "true" errors being committed by the sub-optimal filter. If the covariance of the error vector closely matches the covariance of the filter's state vector, the filter is accurately estimating the errors it is committing. A computer program that can be used to perform the analysis of the sub-optimal filter is General Covariance Analysis Program (GCAP)(Ref 5). This program yields the covariance matrices of the sub-optimal filter state vector and the error-vector at specified points in time. GCAP generates the filter covariance through the Kalman filter equations presented above. To show how the covariance of the error vector is obtained in this program, the following derivation is presented (Ref 5:20-32).

The following augmented state vector is defined:

$$\underline{X}_{aug} = \begin{bmatrix} \underline{E} \\ \hline \underline{\hat{X}}_F \end{bmatrix} = \begin{bmatrix} \underline{X}_S - T\underline{X}_F \\ \hline \underline{\hat{X}}_F \end{bmatrix} \tag{32}$$

differentiating both sides and substituting Equations (19) and (21) for $\dot{\underline{X}}_S$ and $\dot{\underline{\hat{X}}}_F$,

$$\dot{\underline{X}}_{aug} = \begin{bmatrix} F_S\underline{X}_S + G_S\underline{W}_S - TF_F\underline{\hat{X}}_F \\ \hline F_F\underline{\hat{X}}_F \end{bmatrix} \tag{33}$$

which can be rewritten as:

$$\dot{\underline{X}}_{aug} = \begin{bmatrix} F_S\underline{X}_S + G_S\underline{W}_S - TF_F\hat{\underline{X}}_F - F_ST\hat{\underline{X}}_F + F_ST\hat{\underline{X}}_F \\ \hline F_F\hat{\underline{X}}_F \end{bmatrix}$$

and simplified to

$$\dot{\underline{X}}_{aug} = \begin{bmatrix} F_S\underline{E} + (F_ST - TF_F)\hat{\underline{X}}_F + G_S\underline{W}_S \\ \hline F_F\hat{\underline{X}}_F \end{bmatrix}$$

This equation can be factored into the following form:

$$\dot{\underline{X}}_{aug} = \left[\begin{array}{c|c} F_S & (F_ST - TF_F) \\ \hline 0 & F_F \end{array}\right] \underline{X}_{aug} + \left[\begin{array}{c} G_S \\ \hline 0 \end{array}\right] \underline{W}_S \qquad (34)$$

or for simplicity,

$$\dot{\underline{X}}_{aug} = F_{aug}\,\underline{X}_{aug} + G_{aug}\,\underline{W}_S \qquad (35)$$

This equation is in state-space form with the covariance of the augmented state vector satisfying the differential equation

$$\dot{P} = FP + PF^T + GQG^T \qquad (36)$$

where

$$P = \left[\begin{array}{c|c} P_E & P_{12} \\ \hline P_{21} & P_{22} \end{array}\right]$$

$$F = \left[\begin{array}{c|c} F_S & (F_ST - TF_F) \\ \hline 0 & F_F \end{array}\right]$$

Equation (36) shows the covariance propagation of the augmented state vector, with the upper left partition the desired entity; i.e., the covariance of the error vector. The covariance of the error vector is updated after a measurement using the following relationships:

$$\underline{X}_S^+ = \underline{X}_S^- \tag{37}$$

$$\hat{\underline{X}}_F^+ = \hat{\underline{X}}_F^- + K_F(H_S\underline{X}_S^- - H_F\hat{\underline{X}}_F^- + \underline{U}_S) \tag{38}$$

$$\underline{E}^+ = \underline{X}_S^+ - T\underline{X}_F^+ \tag{39}$$

Substituting Equations (37) and (38) into Equation (39) and rearranging terms,

$$\underline{E}^+ = \underline{X}_S^- - T\left[\hat{\underline{X}}_F + K_F(H_S\underline{X}_S^- - H_F\hat{\underline{X}}_F + \underline{V}_S)\right] + TK_FH_ST\hat{\underline{X}}_F^- - TK_FH_S\hat{T\underline{X}}_F \tag{40}$$

the associated error vector covariance after update is

$$P^+ = AP^-A^T + BR_SB^T \tag{41}$$

where

$$A = \left[\begin{array}{c|c} I - TK_FH_S & TK_F(H_F - H_ST) \\ \hline K_F + H_s & I + K_FH_ST - K_FH_F \end{array}\right]$$

and

$$B = \begin{bmatrix} -TK_F \\ K_F \end{bmatrix}$$

GCAP iteratively solves the continuous time equations presented above using a fourth-order Runge-Kutta approximation integration routine and then performs the discrete-time measurement updates.

IV. System Models

The highly dimensioned system models (one each for the Sperry and Hamilton-Standard inertial navigation systems) used in the covariance analysis of the sub-optimal filter designs were developed by Professor Maybeck (Ref 1; Ref 2). Because the states of the two linear system models are modeled as initially Gaussian and driven by white Gaussian noise, the first section of this chapter will discuss noise modeling. The second section will define the state variables used in each system model and their associated initial conditions and noise strengths. In the last section, the dynamics matrix, F_S, noise gain matrix, G_S, and the measurement matrix, H_S, for each system will be presented, along with some justification for the difference in states and state dimension between the two models.

Noise Modeling

The system model state equation is representative of the best mathematical model that can be used to describe a given system. It is necessarily complex to include the dynamics associated with all the significant factors influencing performance. In some cases, a systems second-order effects are so small a factor in overall performance that they can be disregarded and a linear mathematical model

generated. Such is the case for an inertial navigation system. Although the linear equations governing the error response of an INS are well documented in the literature (Ref 3; Ref 6; Ref 7), certain influencing factors and initial conditions cannot be specified exactly due to limitations in the developed theory, testing procedures, and measuring devices. Although an exact magnitude cannot be put on these "influencing factors and initial conditions," careful observation may allow the designer to propose stochastic process models whose power spectral densities are good approximations to these unknowns. In the INS portion of the system state equation, these uncertainties are modeled as additional states driven by white Gaussian noise, and their relationship to the position, velocity, and attitude states is expressed by augmenting the F_S matrix. Similarly, uncertainties associated with the RAC can be modeled as "noise states" and augmented into the system dynamics matrix. The following two noise models are presented to show the effects an augmented "noise state" introduces into the system state equation.

Random Bias. The random bias models a constant of unknown magnitude. It is formed by setting an undriven integrator with a random initial condition. Figure 5 shows the random bias in block diagram form (Ref 4:174). From this block diagram, it can be seen that the state equation for a random bias is $\dot{X}(t) = 0$. As the integrator is not

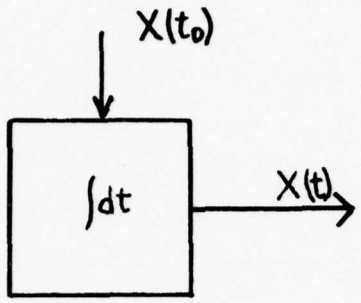

Figure 5. Random Bias

driven by white Gaussian noise, the Q_S element for this state is 0. The initial condition is supplied in the Gaussian random vector $\underline{X}_S(t_0)$ with mean equal to $\hat{X}_S(t_0)$. Careful testing may limit the range of values this constant may initially assume; this information is embodied in the $P_S(t_0)$ matrix for the system as the variance of the state. Examples of errors that are modeled as random biases in the system model are accelerometer and gyroscope scale factor errors.

Exponentially Time-Correlated Noise Model. The exponentially time-correlated noise model is a useful representation of a random quantity whose variance kernel is a decreasing exponential in the difference. This can be

expressed as follows for the scalar case:

$$E[X(t)X(t+\Delta t)] = \sigma^2 e^{-\alpha|\Delta t|} \tag{42}$$

where $E[\cdot]$ is again the expectation operator

and

$\underline{X}(t)$ = random quantity being modeled

σ^2 = the variance of $\underline{X}(t)$

α = 1/T where T is the correlation time of the random quantity

Figure 6 illustrates the exponentially time-correlated noise in block diagram form (Ref 4:178).

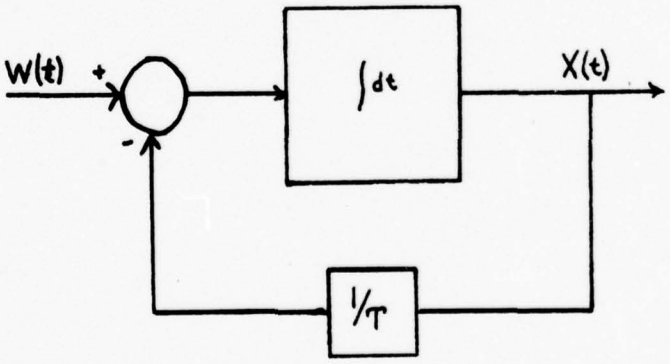

Figure 6. Exponentially Time-Correlated Noise Model

From Figure 6, it can be seen that the uncertainty X(t) is the output of a first order lag driven by white Gaussian noise. The state equation for the noise X(t) is

$$\dot{X}(t) = -\frac{1}{T} X(t) + w(t) \tag{43}$$

As it is desired to model a stationary process, the appropriate strength, Q_S, of the white Gaussian noise can be found by setting the variance propagation equation equal to zero and solving for the Q_S magnitude which achieves a desired σ^2 value. The equation is solved below:

$$\dot{P}_S = F_S P_S + P_S F_S^T + G_S Q_S G_S^T = 0 \tag{44}$$

or for this scalar case

$$0 = -\frac{1}{T} \sigma^2 - \sigma^2 \frac{1}{T} + Q_S \tag{45}$$

$$Q_S = \frac{2\sigma^2}{T} \tag{46}$$

Therefore, the uncertainty being modeled as exponentially time-correlated requires an input noise strength numerically equal to twice the state variance divided by the correlation time. In the system models, certain accelerometer and gyro error characteristics are modeled as exponentially time-correlated.

An exponentially distance-correlated process can be modeled following the above development and making the substitution V/D for T, where D is the correlation distance of

the process and V the velocity in the appropriate direction. Gravity deflections and anomalies are expressed as exponentially distance-correlated processes in the system models.

System Model State Variables

In this section, the state variables used in the Sperry and Hamilton-Standard system models will be defined. As stated in Chapter II, the Kalman filter formulation being implemented in the RAC-INS system is the indirect feedback filter. In this configuration, the Kalman filter estimates the errors being committed by the system rather than the quantities of direct interest such as position, velocity, and altitude. Thus, the first nine states in each system model are the error states associated with the three axes of the east-north-up coordinate frame (three error states for each axis, one each for position, velocity, and attitude errors). A modeling assumption made for the two system models is that, on an ensemble basis, all errors at time t_0 will be zero mean; thus the initial condition for the states of both systems is a zero vector, i.e.,

$$\hat{x}_S(t_0) = [\underline{0}] \tag{47}$$

In addition, the $P_S(t_0)$ matrix is assumed to be diagonal.

Sperry System Model. The 46 states embodied in the Sperry system model, together with their initial variances and appropriate noise strengths, are listed in Table I.

Table I

Sperry System Model States

	State	Description	$P_S(t_0)$ Term	Q_S Term
1.	δX_E		$(1500 \text{ ft})^2$	$\frac{(.0626)^2}{12}$ ft^2/sec
2.	δX_N	position errors	$(1500 \text{ ft})^2$	$\frac{(.0625)^2}{12}$ ft^2/sec
3.	δX_U		$(1500 \text{ ft})^2$	$\frac{(.0625)^2}{12}$ ft^2/sec
4.	δV_E		$(2 \text{ ft/sec})^2$	0
5.	δV_N	velocity errors	$(2 \text{ ft/sec})^2$	0
6.	δV_U		$(2 \text{ ft/sec})^2$	0
7.	Φ_E		$(0.5 \text{ millirad})^2$	(7.61×10^{-11}) rad^2/sec
8.	Φ_N	attitude errors	$(0.5 \text{ millirad})^2$	(7.61×10^{-11}) rad^2/sec
9.	Φ_U		$(0.5 \text{ millirad})^2$	(7.61×10^{-11}) rad^2/sec

Table I (continued)

	State	Description	$P_S(t_0)$ Term	Q_S Term
10.	a_{bx}	accelerometer biases (day-to-day non-repeatibility)	$(250\ \mu g)^2$	0
11.	a_{by}		$(250\ \mu g)^2$	0
12.	a_{bz}		$(250\ \mu g)^2$	0
13.	δk_{ax}	accel. scale factor errors	$(500^*\text{ppm})^2$	0
14.	δk_{ay}		$(500\ \text{ppm})^2$	0
15.	δk_{az}		$(500\ \text{ppm})^2$	0
16.	δk_{axy}	accel. input axis misalignments	$(10\ \text{arc sec})^2$	0
17.	δk_{axz}		$(10\ \text{arc sec})^2$	0
18.	δk_{ayx}		$(10\ \text{arc sec})^2$	0
19.	δk_{ayz}		$(10\ \text{arc sec})^2$	0
20.	δk_{azx}		$(10\ \text{arc sec})^2$	0
21.	δk_{azy}		$(10\ \text{arc sec})^2$	0

*ppm = parts per million

Table I (continued)

	State	Description	$P_S(t_0)$ Term	Q_S Term
22.	a_{rbx}		$(40\ \mu g)^2$	$2P_S(t_0)/T_1$
23.	a_{rby}	accel. bias T_1 = 60 min.	$(40\ \mu g)^2$	$2P_S(t_0)/T_1$
24.	a_{rbz}		$(40\ \mu g)^2$	$2P_S(t_0)/T_1$
25.	a_{rb2x}		$(20\ \mu g)^2$	$2P_S(t_0)/T_2$
26.	a_{rb2y}	accel. bias T_2 = 15 min.	$(20\ \mu g)^2$	$2P_S(t_0)/T_2$
27.	a_{rb2z}		$(20\ \mu g)^2$	$2P_S(t_0)/T_2$
28.	δg_E	gravity deflections d_1 = 10n. mi.	$(26\ \mu g)^2$	$2P_S(t_0)V/d_1$
29.	δg_N		$(17\ \mu g)^2$	$2P_S(t_0)V/d_1$
30.	δg_U	gravity anomaly d_2 = 60n. mi.	$(35\ \mu g)^2$	$2P_S(t_0)V/d_2$
31.	ε_{gx}		$(.09\ deg/hr)^2$	$1.47x10^{-18} rad^2/sec^3$
32.	ε_{gy}	gyro drift rate biases (Brownian motion)	$(.09\ deg/hr)^2$	$1.47x10^{-18} rad^2/sec^3$
33.	ε_{gz}		$(.09\ deg/hr)^2$	$1.47x10^{-18} rad^2/sec^3$

Table I (continued)

	State	Description	$P_S(t_0)$ Term	Q_S Term
34.	δk_{gx}	gyro scale factor errors	$(100 \text{ ppm})^2$	0
35.	δk_{gy}		$(100 \text{ ppm})^2$	0
36.	δk_{gz}		$(100 \text{ ppm})^2$	0
37.	δk_{gxy}	gyro input axis misalignments	$(6 \text{ arc sec})^2$	0
38.	δk_{gxz}		$(6 \text{ arc sec})^2$	0
39.	δk_{gyx}		$(6 \text{ arc sec})^2$	0
40.	δk_{gyz}		$(6 \text{ arc sec})^2$	0
41.	δk_{gzx}		$(6 \text{ arc sec})^2$	0
42.	δk_{gzy}		$(6 \text{ arc sec})^2$	0
43.	b_E	RAC biases	Θ_{be}	0
44.	b_N		Θ_{bn}	0

Table I (continued)

	State	Description	$P_S(t_0)$ Term	Q_S Term
45.	e_{hb}	altimeter bias (d = 250n. mi.)	$(500\ ft)^2$	$2P_S(t_0)V/d$
46.	e_{hsf}	altimeter scale factor error	$(.03)^2$	0

This table is taken directly from Professor Maybeck's report (Ref 1) in which an explanation of how the $P_S(t_0)$ and Q_S magnitudes were chosen can be found. The first nine states represent the errors committed by the system in estimating position, velocity, and attitude expressed relative to the ENU coordinate frame for convenience. States 10 through 27 represent accelerometer errors committed with respect to the X_P-Y_P-Z_P platform frame (From Chapter II, the platform frame of the accelerometers and gyros is related to the navigation frame through the $C_B^N C_P^B$ direction cosine matrix). These errors are described by means of a day-to-day repeatability bias, scale factor error, input-axis misalignment angles about two orthogonal directions, and two exponentially time-correlated biases for each accelerometer. States 28 through 30 describe the errors between the true earth geoid and the reference ellipsoid assumed in the onboard navigation algorithm through exponentially distance-correlated processes. States 31 through 42 describe the laser gyro errors in terms of a gyro drift rate process, gyro scale factor error, and input-axis misalignment angles about two directions for each gyro, again with respect to the X_P-Y_P-Z_P platform frame. The reason this simplistic model of gyro errors is implemented will be summarized when the differences between the Sperry and Hamilton-Standard system models are discussed later in this chapter. States 43 and 44 model a bias error in the RAC estimates of

position along the east and north axes of the reference frame. The initial variance for these states is classified. The last two states, 45 and 46, are altimeter errors, one a time-correlated noise process, and the other a scale factor error. The dynamics matrices relating these states will be presented in the next section.

Hamilton-Standard System Model. Table II lists the 61 states comprising the Hamilton-Standard system model together with their initial variances and appropriate noise strengths. Again, this table is taken directly from Professor Maybeck's report (Ref 2). The first 42 states are identical to those of the Sperry system model, with initial conditions and noise strengths that differ from the Sperry system due to the quality of the accelerometers and gyroscopes used. Table III summarizes the initial variance of similar error sources for the two systems. This table indicates that the quality of the accelerometers and gyroscopes used in the Sperry INS is better than that of those used in the Hamilton-Standard INS.

In addition to the errors analogous to those by the laser gyros of the Sperry system, the conventional dry-tuned gyros of the Hamilton-Standard INS introduce four additional sources of error. These sources of error are modeled in states 43 through 57 as two time-correlated gyro drift rate processes, a two-axis gravity-sensitive drift rate error, and a G^2-sensitive drift rate error for each

Table II

Hamilton-Standard System Model States

	State	Description	$P_S(t_0)$ Term	Q_S Term
1.	δX_E		$(1500 \text{ ft})^2$	0
2.	δX_N	position errors	$(1500 \text{ ft})^2$	0
3.	δX_U		$(1500 \text{ ft})^2$	0
4.	δV_E		$(2\text{ft/sec})^2$	0
5.	δV_N	velocity errors	$(2\text{ft/sec})^2$	0
6.	δV_U		$(2\text{ft/sec})^2$	0
7.	Φ_E		$(0.5 \text{ millirad})^2$	0
8.	Φ_N	attitude errors	$(0.5 \text{ millirad})^2$	0
9.	Φ_U		$(0.5 \text{ millirad})^2$	0
10.	a_{bx}	accelerometer biases (day-to-day non-repeatibility)	$(200\ \mu g)^2$	0
11.	a_{by}		$(200\ \mu g)^2$	0
12.	a_{bz}		$(200\ \mu g)^2$	0

Table II (continued)

	State	Description	$P_S(t_0)$ Term	Q_S Term
13.	δk_{ax}	accel. scale factor errors	$(405.6\text{ppm})^{2*}$	0
14.	δk_{ay}		$(405.6\text{ppm})^{2*}$	0
15.	δk_{az}		$(405.6\text{ppm})^{2*}$	0
16.	δk_{axy}	accel. input axis misalignment	$(30\text{ arc sec})^2$	0
17.	δk_{axz}		$(30\text{ arc sec})^2$	0
18.	δk_{ayx}		$(30\text{ arc sec})^2$	0
19.	δk_{ayz}		$(30\text{ arc sec})^2$	0
20.	δk_{azx}		$(30\text{ arc sec})^2$	0
21.	δk_{azy}		$(30\text{ arc sec})^2$	0
22.	a_{rbx}	accel. bias (T_1 = 60 min)	$(60\ \mu g)^2$	$2P_S(t_0)/T_1$
23.	a_{rby}		$(60\ \mu g)^2$	$2P_S(t_0)/T_1$
24.	a_{rbz}		$(60\ \mu g)^2$	$2P_S(t_0)/T_1$

* $[400^2 + 30^2 + 60^2]\,\text{ppm}^2$

Table II (continued)

	State	Description	$P_S(t_0)$ Term	Q_S Term
25.	a_{rb2x}	accel. bias (T_2 = 15 min)	$(30\ \mu g)^2$	$2P_S(t_0)/T_2$
26.	a_{rb2y}		$(30\ \mu g)^2$	$2P_S(t_0)/T_2$
27.	a_{rb2z}		$(30\ \mu g)^2$	$2P_S(t_0)/T_2$
28.	δg_E	gravity deflections (d_1 = 10 n. mi.)	$(26\ \mu g)^2$	$2P_S(t_0)V/d_1$
29.	δg_N		$(17\ \mu g)^2$	$2P_S(t_0)V/d_1$
30.	δg_U	gravity anomaly (d_2 = 60 n. mi.)	$(35\ \mu g)^2$	$2P_S(t_0)V/d_2$
31.	ε_{gx}	gyro drift rate biases (Brownian motion)	$(2.0^\circ/hr)^2$	0
32.	ε_{gy}		$(1.33^\circ/hr)^2$	0
33.	ε_{gz}		$(1.33^\circ/hr)^2$	0
34.	δk_{gx}	gyro scale factor errors	(500 ppm)^2	0
35.	δk_{gy}		(500 ppm)^2	0
36.	δk_{gz}		(500 ppm)^2	0

Table II (continued)

	State	Description	$P_S(t_0)$ Term	Q_S Term
37.	δk_{gxy}		$(30 \text{ arc sec})^2$	0
38.	δk_{gxz}		$(30 \text{ arc sec})^2$	0
39.	δk_{gyx}	gyro input axis misalignments	$(30 \text{ arc sec})^2$	0
40.	δk_{gyz}		$(30 \text{ arc sec})^2$	0
41.	δk_{gzx}		$(30 \text{ arc sec})^2$	0
42.	δk_{gzy}		$(30 \text{ arc sec})^2$	0
43.	ε_{rgx}		$(0.4\text{oav}-0.6\text{iav}^{\circ}/\text{hr})^2$	$2P_S(t_0)/T_1$
44.	ε_{rgy}	gyro drift rate (T_1 = 60 min)	$(0.4\text{oav}-0.6\text{iav}^{\circ}/\text{hr})^2$	$2P_S(t_0)/T_1$
45.	ε_{rgz}		$(0.4\text{oav}-0.6\text{iav}^{\circ}/\text{hr})^2$	$2P_S(t_0)/T_1$
46.	ε_{rg2x}		$(0.2\text{oav}-0.3\text{iav}^{\circ}/\text{hr})^2$	$2P_S(t_0)/T_2$
47.	ε_{rg2y}	gyro drift rate (T_2 = 15 min)	$(0.2\text{oav}-0.3\text{iav}^{\circ}/\text{hr})^2$	$2P_S(t_0)/T_2$
48.	ε_{rg2z}		$(0.2\text{oav}-0.3\text{iav}^{\circ}/\text{hr})^2$	$2P_S(t_0)/T_2$

Table II (continued)

	State	Description	$P_S(t_0)$ Term	Q_S Term
49.	k_{gxi}		$(2.0^\circ/hr/g)^2$	0
50.	k_{gxs}		$(2.0^\circ/hr/g)^2$	0
51.	k_{gyi}		$(2.0^\circ/hr/g)^2$	0
52.	k_{gys}	g-sensitive drift coefficients (spin and input axes)	$(2.0^\circ/hr/g)^2$	0
53.	k_{gzi}		$(2.0^\circ/hr/g)^2$	0
54.	k_{gzs}		$(2.0^\circ/hr/g)^2$	0
55.	k_{gxsi}		$(0.1^\circ/hr/g^2)^2$	0
56.	k_{gysi}	g^2-sensitive drift coefficients (major spin-input coefficients)	$(0.1^\circ/hr/g^2)^2$	0
57.	k_{gzsi}		$(0.1^\circ/hr/g^2)^2$	0
58.	b_E	RAC biases	Θ_{bE}	0
59.	b_N		Θ_{bN}	0
60.	e_{hb}	altimeter bias (d = 250 n. mi.)	$(500\ ft)^2$	$2P_S(t_0)/d$
61.	e_{hsf}	altimeter scale factor error	$(.03)^2$	0

Table III

Comparison of Initial Variance in Accelerometer and Gyroscope Errors Between the Sperry and Hamilton-Standard System Models

Error Source	Initial Variance Sperry	Initial Variance Hamilton-Standard
Accelerometer Bias (Day-to-Day Nonrepeatibility)	$(250\ \mu g)^2$	$(200\ \mu g)^2$
Accelerometer Scale Factor Errors	$(500 ppm)^2$	$(405.6 ppm)^2$
Accel. Input Axis Misalignment	$(10$ arc sec$)^2$	$(30$ arc sec$)^2$
Accelerometer Bias (Correlation Time 60 min)	$(40\ \mu g)^2$	$(60\ \mu g)^2$
Accel. Bias (Correlation Time 15 min)	$(20\ \mu g)^2$	$(30\ \mu g)^2$
Gyro Drift Rate Bias	$(.09$ deg/hr$)^2$	$(1.33$ deg/hr$)^2$
Gyro Scale Factor Errors	$(100 ppm)^2$	$(500 ppm)^2$
Gyro Input Axis Misalignment	$(6$ arc sec$)^2$	$(30$ arc sec$)^2$

gyroscope. An explanation for this modeling versus that for the Sperry gyroscopes is presented in the last section of this chapter. The last four states model the RAC and altimeter errors committed by the system and are identical to the last four states in the Sperry model.

Dynamics of the Sperry Models

In Chapter III, the state equation of the system model was defined as

$$\dot{\underline{X}}_S = F_S\underline{X}_S + B_S\underline{U}_S + G_S\underline{W}_S$$

In this section, the F_S and G_S matrices relating the state variables and additive white Gaussian noise for each system will be defined. The B_S matrix is not relevant to this analysis, because there are no deterministic open-loop control inputs for this analysis. The measurement matrix H_S associated with the system models will also be presented in this section.

Sperry Dynamic's Matrices. The F_S matrix for the 46 state Sperry system model may be partitioned as shown on the following page in Equation (48). The F_{ij} partitions of Equation (48) will be displayed in the following development.

The F_{1-1} partition is the fundamental matrix relating the error states of the INS. Professor Maybeck used the fundamental matrix presented in Inertial Navigation System Error Models (Ref 8:26) as the F_{1-1} matrix for this system

$$F_S = \begin{bmatrix} F_{1-1} & F_{1-2} & F_{1-3} & F_{1-4} & F_{1-5} & F_{1-6} & F_{1-7} & F_{1-8} & F_{1-9} & F_{1-10} & F_{1-11} & F_{1-12} \\ & F_{2-2} & & & & & & & & & & \\ & & F_{3-3} & & & & & & & & & \\ & & & F_{4-4} & & & & & & & & \\ & & & & F_{5-5} & & & & & & & \\ & & & & & F_{6-6} & & & & & & \\ & & & & & & F_{7-7} & & & & & \\ & & & & & & & F_{8-8} & & & & \\ & & & & & & & & F_{9-9} & & & \\ & & & & & & & & & F_{10-10} & & \\ & & & & & & & & & & F_{11-11} & \\ & & & & & & & & & & & F_{12-12} \end{bmatrix} \quad (48)$$

model with one change: the error-states $\delta\lambda$ and $\delta\ell$, representing the errors in longitude and latitude, expressed in degrees or radians have been transformed to the error-states δX_E and δX_N expressed in feet. The F_{1-1} matrix is shown explicitly in Figures 7 and 7a.

The remainder of the F_{i-j} matrices relate the "noise states" to the error states. These matrices are presented

	δX_E	δX_N	δX_U	δV_E
$\dot{\delta X}_E$	0	$\frac{V_E}{R}\tan(L)$	$-\frac{V_E}{R}$	1
$\dot{\delta X}_N$	0	0	$-\frac{V_N}{R}$	0
$\dot{\delta X}_U$	0	0	0	0
$\dot{\delta V}_E$	0	$2\left[-\frac{V_U}{R}\omega_{IE}\sin(L) + \frac{V_N}{R}\omega_{IE}\cos(L)\right] + \frac{V_E V_N}{R^2}\cos^2(L)$	$-\frac{V_N V_E}{R^2}\tan(L) + \frac{V_E V_U}{R^2}$	$\frac{V_N}{R}\tan(L) - \frac{V_U}{R}$
$\dot{\delta V}_N$	0	$-2\left[\frac{\omega_{IE} V_E}{R}\cos(L) - \frac{V_E^2}{R^2\cos^2(L)}\right]$	$\frac{V_E^2\tan(L)}{R^2} - \frac{V_N V_U}{R^2}$	$-2\left[\frac{V_E\tan(L)}{R} + \omega_{IE}\sin(L)\right]$
$\dot{\delta V}_U$	0	$\frac{-2}{R}\omega_{IE} V_E \sin(L)$	$\frac{2G}{R} - \frac{V_E^2 + V_N^2}{R^2}$	$2\left[\frac{V_E}{R} + \omega_{IE}\cos(L)\right]$
$\dot{\Phi}_E$	0	0	$\frac{V_N}{R^2}$	0
$\dot{\Phi}_N$	0	$\frac{-\omega_{IE}\sin(L)}{R}$	$-\frac{V_E}{R^2}$	$\frac{1}{R}$
$\dot{\Phi}_U$	0	$\frac{V_E}{R^2} + \frac{\omega_{IE}\cos(L)}{R} + \frac{V_E}{R^2}\tan^2(L)$	$\frac{-V_E\tan(L)}{R^2}$	$\frac{\tan(L)}{R}$

Figure 7. INS Fundamental Error Matrix

	δV_N	δV_U	Φ_E	Φ_U	
$\delta\dot{X}_E$	0	0	0	0	0
$\delta\dot{X}_N$	1	0	0	0	0
$\delta\dot{X}_U$	0	1	0	0	0
$\delta\dot{V}_E$	$\frac{V_E}{R}\tan(L) + 2\omega_{IE}\sin(L)$	$-\frac{V_E}{R} + 2\omega_{IE}\cos(L)$	0	$-f_U$	f_N
$\delta\dot{V}_N$	$-\frac{V_U}{R}$	$-\frac{V_N}{R}$	f_U	0	$-f_E$
$\delta\dot{V}_U$	$\frac{2V_N}{R}$	0	$-f_N$	f_E	0
$\dot{\Phi}_E$	$-\frac{1}{R}$	0	0	$\frac{V_E}{R}\tan(L) + \omega_{IE}\sin(L)$	$-\left[\frac{V_E}{R} + \omega_{IE}\cos(L)\right]$
$\dot{\Phi}_N$	0	0	$-\left[\frac{V_E}{R}\tan(L) + \omega_{IE}\sin(L)\right]$	0	$-\frac{V_N}{R}$
$\dot{\Phi}_U$	0	0	$\frac{V_E}{R}+\omega_{IE}\cos(L)$	$\frac{V_N}{R}$	0

Figure 7a. INS Fundamental Error Matrix

as Equations (49) through (57).

$$F_{1-2} = \begin{bmatrix} \underline{0}\ (3x3) \\ \hline C_{EX} & C_{EY} & C_{EZ} \\ C_{NX} & C_{NY} & C_{NZ} \\ C_{uX} & C_{uY} & C_{uZ} \\ \hline \underline{0}\ (3x3) \end{bmatrix} \tag{49}$$

$$F_{1-3} = \begin{bmatrix} \underline{0}\ (3x3) \\ \hline C_{EX}f_X & C_{EY}f_Y & C_{EZ}f_Z \\ C_{NX}f_X & C_{NY}f_Y & C_{NZ}f_Z \\ C_{uX}f_X & C_{uY}f_Y & C_{uZ}f_Z \\ \hline \underline{0}\ (3x3) \end{bmatrix} \tag{50}$$

$$F_{1-4} = \begin{bmatrix} \underline{0}\ (3x6) \\ \hline C_{EX}f_Y & -C_{EX}f_Z & -C_{EY}f_X & C_{EY}f_X & C_{EZ}f_X & -C_{EZ}f_Y \\ C_{NX}f_Y & -C_{NX}f_Z & -C_{NY}f_X & C_{NY}f_Z & C_{NZ}f_X & -C_{NZ}f_Y \\ C_{uX}f_Y & -C_{uX}f_Z & -C_{uY}f_X & C_{uY}f_Z & C_{uZ}f_X & -C_{uZ}f_Y \\ \hline \underline{0}\ (3x6) \end{bmatrix} \tag{51}$$

$$F_{1-5} = F_{1-6} = F_{1-2} \tag{52}$$

$$F_{1-7} = \begin{bmatrix} \underline{0}\ (3x3) \\ \hline 1 & 0 & 0 \\ 0 & 1 & 0 \\ 0 & 0 & 1 \\ \hline \underline{0}\ (3x3) \end{bmatrix} \tag{53}$$

$$F_{1-8} = \begin{bmatrix} \underline{0}\ (6x3) \\ \hline C_{EX} & C_{EY} & C_{EZ} \\ C_{NX} & C_{NY} & C_{NZ} \\ C_{uX} & C_{uY} & C_{uZ} \\ \hline \end{bmatrix} \tag{54}$$

$$F_{1-9} = \begin{bmatrix} \underline{0}\ (6x3) \\ \hline C_{EX}\omega_X & C_{EY}\omega_Y & C_{EZ}\omega_Z \\ C_{NX}\omega_X & C_{NY}\omega_Y & C_{NZ}\omega_Z \\ C_{uX}\omega_X & C_{uY}\omega_Y & C_{uZ}\omega_Z \end{bmatrix} \tag{55}$$

$$F_{1-10} = \begin{bmatrix} \underline{0}\ (3x6) \\ \hline -C_{EX}\omega_Y & C_{EX}\omega_Z & C_{EY}\omega_X & -C_{EY}\omega_Z & -C_{EZ}\omega_X & C_{EZ}\omega_Y \\ -C_{NX}\omega_Y & C_{NX}\omega_Z & C_{NY}\omega_X & -C_{NY}\omega_Z & -C_{NZ}\omega_X & C_{NZ}\omega_Y \\ -C_{uX}\omega_Y & C_{uX}\omega_Z & C_{uY}\omega_X & -C_{uY}\omega_Z & -C_{uZ}\omega_X & C_{uZ}\omega_Y \\ \hline \underline{0}\ (3x6) \end{bmatrix} \tag{56}$$

$$F_{1-11} = F_{1-12} = [\underline{0}\ (9x2)] \tag{57}$$

For the states modeling accelerometer and gyroscope uncertainties, a transformation is made in their respective partitions from the platform frame to the ENU frame. This transformation is accomplished through the C_P^N direction cosine matrix where the C_{ij} element is the direction cosine between the i^{th} axis of the ENU frame and the j^{th} axis of the platform frame. The X, Y, and Z subscripts on specific

force, $\underline{f}$, and angular velocity, $\underline{\omega}$, denote vector components of these quantities in the platform frame.

The remainder of the F_{ii} matrices represent the "noise state" dynamics. Uncertainties modeled as biases have null dynamics partitions, while those that are modeled as exponentially time or distance-correlated have the negative inverse of their correlation time along the diagonal of their partition (For distance-correlated processes the correlation time is expressed as $T = D/V$.). The F_{2-2} through F_{12-12} partitions are

$$F_{2-2} = F_{3-3} = [\underline{0}\ (3x3)] \tag{58}$$

$$F_{4-4} = [\underline{0}\ (6x6)] \tag{59}$$

$$F_{5-5} = \begin{bmatrix} -1/T_1 & 0 & 0 \\ 0 & -1/T_1 & 0 \\ 0 & 0 & -1/T_1 \end{bmatrix} \tag{60}$$

$$F_{6-6} = \begin{bmatrix} -1/T_2 & 0 & 0 \\ 0 & -1/T_2 & 0 \\ 0 & 0 & -1/T_2 \end{bmatrix} \tag{61}$$

$$F_{7-7} = \begin{bmatrix} -V/D_1 & 0 & 0 \\ 0 & -V/D_1 & 0 \\ 0 & 0 & -V/D_2 \end{bmatrix} \tag{62}$$

$$F_{8-8} = F_{9-9} = F_{10-10} = \left[\underline{0}\ (3x3)\right] \tag{63}$$

$$F_{11-11} = \left[\underline{0}\ (2x2)\right] \tag{64}$$

$$F_{12-12} = \begin{bmatrix} -V/D_3 & 0 \\ 0 & 0 \end{bmatrix} \tag{65}$$

where from Table I,

T_1 = 60 min

T_2 = 15 min

D_1 = 10 nautical miles

D_2 = 60 nautical miles

D_3 = 250 nautical miles

The G_S matrix adds the white Gaussian noises associated with the state vector into the linear differential system equation. This matrix is 46 x 19 where 19 is the number of white noise sources associated with the system. The matrix is composed of ones and zeros, with a one in the ij^{th} element indicating the i^{th} state is corrupted by white noise j of the $\underline{W}_S$ vector. A zero row is used for a state which is not directly corrupted by white noise. This matrix is not shown explicitly.

The discrete-time measurements made available to the filter are the difference between position indications of INS and the RAC. The INS position indications can be

expressed as

$$X_{E\text{-}INS}(t_i) = X_{E\text{-}true} + \delta X_E(t_i) \tag{66}$$

$$X_{N\text{-}INS}(t_i) = X_{N\text{-}true} + \delta X_N(t_i) \tag{67}$$

where

$X_{\_\text{-}INS}(t_i)$ = east or north position indication of the INS at time t_i

$X_{\_\text{-}true}(t_i)$ = the true east or north position at time t_i

The RAC position fixes can similarly be expressed as

$$X_{E\text{-}RAC}(t_i) = X_{E\text{-}true}(t_i) + b_E - V_E(t_i) \tag{68}$$

$$X_{N\text{-}RAC}(t_i) = X_{N\text{-}true}(t_i) + b_N - V_N(t_i) \tag{69}$$

$X_{\_\text{-}RAC}(t_i)$ = east or north position measurement indication of the RAC at time t_i

$b_\_$ = east or north RAC bias (states 43 and 44 in the system model)

$V_\_(t_i)$ = corruptive white Gaussian noise whose strength at time t_i is a function of vehicle altitude (The negative coefficient is adopted for convenience to generate Z = HX + V instead of Z = HX - V)

The strength of the white noise corrupting the measurement can be expressed as

$$R_S(t_i) = \Theta \cdot \text{Altitude}(t_i)^2 \tag{70}$$

where Θ has a classified numerical value.

The appropriate H_S matrix is formed by differencing corresponding INS and RAC position estimates to form the measurement vector. The resultant equation in matrix form is

$$Z(t_i) = \left[\begin{array}{cc|c|cccc} 1 & 0 & & 1 & 0 & 0 & 0 \\ & & \underline{0}(2x40) & & & & \\ 0 & 1 & & 0 & 1 & 0 & 0 \end{array}\right] \underline{X}_S(t_i) + \begin{matrix} V_E(t_i) \\ V_N(t_i) \end{matrix} \quad (71)$$

where the matrix premultiplying the system state vector is the H_S matrix.

Hamilton-Standard Dynamic's Matrices. The F_S matrix for the 61-state Hamilton-Standard system model may be partitioned as follows in Equation (72). The partitions F_{1-1} through F_{1-10} and F_{2-2} through F_{10-10} correspond exactly to the same partitions in the Sperry model.

$$F_S = \begin{bmatrix} F_{1\text{-}1} & F_{1\text{-}2} & F_{1\text{-}3} & F_{1\text{-}4} & F_{1\text{-}5} & F_{1\text{-}6} & F_{1\text{-}7} & F_{1\text{-}8} & F_{1\text{-}9} & F_{1\text{-}10} & F_{1\text{-}11} & F_{1\text{-}12} & F_{1\text{-}13} & F_{1\text{-}14} & F_{1\text{-}15} & F_{1\text{-}16} \\ & F_{2\text{-}2} & & & & & & & & & & & & & & \\ & & F_{3\text{-}3} & & & & & & & & & & & & & \\ & & & F_{4\text{-}4} & & & & & & & & & & & & \\ & & & & F_{5\text{-}5} & & & & & & & & & & & \\ & & & & & F_{6\text{-}6} & & & & & & & & & & \\ & & & & & & F_{7\text{-}7} & & & & & & & & & \\ & & & & & & & F_{8\text{-}8} & & & & & & & & \\ & & & & & & & & F_{9\text{-}9} & & & & & & & \\ & & & & & & & & & F_{10\text{-}10} & & & & & & \\ & & & & & & & & & & F_{11\text{-}11} & & & & & \\ & & & & & & & & & & & F_{12\text{-}12} & & & & \\ & & & & & & & & & & & & F_{13\text{-}13} & & & \\ & & & & & & & & & & & & & F_{14\text{-}14} & & \\ & & & & & & & & & & & & & & F_{15\text{-}15} & \\ & & & & & & & & & & & & & & & F_{16\text{-}16} \end{bmatrix} \tag{72}$$

Partitions $F_{1\text{-}11}$ through $F_{1\text{-}14}$ and $F_{11\text{-}11}$ through $F_{14\text{-}14}$ introduce the additional error characteristics of the dry-tuned gyros of the Hamilton-Standard system. These matrices are as follows:

$$F_{1\text{-}11} = \begin{bmatrix} \underline{0}\ (6\text{x}3) \\ \hline C_{EX} & C_{EY} & C_{EZ} \\ C_{NX} & C_{NY} & C_{NZ} \\ C_{uX} & C_{uY} & C_{uZ} \end{bmatrix} \tag{73}$$

$$F_{1\text{-}12} = F_{1\text{-}11} \tag{74}$$

$$F_{1\text{-}13} = \begin{bmatrix} \underline{0}\ (6\text{x}6) \\ \hline C_{EX}f_X & -C_{EX}f_X & C_{EY}f_Y & C_{EY}f_X & C_{EZ}f_Z & C_{EZ}f_Y \\ C_{NX}f_X & -C_{NX}f_Y & C_{NY}f_Y & C_{NY}f_X & C_{NZ}f_Z & C_{NZ}f_Y \\ C_{uX}f_X & -C_{uX}f_Y & C_{uY}f_Y & C_{uY}f_X & C_{uZ}f_Z & C_{uZ}f_Y \end{bmatrix} \tag{75}$$

$$F_{1\text{-}14} = \begin{bmatrix} \underline{0}\ (6\text{x}3) \\ \hline -C_{EX}f_Xf_Y & C_{EY}f_Xf_Y & C_{EZ}f_Yf_Z \\ -C_{NX}f_Xf_Y & C_{NY}f_Xf_Y & C_{NZ}f_Yf_Z \\ -C_{uX}f_Xf_Y & C_{uY}f_Xf_Y & C_{uZ}f_Yf_Z \end{bmatrix} \tag{76}$$

$$F_{11\text{-}11} = \begin{bmatrix} -1/T_1 & 0 & 0 \\ 0 & -1/T_1 & 0 \\ 0 & 0 & -1/T_1 \end{bmatrix} \tag{77}$$

$$F_{12\text{-}12} = \begin{bmatrix} -1/T_2 & 0 & 0 \\ 0 & -1/T_2 & 0 \\ 0 & 0 & -1/T_2 \end{bmatrix} \tag{78}$$

$$F_{13\text{-}13} = [\underline{0}\ (6\text{x}6)] \tag{79}$$

$$F_{14\text{-}14} = [\underline{0}\ (3\text{x}3)] \tag{80}$$

where from Table II the correlation times T_1 and T_2 are

$$T_1 = 60 \text{ min}$$

$$T_2 = 15 \text{ min}$$

The F_{1-15}, F_{1-16}, F_{15-15}, and F_{16-16} partitions of Equation (72) correspond to the F_{1-11}, F_{1-12}, F_{11-11}, and F_{12-12} matrices of Equations (57), (64), and (65) respectively.

The G_S matrix for the Hamilton-Standard system is formed in the same manner as that for the Sperry system. Its dimension is 61 x 16. This matrix is not shown explicitly.

The discrete-time measurements made available to the filter are composed of the same information as those of the Sperry system. The measurement matrix H_S is

$$H_S = \begin{bmatrix} 1 & 0 & | & & | & 1 & 0 & 0 & 0 \\ & & | & \underline{0}\ (2x56) & | & & & & \\ 0 & 1 & | & & | & 0 & 1 & 0 & 0 \end{bmatrix} \qquad (81)$$

The system equations for the Sperry and Hamilton-Standard systems having been defined, the differences will now be discussed.

System Model Differences. The major difference in the two system models is the additional 15 gyro error sources incorporated into the Hamilton-Standard system model. These error sources representing the G-sensitive and G^2-sensitive drift coefficients of conventional gyros do not appear in the Sperry system model because its laser gyros are virtually gravity insensitive.

The white Gaussian noise associated with the attitude error-states of the Sperry system is again due to the difference in gyroscopes used for the two INS'. A typical gyro

drift rate model is shown in Figure 8 (Ref 1:14). This model indicates that gyro drift rate is composed of an exponentially time-correlated noise ϵ (with a correlation time of T and an independent white Gaussian noise W_2.

> In conventional gyros, the ϵ contribution to drift rate predominates W_2, and typically the strength of the white Gaussian noise W_1 is set at some finite value while the strength of W_2 is set to zero. However, for laser gyros, the effect of W_2 predominates; this noise strength is depicted through the Q_S terms of 7.61×10^{-11} rad^2/sec driving the attitude error differential equations in Table I [Ref 1:13].

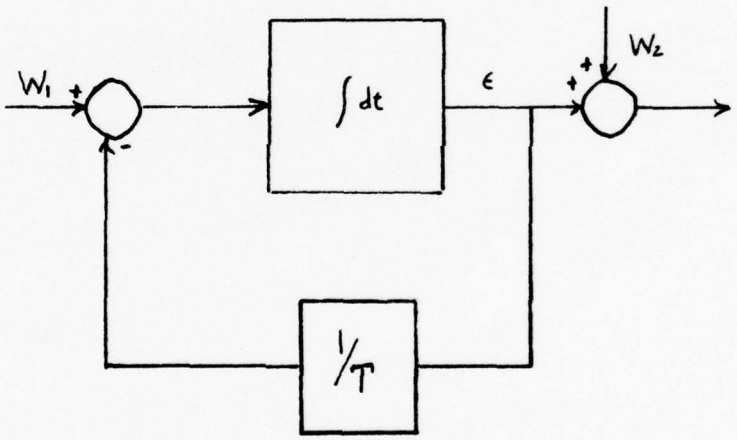

Figure 8. Gyro Drift Model

The system models having been detailed, Chapter V will define the sub-optimal filter models considered in this work.

V. The Lockheed Kalman Filter Design and an Alternate Design

In this chapter, the sub-optimal Kalman filter design as proposed by Lockheed will be presented. In addition, an alternate design based on the Lockheed filter will be developed. A comparison of the merits and possible drawbacks of each of these filters when driven by either INS and updated by the radiometric area correlator will also be made. In Chapter VII the performance of these two filters will be evaluated.

Lockheed's Kalman Filter

The basis for the Lockheed filter is a mathematical model composed of six error states. This model can be decomposed into two decoupled three-state partitions, each embodying errors in position, velocity, and attitude angle in one direction. In this decoupled form, and with the east-north-up coordinate frame instrumented, the state-space equations are (Ref 1:1)

$$\begin{bmatrix} \dot{\delta X}_E \\ \dot{\delta V}_E \\ \dot{\Phi}_N \end{bmatrix} = \begin{bmatrix} 0 & 1 & 0 \\ 0 & 0 & -G \\ 0 & \frac{1}{R} & 0 \end{bmatrix} \begin{bmatrix} \delta X_E \\ \delta V_E \\ \Phi_N \end{bmatrix} + \begin{bmatrix} 0 & 0 \\ 1 & 0 \\ 0 & 1 \end{bmatrix} \begin{bmatrix} W_{E1} \\ W_{E2} \end{bmatrix} \qquad (82)$$

$$\begin{bmatrix} \dot{\delta X}_N \\ \dot{\delta V}_N \\ \dot{\Phi}_E \end{bmatrix} = \begin{bmatrix} 0 & 1 & 0 \\ 0 & 0 & G \\ 0 & -\frac{1}{R} & 0 \end{bmatrix} \begin{bmatrix} \delta X_N \\ \delta V_N \\ \Phi_E \end{bmatrix} + \begin{bmatrix} 0 & 0 \\ 1 & 0 \\ 0 & 1 \end{bmatrix} \begin{bmatrix} W_{N1} \\ W_{N2} \end{bmatrix} \quad (83)$$

where

δX_E is the error in the INS-indicated east position

δX_N is the error in the INS-indicated north position

δV_E is the error in the INS-indicated east velocity

δV_N is the error in the INS-indicated north velocity

Φ_E is the attitude error, east component

Φ_N is the attitude error, north component

R is the equatorial radius of the earth--2.09×10^7 Ft

G is the magnitude of gravity--32.2 Ft/Sec^2

W_{E1}, W_{N1} are white Gaussian noises modeling acceleration associated errors

W_{E2}, W_{N2} are white Gaussian noises modeling attitude angular rate associated errors

These equations form the linear stochastic differential equation upon which the filter is based as described in Chapter III, i.e.,

$$\dot{\underline{X}}_F = F_F \underline{X}_F + G_F \underline{W}_F + B_F \underline{U}_F$$

where for each partition,

$\underline{U}_F$ = control input - a zero vector

$$E[W_{-1}(t_1)W_{-1}(t_2)] = \begin{cases} Q_{22} & \text{for } t_1 = t_2 \\ 0 & \text{for } t_1 \neq t_2 \end{cases} \tag{84}$$

$$E[W_{-1}(t_1)W_{-2}(t_2)] = 0$$

$$E[W_{-2}(t_1)W_{-2}(t_2)] = \begin{cases} Q_{33} & \text{for } t_1 = t_2 \\ 0 & \text{for } t_1 \neq t_2 \end{cases} \tag{85}$$

and the subscripts for each Q were chosen because they assume those positions in the diagonal $G_F Q_F G_F^T$ matrix.

The discrete time measurement for each filter partition is formed by subtracting INS-indicated position from the RAC-indicated position. INS-indicated east position is the sum of true position and the east position error state,

$$X_{E\text{-}INS}(t_i) = X_{E\text{-}TRUE}(t_i) + \delta X_E(t_i) \tag{86}$$

where

$X_{E\text{-}INS}(t_i)$ = INS-indicated east position

$X_{E\text{-}TRUE}(t_i)$ = true east position

Similarly, the RAC-indicated position is the sum of true position and a corruptive white Gaussian noise whose magnitude is proportional to the square of the altitude. This equation is shown below where the negative sign has been

adopted for convenience:

$$X_{E\text{-}RAC}(t_i) = X_{E\text{-}TRUE} - V_{E(t_i)} \tag{87}$$

where

$X_{E\text{-}RAC}(t_i)$ = RAC-indicated east position

$V_E(t_i)$ = zero mean, white Gaussian noise corrupting the RAC position measurement

and

R_F = the strength of the measurement corrupting noise

$V_E = \Theta \cdot (\text{altitude})^2$

with Θ a classified numeric value. Therefore, subtracting Equation (87) from Equation (86) yields the desired measurement equation for the east-position partition as

$$Z(t_i) = \delta X_E(t_i) + V_E(t_i) \tag{88}$$

Because position is the only quantity measured by the RAC, this measurement equation can be expressed as:

$$Z(t_i) = \begin{bmatrix} 1 & 0 & 0 \end{bmatrix} \begin{bmatrix} \delta X_E(t_i) \\ \delta V_E(t_i) \\ \Phi_N(t_i) \end{bmatrix} + V_E(t_i) \tag{89}$$

Similarly, the measurement equation for the north-position partition is

$$Z(t_i) = \begin{bmatrix} 1 & 0 & 0 \end{bmatrix} \begin{bmatrix} \delta X_N(t_i) \\ \delta V_N(t_i) \\ \Phi_E(t_i) \end{bmatrix} + V_N(t_i) \tag{90}$$

These equations correspond to the measurement equation for the sub-optimal filter presented in Chapter III, i.e.,

$$\underline{Z}(t_i) = H_F \underline{X}_F(t_i) + \underline{V}_F(t_i)$$

These filter models are extremely simple, six total states as opposed to the 46 and 61 state optimal filters of the Sperry and Hamilton-Standard systems' truth models respectively, thereby reducing the computational load and storage requirements for the onboard computer. In addition, a simplification to the covariance propagation equation is made in the Lockheed design. The continuous time equation describing the covariance propagation is from Equation (28):

$$\dot{P} = FP + PF^T + GQG^T$$

The equivalent discrete time equation is (Ref 4:163)

$$P(t_i^-) = \Phi(t_i,t_{i-1})P(t_{i-1}^+)\Phi^T(t_i,t_{i-1}) + \int_{t_{i-1}}^{t_i} \Phi(t_i,\tau)GQG^T\Phi^T(t_i,\tau)d\tau \qquad (91)$$

where

τ is a dummy variable representing time

superscript $^+$ is the time instant just after a measurement update

superscript $^-$ is the time instant just before a measurement update

$\Phi(t_i,t_{i-1})$ is the state transition matrix, the matrix which satisfies the differential equation

$$\frac{d}{dt}\,\Phi(t_i,t_{i-1}) = F\Phi(t_i,t_{i-1})$$

over the time interval t_{i-1} to t_i starting from the initial condition

$$\Phi(t_{i-1},t_{i-1}) = I$$

where I is an identity matrix of the same dimension as $\Phi(t_{i-1},t_{i-1})$.

The simplification made by Lockheed is to approximate the full matrix resulting from the integration term in the discrete equation as a diagonal matrix. Thus for each three-state partition the full 3x3 additive noise matrix is approximated as a 3x3 diagonal matrix. This approximation leads to the following discrete time covariance propagation equation for the Lockheed design (Ref 1:2)

$$P(t_i^-) = \Phi(t_i,t_{i-1})P(t_{i-1}^+)\Phi^T(t_i,t_{i-1}) + \begin{bmatrix} q_{11} & 0 & 0 \\ 0 & q_{22} & 0 \\ 0 & 0 & q_{33} \end{bmatrix} \quad (92)$$

where

$$q_{11} = (\tfrac{1}{2}\Delta t^2)^2 Q_{22} + (5.3666\Delta t^3)^2 Q_{33}$$

$$q_{22} = \Delta t^2 Q_{22} + (16.1\Delta t^2)^2 Q_{33}$$

$$q_{33} = \Delta t^2 Q_{33}$$

Q_{22} = strength of white Gaussian noise W_{-1} as expressed in Equation (84)

Q_{33} = strength of white Gaussian noise W_{-2} as expressed in Equation (85)

$$\Delta t = t_i - t_{i-1}$$

Advantages

The major advantage of this design is simplicity. The onboard computer has only to propagate and update two three-state partitions, a considerable computational and storage reduction from tracking even one six-state filter whose states are coupled. In addition, the computer burden is further lessened using a discrete noise formulation obtained through straightforward mathematical "adds" and "multiplies"; a function the computer can accomplish far more efficiently than numerical integration.

Disadvantages

One possible disadvantage of such a simple design is accuracy, whether the tradeoff in accuracy between the six-state filter model and a more sophisticated design is warranted can only be evaluated when system specifications are finalized. Accuracy will also be lost in approximating the full 3x3 additive noise matrix for each filter as diagonal. This loss is illustrated in the following development.

Using Equation (92) the initial covariance matrix, $P_F(t_0)$, is propagated to its first measurement update time, t_1, as follows:

$$P(t_1^-) = \Phi(t_1,0)P_F(t_0)\Phi^T(t_1,0) + \int_0^{t_1} \Phi(t_1,\tau)G_F Q_F G_F^T \Phi^T(t_1,\tau)\,d\tau \qquad (93)$$

The matrix multiplication and integration terms may be expressed in the simplified form below for each partition.

$$P(t_1^-) = \begin{bmatrix} E_{11} & E_{21} & E_{31} \\ E_{12} & E_{22} & E_{32} \\ E_{13} & E_{23} & E_{33} \end{bmatrix} + \begin{bmatrix} N_{11} & N_{21} & N_{31} \\ N_{12} & N_{22} & N_{32} \\ N_{13} & N_{23} & N_{33} \end{bmatrix} \tag{94}$$

where

E_{ij} are elements of the $\Phi(\cdot)P_F(t_0)\Phi^T(\cdot)$ matrix, with

$E_{ij} = E_{ji}$ from symmetry

and

Q_{ij} are elements of the $\int \Phi(\cdot)\ G_F Q_F G_F^T \Phi^T(\cdot) d\tau$ matrix with

$Q_{ij} = Q_{ji}$ from symmetry

The Kalman gain matrix, K, is then calculated:

$$K(t_1) = P_F(t_1^-)H_F^T[H_F P_F(t_1^-)H_F^T + R_F]^{-1} \tag{95}$$

Using Equations (90) and (100), in matrix form this gain for either partition can be expressed as:

$$K(t_1) = \begin{bmatrix} E_{11}+N_{11} & 0 & 0 \\ E_{12}+N_{12} & 0 & 0 \\ E_{13}+N_{13} & 0 & 0 \end{bmatrix} \frac{1}{E_{11}+N_{11}+\Theta\cdot(\text{altitude})^2} \tag{96}$$

This gain matrix is then used to update the covariance matrix according to Equation (30), i.e.,

$$P_F(t_1^+) = P_F(t_1^-) - KH_F P_F(t_1^-)$$

In lower triangular matrix form, this expanded matrix equation is:

$$P_F(t_1^+) = \begin{bmatrix} E_{11}+N_{11} & & \\ E_{12}+N_{12} & E_{22}+N_{22} & \\ E_{13}+N_{13} & E_{23}+N_{23} & E_{33}+N_{33} \end{bmatrix}$$

$$- \begin{bmatrix} (E_{11}+N_{11})^2 & & \\ (E_{12}+N_{12})(E_{11}+N_{11}) & (E_{12}+N_{12})^2 & \\ (E_{13}+N_{13})(E_{11}+N_{11}) & (E_{12}+N_{12})(E_{13}+N_{13}) & (E_{13}+N_{13})^2 \end{bmatrix} \cdot$$

$$\frac{1}{E_{11}+N_{11}+\Theta\cdot(\text{altitude})^2} \qquad (97)$$

Although this equation is quite cumbersome, it serves to point out that every element of the updated covariance matrix, except the upper left, is dependent upon the off-diagonal noise elements. Thus, in ignoring these off-diagonal elements, a certain degree of accuracy will be lost in determining the variance of the error-states.

Alternate Design

Because the computational load and storage requirements placed upon the onboard computer were the ultimate limiting factors in any design for this application, the six error-states as proposed by Lockheed were used in the following filter formulation. The alternate design utilizes an approximation to the full 3x3 additive noise matrix that is

generated from the covariance propagation equation for each of the three-state partitions, instead of Lockheed's diagonalized approximation. Since the best performance for the two three-state filter models can be obtained using the correct covariance propagation equation, an approximation closely matching the full noise matrix rather than just the diagonal elements should provide better filter estimation precision than the Lockheed design. Although this formulation should provide a better estimate of the system navigation errors than the Lockheed design when properly "tuned" (the tuning process is described in Chapter VII), the enhanced estimation precision is bought at a "cost" of additional storage space in the onboard computer, a critical consideration. The additional storage space is required because the three equations in the Lockheed design involving "adds" and "multiplies" would be extended to six in the alternate design. The additional three equations characterize the noise added to the off-diagonal elements of the covariance matrix during propagation; three equations are sufficient because through symmetry, the upper three triangular elements of each partition's covariance matrix are equivalent to the lower three triangular elements. The following is the derivation used to obtain the six additive noise equations.

The term for which an equivalent set of simple equations is sought is

$$\begin{bmatrix} N_{11} & N_{12} & N_{13} \\ N_{21} & N_{22} & N_{23} \\ N_{31} & N_{32} & N_{33} \end{bmatrix} = \int_{t_{i-1}}^{t_i} \Phi(t_i,\tau) G_F Q_F G_F^T \Phi^T(t_i,\tau) d\tau \qquad (98)$$

The state transition matrix, $\Phi(t_i,\tau)$, for a time period t_{i-1} to t_i, Δt, can be found through straightforward manipulation of the filter F_F matrix using Laplace transformation methods since F_F is the time invariant (Ref 9:161).

$$\Phi(t_i,t_{i-1}) = \Phi(\Delta t) = \begin{bmatrix} 1 & \frac{1}{\omega}\sin(\omega\Delta t) & -R[1-\cos(\omega\Delta t)] \\ 0 & \cos(\omega\Delta t) & -R\omega\sin(\omega\Delta t) \\ 0 & \frac{1}{R\omega}\sin(\omega\Delta t) & \cos(\omega\Delta t) \end{bmatrix} \qquad (99)$$

where the substitution $\omega = \sqrt{\frac{G}{R}}$ has been made.

Substituting this equation together with the filter G_F and Q_F matrices into Equation (98) and performing the integration, the following results are obtained:

$$N_{11} = \frac{Q_{22}}{\omega^2}\left[\frac{-1}{2\omega}\cos(\omega\Delta t)\sin(\omega\Delta t)+\frac{\Delta t}{2}\right] + Q_{33}R^2\left[\frac{3\Delta t}{2} - \frac{2}{\omega}\sin(\omega\Delta t) + \frac{1}{2\omega}\sin(\omega\Delta t)\cos(\omega\Delta t)\right] \qquad (100)$$

$$N_{22} = Q_{22}\left[\frac{1}{2\omega}\sin(\omega\Delta t)\cos(\omega\Delta t)+\frac{\Delta t}{2}\right] + Q_{33}R^2\omega^2\left[\frac{-1}{2\omega}\cos(\omega\Delta t)\sin(\omega\Delta t)+\frac{\Delta t}{2}\right] \qquad (101)$$

$$N_{33} = \frac{Q_{22}}{R^2\omega^2}\left[\frac{-1}{2\omega}\cos(\omega\Delta t)\sin(\omega\Delta t)+\frac{\Delta t}{2}\right] + Q_{33}\left[\frac{1}{2\omega}\sin(\omega\Delta t)\cos(\omega\Delta t)+\frac{\Delta t}{2}\right] \quad (102)$$

$$N_{21} = \frac{Q_{22}}{2\omega^2}\sin^2(\omega\Delta t) - Q_{33}R^2\left[\frac{1}{2}\sin^2(\omega\Delta t)+\cos(\omega\Delta t)-1\right] \quad (103)$$

$$N_{31} = \frac{Q_{22}}{R\omega^2}\left[\frac{-1}{2\omega}\cos(\omega\Delta t)\sin(\omega\Delta t) + \frac{\Delta t}{2}\right] + Q_{33}R\left[\frac{1}{2\omega}\sin(\omega\Delta t)\cos(\omega\Delta t)+\frac{\Delta t}{2} - \frac{1}{\omega}\sin(\omega\Delta t)\right] \quad (104)$$

$$N_{32} = \frac{Q_{22}}{2R\omega^2}\sin^2(\omega\Delta t) - \frac{Q_{33}R}{2}\sin^2(\omega\Delta t) \quad (105)$$

$$N_{12} = N_{21} \quad (106)$$

$$N_{13} = N_{31} \quad (107)$$

$$N_{23} = N_{32} \quad (108)$$

These equations can be further simplified by introducing the power series expansions of the trigonometric terms. The relationships used are (Ref 10:456):

$$\sin(\omega\Delta t)\cos(\omega\Delta t) = \frac{1}{2}\sin(2\omega\Delta t) = \frac{1}{2}\left[2\omega\Delta t - \frac{(2\omega\Delta t)^3}{3!} + \frac{(2\omega\Delta t)^5}{5!} + \text{---}\right] \quad (109)$$

$$\sin(\omega\Delta t) = \omega\Delta t - \frac{(\omega\Delta t)^3}{3!} + \frac{(\omega\Delta t)^5}{5!} + \text{----} \quad (110)$$

$$\cos(\omega\Delta t) = 1 - \frac{(\omega\Delta t)^2}{2} + \frac{(\omega\Delta t)^4}{4} + \text{-----} \tag{111}$$

When these substitutions are made into Equations (100) thru (105) the results, disregarding higher order terms, are:

$$N_{11} \simeq \frac{Q_{22}\Delta t^3}{3} + \frac{Q_{33}R^2\omega^4\Delta t^5}{20} \tag{112}$$

$$N_{22} \simeq Q_{22}\Delta t + \frac{Q_{33}R^2\omega^4\Delta t^3}{3} \tag{113}$$

$$N_{33} \simeq \frac{Q_{22}\Delta t^3}{3R^2} + Q_{33}\Delta t \tag{114}$$

$$N_{21} \simeq \frac{Q_{22}\Delta t^2}{2} + \frac{Q_{33}R^2\omega^4\Delta t^4}{8} \tag{115}$$

$$N_{31} \simeq \frac{Q_{22}\Delta t^3}{3R} - \frac{Q_{33}R\omega^2\Delta t^3}{6} \tag{116}$$

$$N_{32} \simeq \frac{Q_{22}\Delta t^2}{2R} - \frac{Q_{33}R\omega^2\Delta t^2}{2} \tag{117}$$

Because the covariance can be propagated and updated without the need for an external measurement, Ref Chapter III, a shorter time span than that between measurements is used to keep the covariance estimate current. A time period of four seconds was used in the computer simulation until just prior to pitchover, and this time period will be used to show the accuracy of the six equation approximation to the additive noise integral solution. Table IV depicts the

exact solution, power series approximation, and Lockheed approximation to Equation (105) over a period of four seconds.

Table IV indicates that the power series approximation is very accurate, which leads to the conclusion that implementing a filter that uses this approximation instead of the exact Kalman filter equations will suffer little loss of accuracy. The Lockheed approximations differ greatly from the elements of the exact solution; however, this difference may be an attempt to negate the effects of ignoring the off-diagonal noise elements. Chapter VII will compare the performance of these filters.

Table IV

Comparison of Filter Additive Noise Elements Over a Four Second Time Span

Element	Exact Solution	Power Series Approx.	Lockheed Approx.
N_{11}	$21.33Q_{22}+53005.32Q_{33}$	$21.33Q_{22}+52995.57Q_{33}$	$64.0Q_{22}+117966.4Q_{33}$
N_{22}	$3.99997Q_{22}+2.2081E+4Q_{33}$	$4.0Q_{22}+2.2081E+4Q_{33}$	$16.0Q_{22}+66357.8Q_{33}$
N_{33}	$4.9E-14Q_{22}+3.99997Q_{33}$	$4.9E-14Q_{22}+4.0Q_{33}$	$0.0Q_{22}+16.0Q_{33}$
N_{21}	$7.99993Q_{22}+33123.7Q_{33}$	$8.0Q_{22}+33122.2Q_{33}$	
N_{31}	$1.019E-6Q_{22}-343.1704Q_{33}$	$1.019E-6Q_{22}-343.1733Q_{33}$	
N_{32}	$3.82E-7Q_{22}-257.38Q_{33}$	$3.82E-7Q_{22}-257.38Q_{33}$	

VI. Trajectory

This work analyzes the navigation errors committed by a Kalman filter as the weapon system "flies" a typical trajectory. The trajectory was provided by AFATL in the form of strip charts. These strip charts represent a six-degree-of-freedom glide-to-impact time history of the variables of interest as simulated on an analog computer. The glide-to-impact simulation is indicative of the maximum range the unpowered vehicle possesses. Although six degrees-of-freedom were simulated, the fact that it was a no-wind flight, with the vehicle maneuvering only in pitch, limited the geometry to two dimensions, i.e., the vertical plane. The strip charts are classified Secret; however, Figures 9 thru 12 characterize some of the dynamics of the vehicle. The figures are not to scale and do not accurately reflect relative time periods, distances, altitudes, or velocities.

After release at altitude, the system goes into an extended glide. Through this glide period, a pronounced phugoid motion is present which affects position, velocity, normal acceleration, glide-path angle, and pitch rate. The angle of attack is kept relatively constant by an autopilot and thus does not reflect the phugoid.

AD-A034 278 AIR FORCE INST OF TECH WRIGHT-PATTERSON AFB OHIO SCH--ETC F/G 17/7
COVARIANCE ANALYSIS OF KALMAN FILTERS PROPOSED FOR A RADIOMETRI--ETC(U)
DEC 76 C K FITSCHEN

UNCLASSIFIED GE/EE/76D-23 NL

2 OF 2
AD
A034 278

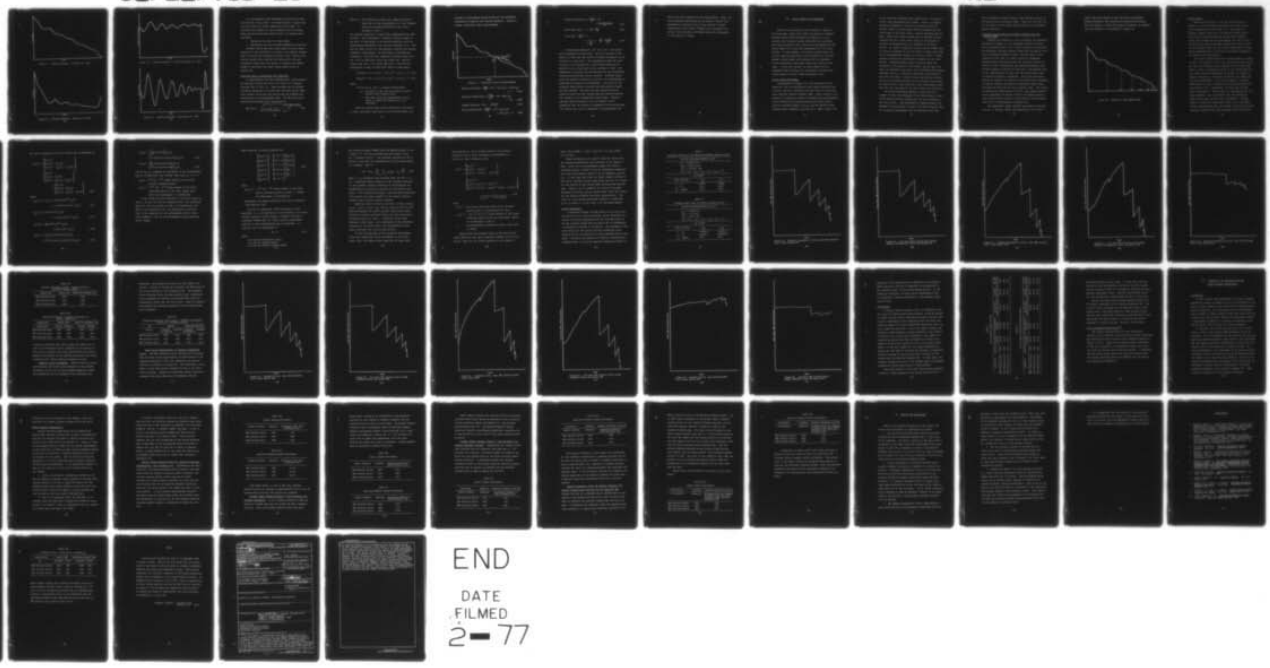

END

DATE
FILMED
2-77

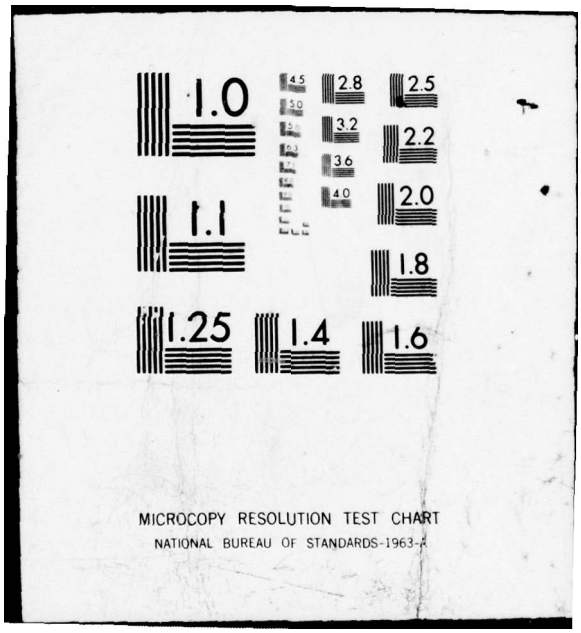
1.0
1.1
1.25
1.4
1.6
1.8
2.0
2.2
2.5
2.8
3.2
3.6
4.0
4.5
5.0
MICROCOPY RESOLUTION TEST CHART
NATIONAL BUREAU OF STANDARDS-1963-A

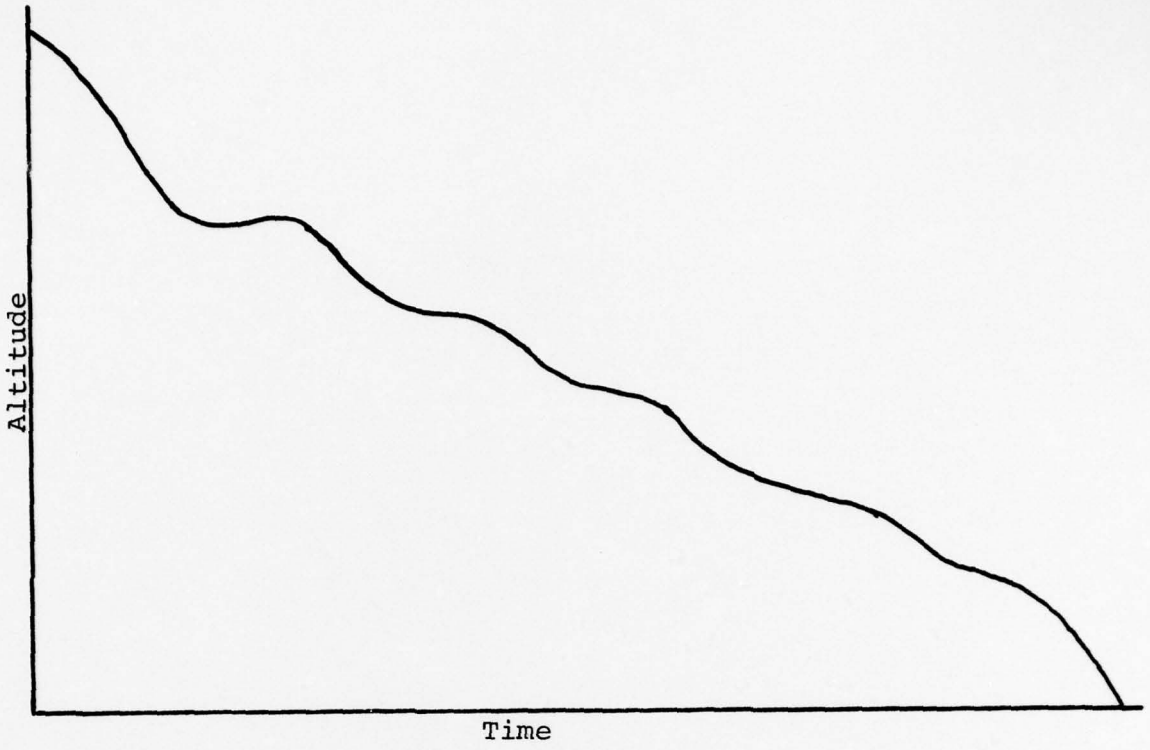

Figure 9. Vehicle Dynamics: Altitude vs. Time

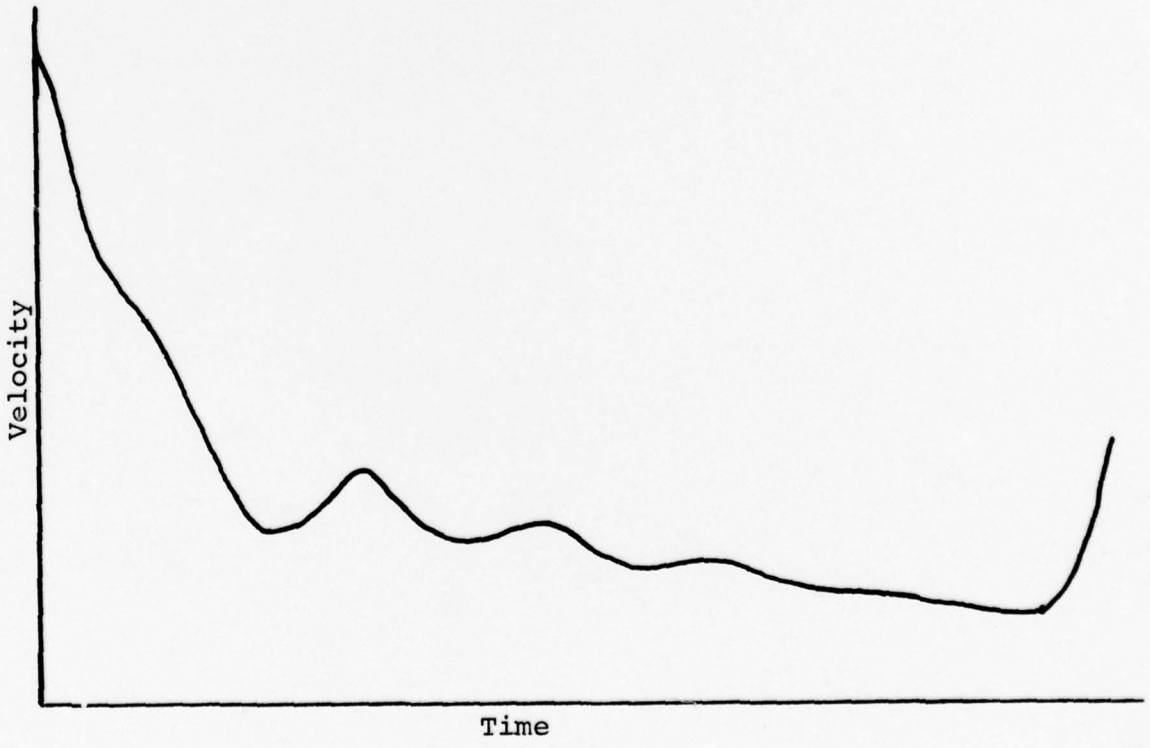

Figure 10. Vehicle Dynamics: Velocity vs. Time

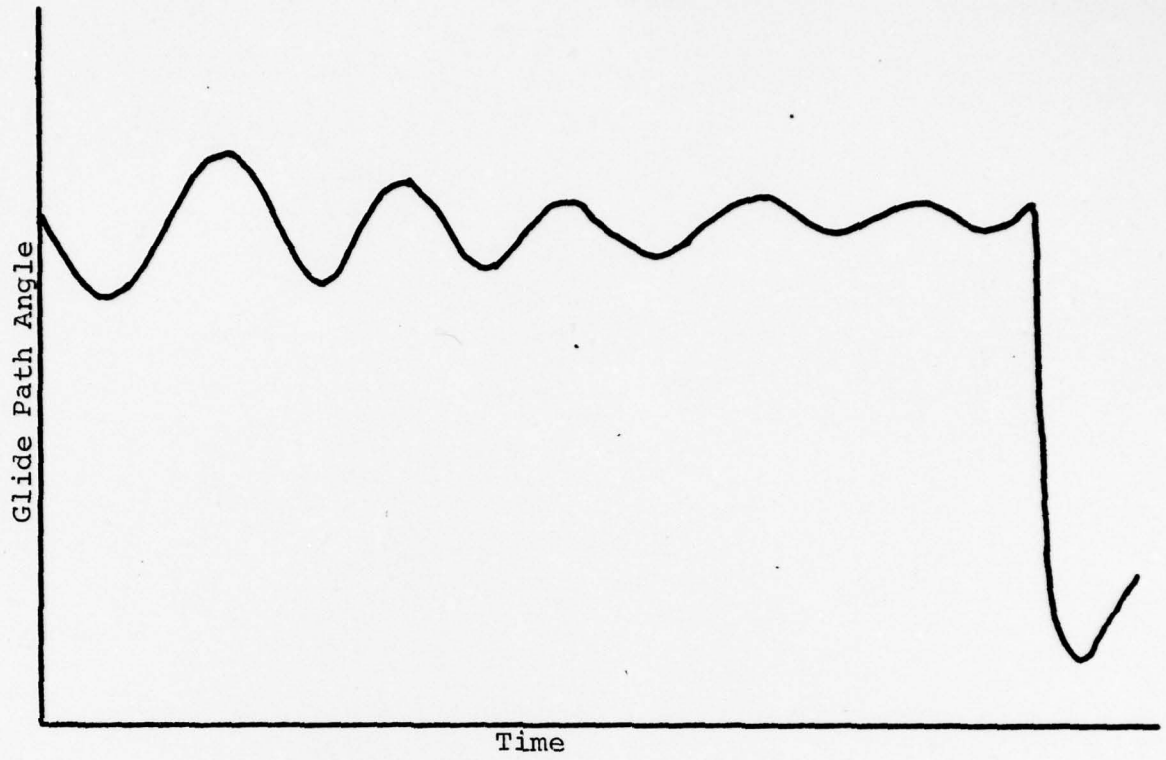

Figure 11. Vehicle Dynamics: Glide-Path Angle vs. Time

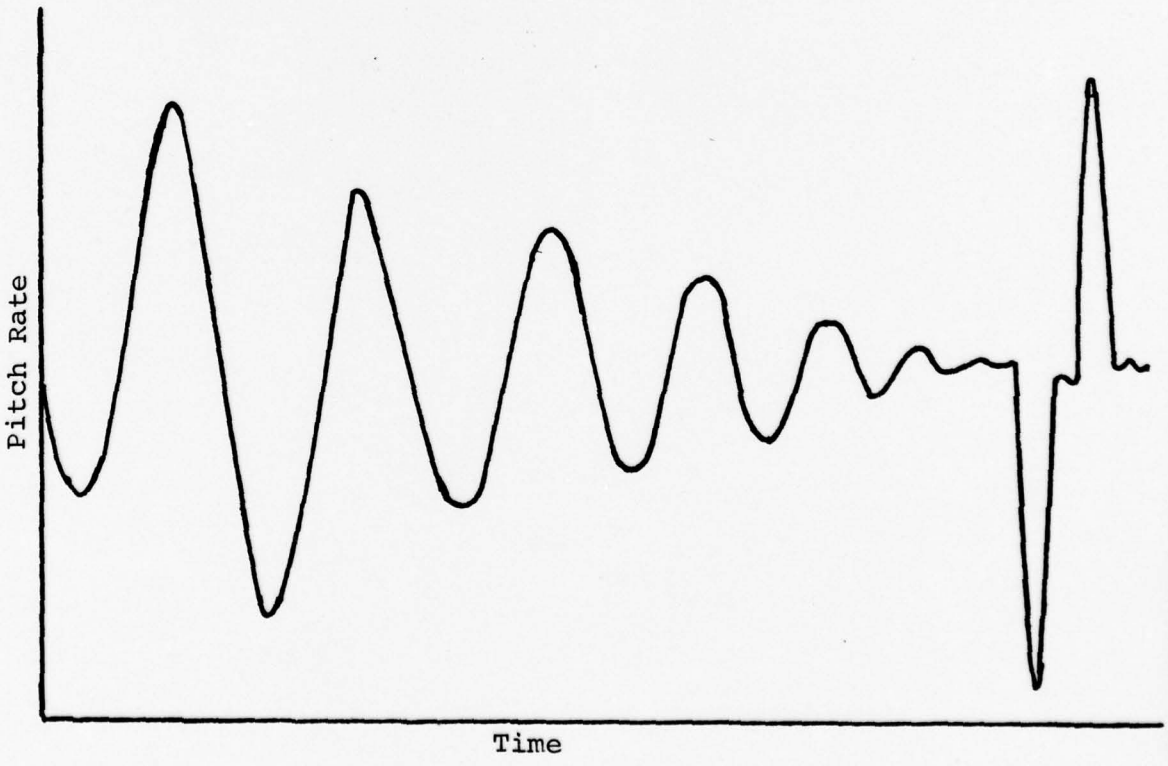

Figure 12. Vehicle Dynamics: Pitch Rate vs. Time

At a geographical point dependent on vehicle altitude and distance to the target, the system begins a rapid pitch-over that ends just before impact with the ground. To introduce the dynamics of this trajectory into the system model and the sub-optimal Kalman filter, two options were available:

1. Tabularize the data for table lookup
2. Approximate the data through mathematical functions

Although tabularized data would enable an exact representation of the trajectory to be made, the computer program used to perform the covariance analysis, GCAP, uses an integration routine that requires four data points for each integration step; thus, the amount of computer core memory needed to facilitate the table lookup scheme would be prohibitive.

Functions Used to Approximate the Trajectory

In approximating the data mathematically, good accuracy was obtained through the use of two "curve fit" computer routines (Ref 11; Ref 12). These routines use an orthogonalization technique to minimize the root mean square (RMS) error between the actual data points and the computer generated points at corresponding times. The RMS error minimized may be mathematically represented as

$$\text{RMS Error} = \sqrt{\frac{1}{\#\text{ of data points}} \sum_{i=1}^{\#\text{ of data points}} R_i^2} \qquad (118)$$

where R_i = the difference between user supplied ordinate magnitude at time corresponding to i and computer generated ordinate magnitude at time corresponding to time i

The computer generates 27 third-order polynominals for each variable. Each polynominal, covering a certain length of the axis, is continuous to the second derivative with the polynominals representing the time axis adjacent to it. Two sets of these "curve fit" polynominals, coupled with certain kinematic relationships, are sufficient to describe the trajectory. The first set, depicting altitude versus time, has a 24.2 ft RMS error, while the second set, velocity versus time, has a 1.65 ft/sec RMS error. The form one polynominal of each of these sets takes is shown below.

$$\text{Altitude} = H = A(t-t_0)^3 + B(t-t_0)^2 + C(t-t_0) + D \quad (119)$$

$$\text{Velocity} = VT = E(t-t_0)^3 + F(t-t_0)^2 + G(t-t_0) + P \quad (120)$$

where

A,B,C,D,E,F,G, and P = constant coefficients

t_0 = the point on the time axis where the polynominal first becomes valid

t = the time, within the polynominal's valid range, at which the function is to be evaluated

With the altitude and velocity specified as functions of time, and motion restricted to the vertical plane, the

kinematic relationships below provide all the necessary information to specify the vehicles dynamics. Figure 13 further illustrates these relationships.

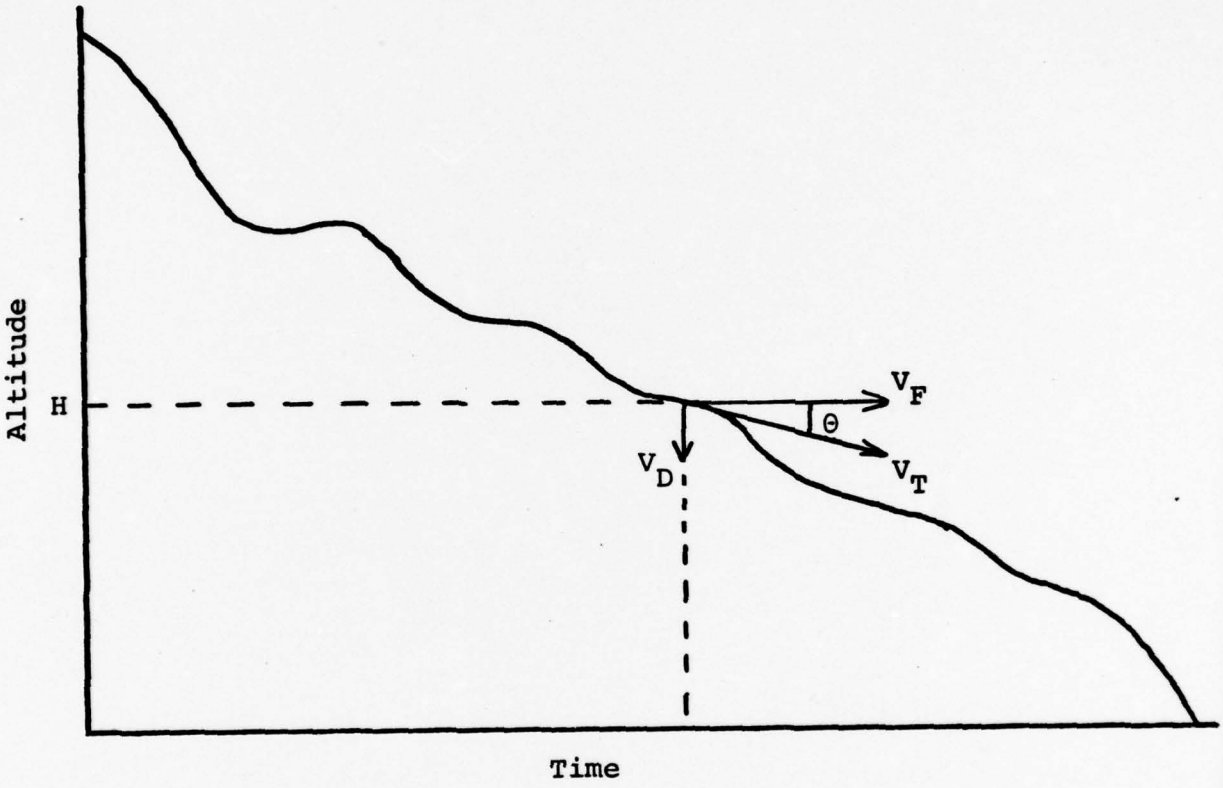

Figure 13. Trajectory Vector Relationships

$$\text{Vertical Velocity} = \frac{d(H)}{dt} = \dot{VD} = 3A(t-t_0)^2 + 2B(t-t_0) + C \quad (121)$$

$$\text{Vertical Acceleration} = \frac{d^2(H)}{dt^2} = VD = 6A(t-t_0) + 2B \quad (122)$$

$$\text{Forward Velocity} = VF = VT^2-VD^2 \quad (123)$$

$$\text{Total Acceleration} = \frac{d(VT)}{dt} = \dot{VT} = 3E(t-t_0)^2 + 2F(t-t_0) + G \quad (124)$$

$$\text{Forward Acceleration} = \frac{d(VF)}{dt} = \dot{VF}$$

$$= \frac{VT(\dot{VT}) - VD(\dot{VD})}{VF} \qquad (125)$$

$$\text{Glide Path Angle} = \theta = TAN^{-1}\frac{VD}{VF} \qquad (126)$$

$$\text{Pitch Rate} = \frac{d(\theta)}{dt} = \dot{\theta}$$

$$= \frac{1}{1+\left(\frac{VD}{VF}\right)^2} \times \frac{\dot{VD}}{VF} - \frac{VD(\dot{VF})}{VF^2} \qquad (127)$$

In developing Equations (121) thru (127), one simplifying assumption has been made: that the attitude of the vehicle is such that the vehicle is always tangential to the altitude vs. time curve. This assumption allows the total velocity to be expressed as a vector whose direction is parallel to the flight path at any instance of time. The components of velocity and acceleration are then determined through straightforward vector calculus. Although simplifying the vehicle's equations of motion, one disadvantage is encountered by making this assumption: the effect of the autopilot maintaining a constant positive angle-of-attack has been ignored. The fact that the constant positive angle-of-attack has been ignored does not greatly diminish the validity of the mathematical model above. Because a constant angle-of-attack of zero is implied in the assumption that the vehicle is tangential to the glide-path, the vehicle will still be subjected to approximately the

same pitch rates indicated on the strip-charts. Thus, the actual dynamics experienced by the vehicle "flying" the mathematical trajectory will be very similar to those experienced by the vehicle "flying" the strip-chart trajectory, with the major difference being the orientation of the vehicle in flight.

VII. Filter Tuning and Performance

Because the sub-optimal filter designs of Chapter V have many fewer states than either the Sperry or Hamilton-Standard system models presented in Chapter IV, it is unlikely that the same initial conditions and corruptive white noise strengths that reflect true performance in the system models will yield best performance for the filter designs. In this chapter, the process through which the initial conditions and white noise strengths for the sub-optimal filter models were obtained will be described. Filter performance using these values will then be evaluated. In the last section, an error budget will be presented which indicates the contribution various error sources make to overall system navigation error.

Filter Tuning Philosophy

As presented in Chapter III, the covariance of the states for the two sub-optimal filter model partitions and the error vector's covariance form the output of the covariance analysis computer program, GCAP. Filter tuning is the process of aligning as closely as possible the corresponding error statistics by properly setting the filter model's initial covariance matrix, $P_F(t_0)$, and the additive white Gaussian noise strengths, Q_F's and R_F's. When "tuned," the

filter correctly estimates true system error. In tuning a filter, many approaches can be taken. Since it is mathematically impossible to match the variance of the sub-optimal filter's states exactly with the appropriate variance terms of the error vector, certain decisions must be made. Should the tuning process seek to optimize the performance for one or more "key" states at the expense of accuracy in estimating the true variance of the other states. Or, should a medium be struck, and an attempt made to align the variance of all the filter's states with those of the corresponding elements of the error vector, thereby possibly reducing the performance capability on the "key" states. Professor Maybeck chose to closely match the variances of the position error-states, δX_E and δX_N, with their corresponding true error vector variances and achieved excellent results. Although he attained a close match in the first two states of each filter, position and velocity errors, the variance estimates of the attitude error state, the third state of each partition, were significantly lower than the true variances of the error vector for this state.

The tuning philosophy adopted in this work is to attempt to align the variances of all three states in each filter model partition closely with the true variances of the error-vector. This philosophy is adopted because the movement of the platform to "point" the RAC vertically down for a position measurement will be governed by the INS/

filter generated attitude angles of the vehicle relative to the east-north-up coordinate frame. Thus, for this work all of the states in each filter model partition are considered equally important.

Trajectory Specifications and Update Schedule Used for Filter Tuning

Although the kinematics of the trajectory are completely described in Chapter VI, the geographic starting location and the heading angle of the "flight" remain to be specified. The geographic starting location chosen was the same as that used in Professor Maybeck's study, latitude $39^{\circ}50'$ north, longitude $83^{\circ}40'$ west, to afford a means of comparison between system performance along the relatively benign trajectory of that investigation and system performance along the more dynamic trajectory of this work. The heading angle is 45°, approximately 8° less than the heading angle used in Professor Maybeck's simulation. This angle was chosen because it subjects the vehicle to the same vector components of angular velocity and angular acceleration inputs along the east and north axes of the navigation frame. The effects of varying the heading angle from 45°, thus causing greater vector components of angular velocity and angular acceleration along either the east or north axis of the navigation frame will be investigated in Chapter VIII.

The measurement update schedule was verbally obtained from Mr. P. Richter, AFATL, and consisted of six "fixes."

These fixes were spaced in time such that the distance between successive RAC updates was progressively smaller. The last update is taken after vehicle pitchover is complete. This fix schedule is illustrated in Figure 14.

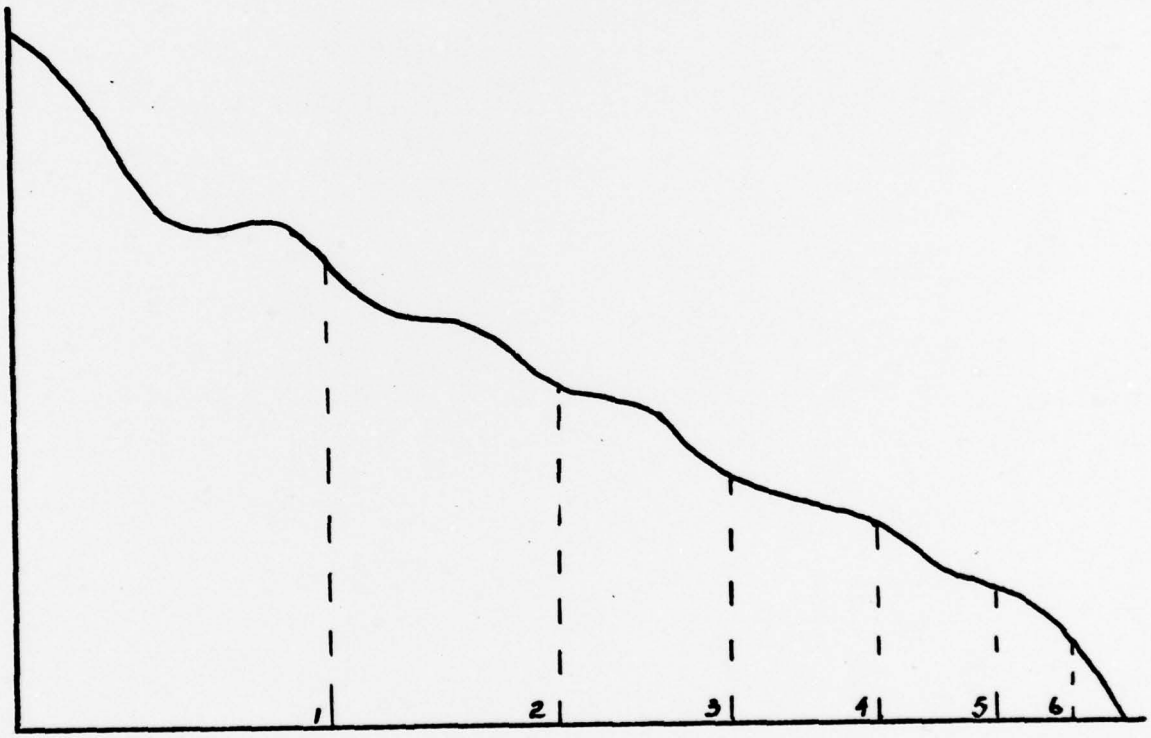

Figure 14. Spacing of RAC Update Fixes

Filter Tuning

Rather than tune each of the two filter designs of Chapter VI, only the design reflecting the correct covariance propagation will be tuned (i.e., the proper non-diagonal integral solution to the additive noise matrix). The initial covariance matrices and the white Gaussian noises that provide the best performance for this filter in the Sperry and Hamilton-Standard systems will then be used in the Lockheed filter and the filter incorporating a power series approximation to the correct covariance propagation to evaluate their performance.

The actual tuning process can be approached in a number of ways. One method is to set the initial covariance matrix and the white Gaussian noise strengths of the filter model equal to their corresponding values in the system model and vary these numerical magnitudes one-by-one in a number of computer simulations, observing the effect each change has on filter performance. With this information, different combinations of noise strengths and initial conditions can be simulated until a combination is found that provides "best performance." This "cut and try" approach can be very time consuming, with no guarantee that the combination chosen really does provide "best" performance. Another method of tuning the sub-optimal filter is to find mathematical relationships that give insight into how the initial covariance elements and noise strengths affect individual

states, and set these elements to increase the filter's accuracy. A combination of these methods was used to tune the filter model of Chapter VI which reflected the true covariance propagation. In setting the initial covariance matrix and white noise strengths equal to their corresponding system model elements, and then varying the magnitudes of these elements slightly in succeeding computer simulations, five filter characteristics were noted:

1. The variances of corresponding error states in the two three-state partitions were essentially the same, i.e.,:

Error variance of $\hat{\delta X}_E$ = error variance of $\hat{\delta X}_N$

Error variance of $\hat{\delta V}_E$ = error variance of $\hat{\delta V}_N$

Error variance of $\hat{\Phi}_N$ = error variance of $\hat{\Phi}_E$

2. The two three-state partitions had a noticeable "transient" lasting through approximately the first two updates, during which they consistently underestimated the variance of errors they were committing.

3. After a measurement update, the variances of the errors in the estimates of positions δX_E and δX_N and their corresponding error-vector variances were very close.

4. The variances of the errors in estimates of attitudes Φ_N and Φ_E were consistently underestimated.

5. The covariance of the error-vector formed a numerical pattern, through the first two updates, that was essentially the same in all computer simulations run, even when

the filters were estimating very poorly.

These characteristics were displayed when the three-state filters were estimating the errors for either the Hamilton-Standard or Sperry system models.

Since the two three-state filter model partitions yielded the same variance estimates when supplied identical initial conditions and noise strengths, mathematical insight was sought from only one set of filter equations, the east position set, and the results applied to the other partition. Using the development of Chapter VI, the initial covariance matrix, a 3x3 diagonal matrix, is propagated to the first update time, t_1, as follows:

$$P_F(t_1^-) = \Phi(t_1,0)P_F(0)\Phi^T(t_1,0) + \int_0^{t_1} \Phi(t_1,\tau)G_F Q_F G_F^T \Phi^T(t_1,\tau)d\tau \qquad (128)$$

After performing the matrix multiplication and integration,

the lower triangular 3x3 $P_F(t_1^-)$ matrix may be expressed as:

$$P_F(t_1^-) = \begin{bmatrix} P_{11}(t_1^-) & & \\ P_{12}(t_1^-) & P_{22}(t_1^-) & \\ P_{13}(t_1^-) & P_{23}(t_1^-) & P_{33}(t_1^-) \end{bmatrix}$$

$$= \begin{bmatrix} E_{11}(t_1) & & \\ E_{12}(t_1) & E_{22}(t_1) & \\ E_{13}(t_1) & E_{23}(t_1) & E_{33}(t_1) \end{bmatrix}$$

$$+ \begin{bmatrix} N_{11}(t_1) & & \\ N_{12}(t_1) & N_{22}(t_1) & \\ N_{13}(t_1) & N_{23}(t_1) & N_{33}(t_1) \end{bmatrix} \qquad (129)$$

where

$$E_{11}(t_1) = P_{11}(0) + \left[\frac{1}{\omega}\sin(\omega\Delta t)\right]^2 P_{22}(0) + \left[-R(1-\cos(\omega\Delta t))\right]^2 P_{33}(0) \qquad (130)$$

$$E_{22}(t_1) = \left[\cos(\omega\Delta t)\right]^2 P_{22}(0) + \left[-R\omega\sin(\omega\Delta t)\right]^2 P_{33}(0) \qquad (131)$$

$$E_{33}(t_1) = \left[\frac{1}{R\omega}\sin(\omega\Delta t)\right]^2 P_{22}(0) + \left[\cos(\omega\Delta t)\right]^2 P_{33}(0) \qquad (132)$$

$$E_{12}(t_1) = \left[\frac{1}{\omega}\sin(\omega\Delta t)\cos(\omega\Delta t)\right] P_{22}(0) + \left[R^2\omega\sin(\omega\Delta t)(1-\cos(\omega\Delta t))\right] P_{33}(0) \qquad (133)$$

$$E_{13}(t_1) = \left[\frac{1}{R\omega^2}\sin^2(\omega\Delta t)\right] P_{22}(0) + \left[-R\cos(\omega\Delta t)(1-\cos(\omega\Delta t))\right] P_{33}(0) \quad (134)$$

$$E_{23}(t_1) = \left[\frac{1}{R\omega}\sin(\omega\Delta t)\cos(\omega\Delta t)\right] P_{22}(0) + \left[-R\omega\cos(\omega\Delta t)\sin(\omega\Delta t)\right] P_{33}(0) \quad (135)$$

and the $N_{ij}(t_1)$ elements are equivalent to the corresponding $N_{ij}(\Delta t)$ of Equations (103) through (108) with $\Delta t = t_1 - 0$.

$P_{ij}(0)$ = i^{th} row - j^{th} column element of the filter initial covariance matrix

$P_{ij}(t_1^-)$ = i^{th} row - j^{th} column element of the filter covariance matrix at the first update time, before the measurement is incorporated.

If the values for the covariance of the error vector at time t_1 (in the "cut and try" approach above, the covariance matrix of the error vector at time t_1 was essentially the same in all simulations run) are substituted on the left side of this equation for the corresponding filter covariance elements, a set of six simultaneous linear equations can be formed.

These equations in matrix notation are:

$$\begin{bmatrix} P_{E11}(t_1^-) \\ P_{E22}(t_1^-) \\ P_{E33}(t_1^-) \\ P_{E12}(t_1^-) \\ P_{E13}(t_1^-) \\ P_{E23}(t_1^-) \end{bmatrix} = \begin{bmatrix} 1 & A & B & C & D \\ 0 & E & F & G & H \\ 0 & I & J & K & L \\ 0 & M & N & P & Q \\ 0 & R & S & T & U \\ 0 & V & W & Y & Z \end{bmatrix} \begin{bmatrix} P_{11}(0) \\ P_{22}(0) \\ P_{33}(0) \\ Q_{22} \\ Q_{33} \end{bmatrix} \tag{136}$$

where

$P_{Eij}(t_1^-)$ = i^{th} row - j^{th} column element of the error vector covariance matrix at time t_1 - before the measurement is incorporated.

Expressions for dummy coefficients A-Z can be obtained from Equation (129).

This set of independent linear equations is over-specified, i.e., six equations in five unknowns, so an exact solution cannot be found; however a computer routine is available, LSQUAR (Ref 13), which yields an approximate solution to such overspecified sets of equations. If Equation (136) is represented as

$$AX + B \tag{137}$$

where

A is the 6x5 coefficient matrix
X is the 5x1 variable matrix
B is the 6x1 desired variance matrix

The software package LSQUAR forms the pseudo-inverse of the A matrix, A^+, and then premultiplies both sides of the AX = B equation with A^+. The resultant solution for the X matrix is such that the Euclidean norm of the system matrix is a minimum. That is

$$||AX - B||_E = \left[\sum_{i=1}^{6} \sum_{k=1}^{5} A_{ik}X_{kl} - B_{il}\right]^2 \frac{1}{2} \quad (138)$$

where $||\cdot||_E$ represents the Euclidean norm, and the i, k, and l subscripts denote elements of the indicated matrices In using LSQUAR, relative weighting of the equations was accomplished by multiplying through with appropriate constants. This procedure precluded a solution which minimized errors about the larger elements of the desired variance elements while ignoring smaller elements.

LSQUAR was used to find the two sets of filter values, $P_{11}(0)$, $P_{22}(0)$, $P_{33}(0)$, Q_{22}, and Q_{33} (one set each for the Hamilton-Standard and Sperry systems) which most closely aligned the filter covariance matrix with the error-vector covariance matrix at time t_1. Excellent results were obtained in both cases. As a percentage of the individual variances of the error-vector, the corresponding filter states variances fell in the range 99-101%.

To find the magnitude of the corruptive measurement noise that yields best filter performance at the first update time, the Kalman filter equations are again used.

From Chapter VI, the covariance matrix of the filter's states at time t_1 after including the measurement is, written in lower triangular form:

$$P(t_1^+) = \begin{bmatrix} P_{11}(t_1^-) & & \\ P_{12}(t_1^-) & P_{22}(t_1^-) & \\ P_{13}(t_1^-) & P_{23}(t_1^-) & P_{33}(t_1^-) \end{bmatrix}$$

$$- \begin{bmatrix} P_{11}(t_1^-)^2 & & \\ P_{12}(t_1^-)\cdot P_{11}(t_1^-) & P_{22}(t_1^-)^2 & \\ P_{13}(t_1^-)\cdot P_{11}(t_1^-) & P_{12}(t_1^-)\cdot P_{13}(t_1) & P_{33}(t_1^-)^2 \end{bmatrix} \cdot$$

$$\frac{1}{P_{11}(t_1^-) + \Theta\cdot(\text{altitude})^2} \qquad (139)$$

where

$P(t_1^+)$ = the filter covariance matrix after the measurement update is incorporated at time t_1

$P_{ij}(t_1^-)$ = the i^{th} row x j^{th} column element of the filter covariance matrix before the measurement update is incorporated at time t_1

Θ = the measurement variable for which a best value is sought.

Substituting the variance values of the error-vector after update for the lower triangular elements of the $P(t_1^+)$ matrix, there are six linear equations in one unknown, Θ.

Again using LSQUAR, a "best" value for Θ at this update can be found.

These techniques can be used to tune the filter over the remaining measurement time intervals if one change is made. After the first measurement update the filter's covariance matrix is known so the six propagation equations until the second update contain only two unknowns, Q_{22} and Q_{33}. It was found that after the second update (the end of the filter transient period noted above) one set of Q values for the filters of each system model provided good performance. Tables V and VI summarize the initial covariance matrices and the Q_{22} and Q_{33} values which "tune" the filters for the Hamilton-Standard and Sperry system models. The value of Θ used during measurement updates is classified as it is within 1% of the "true" Θ of the system models.

Filter Performance

A comparison between the RMS values of the state estimate errors of the tuned sub-optimal filter reflecting the correct covariance propagation and the true RMS errors of the RAC guidance system when the Sperry INS is implemented is presented in Figures 15 through 20. The variances of the error-states for the filter partition estimating north position errors are identical to those presented and are not shown. The plots are unscaled for security classification considerations, so a direct numerical comparison cannot be

Table V

Variables Which Tune the Hamilton-Standard System Filters

Initial Covariance Matrix, $P_F(0)$		
P_{11} = 2.27E+6 ft^2		
P_{22} = 4.051 ft/sec		
P_{33} = 3.2371E-7 rad		
$P_{12} = P_{13} = P_{23} = P_{21} = P_{31} = P_{32} = 0.0$		
Q_F Values		
Time Interval	Q_{22}	Q_{33}
0 - t_1	-.43491	.15884
t_1 - t_2	.1E-4	.22E-7
t_2 - impact	.1E-4	.16E-7

Table VI

Variables Which Tune the Sperry System Filters

Initial Covariance Matrix, $P_F(0)$		
P_{11} = 2.22E+6 ft^2		
P_{22} = 3.9 ft/sec		
P_{33} = 2.5E-7 rad		
$P_{12} = P_{13} = P_{23} = P_{21} = P_{31} = P_{32} = 0.0$		
Q_F Values		
Time Interval	Q_{22}	Q_{33}
0 - t_1	.31489E-1	.12057E-9
t_1 - t_2	.87651E-1	.98724E-10
t_2 - impact	.1E-6	.3E-9

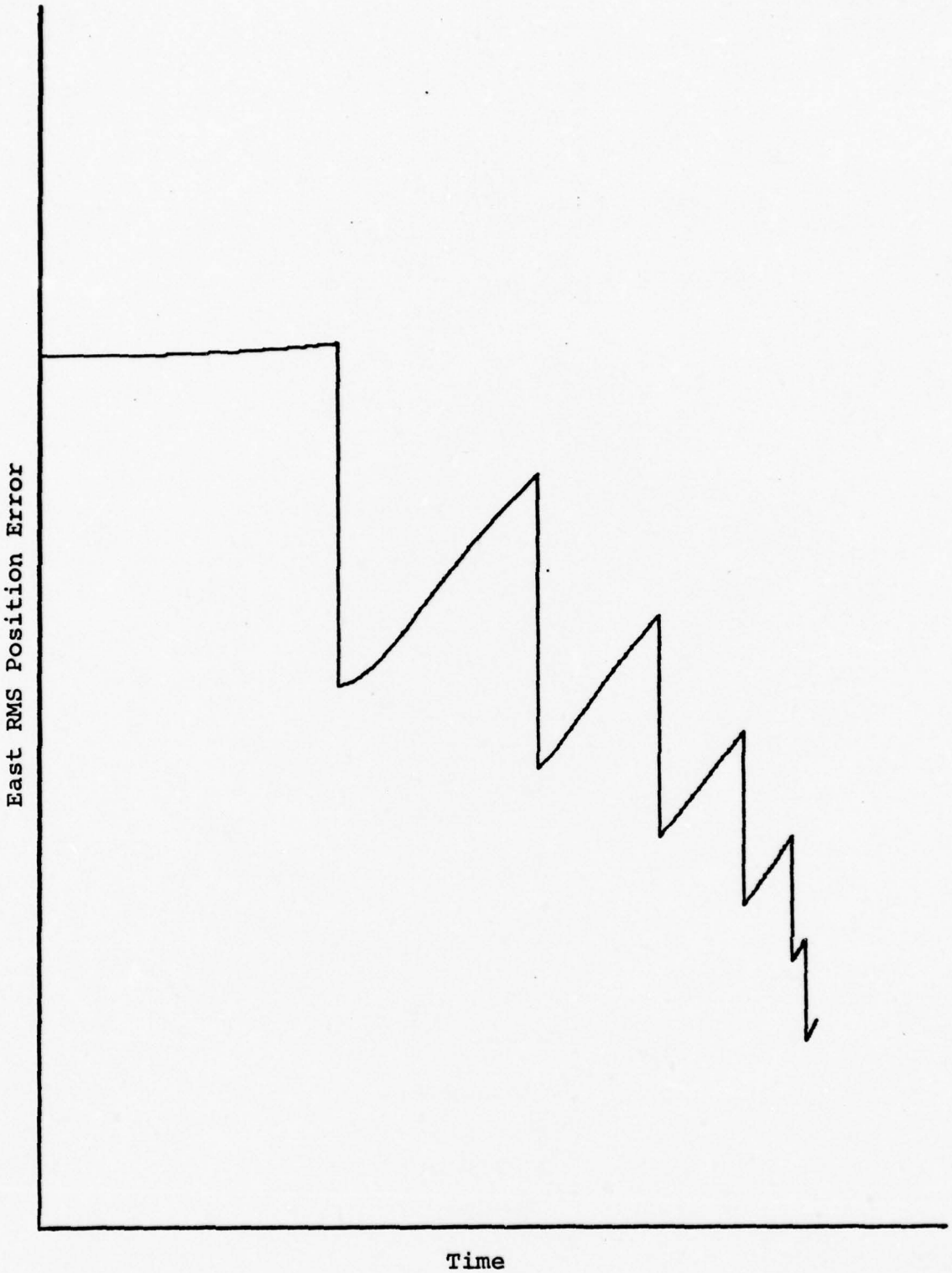

Figure 15. Standard Propagation Filter, East RMS Position Error Using Sperry INS

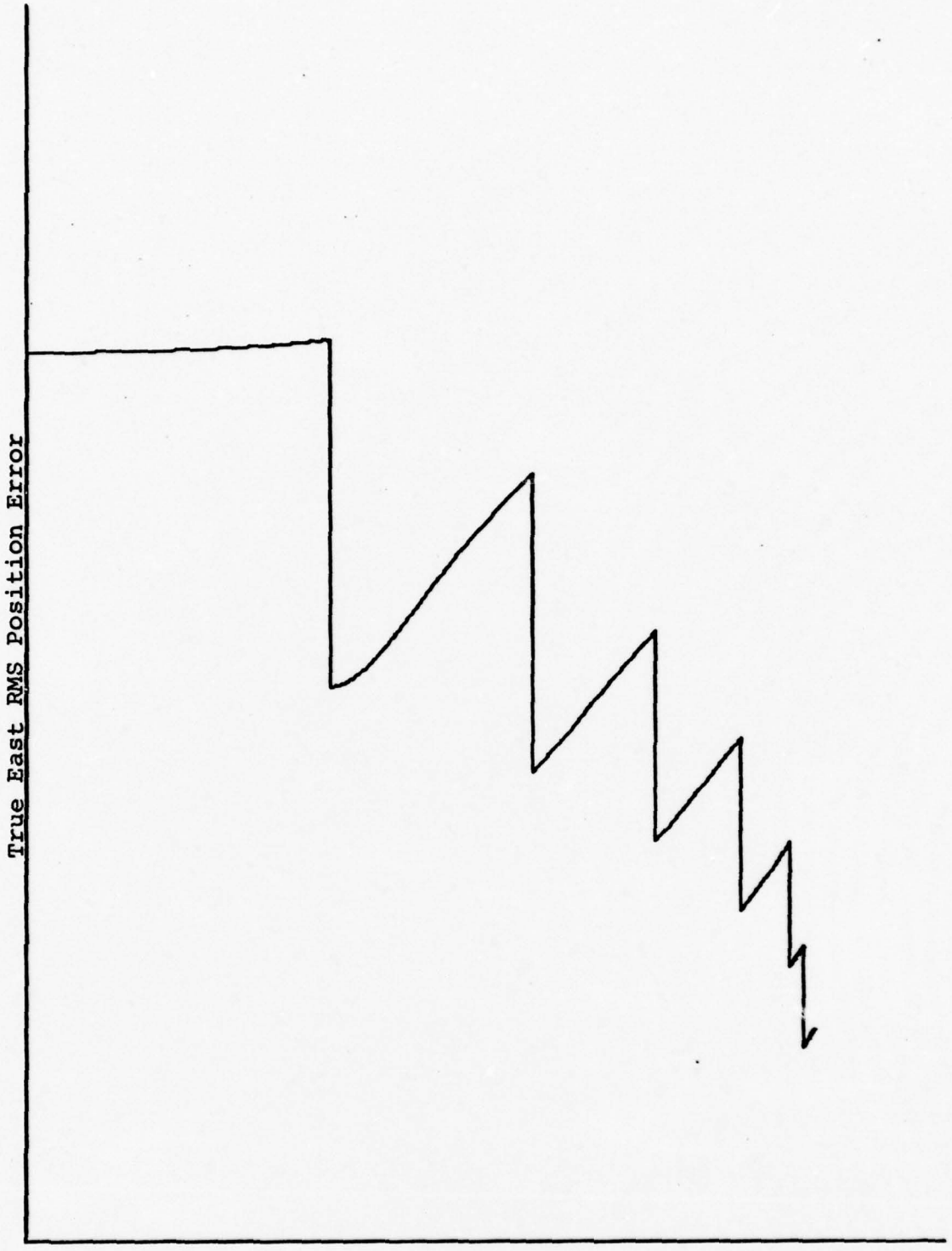

Figure 16. True East RMS Position Error Using Standard Propagation Filter and Sperry INS

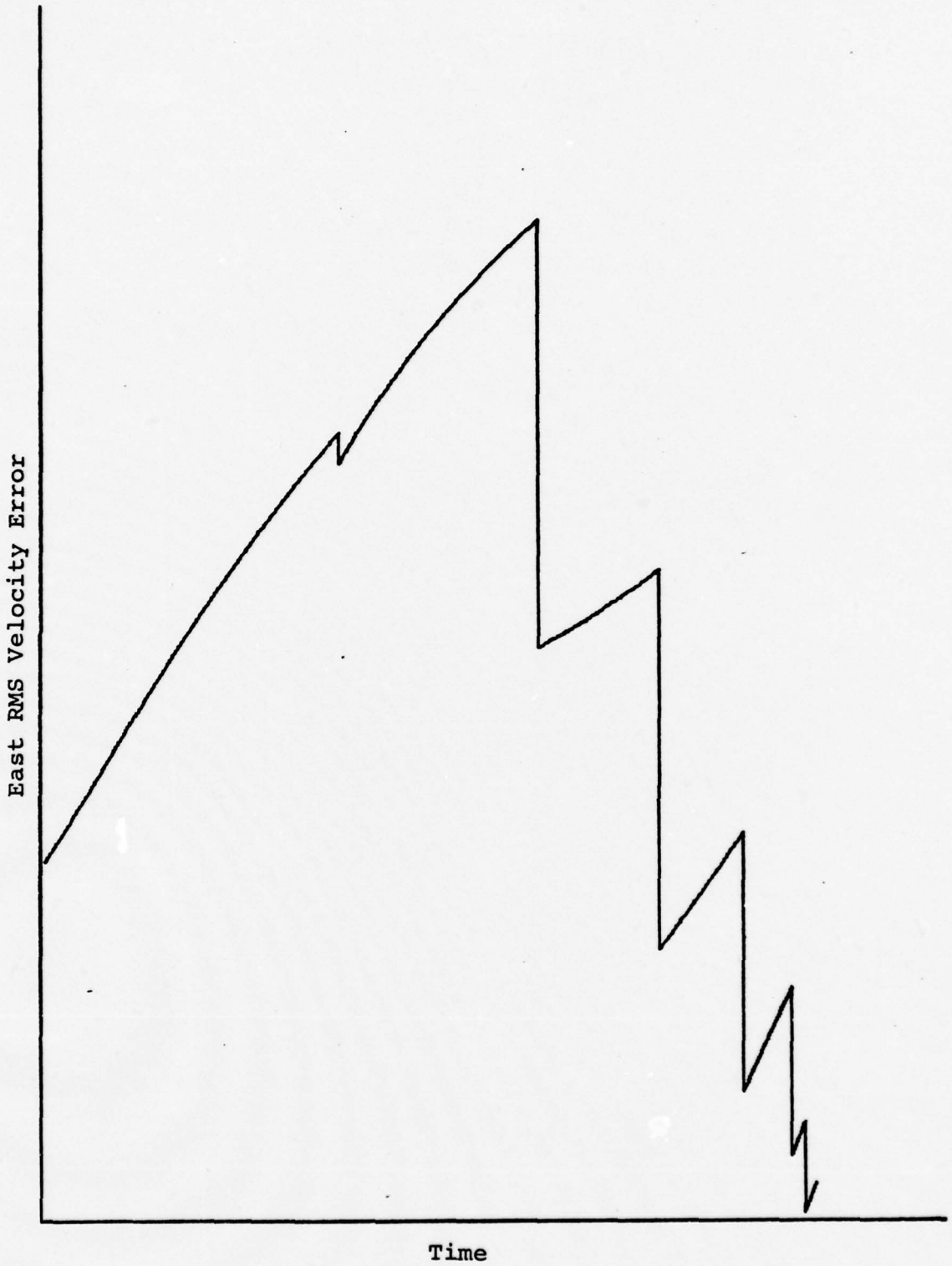

Figure 17. Standard Propagation Filter, East RMS Velocity Error Using Sperry INS

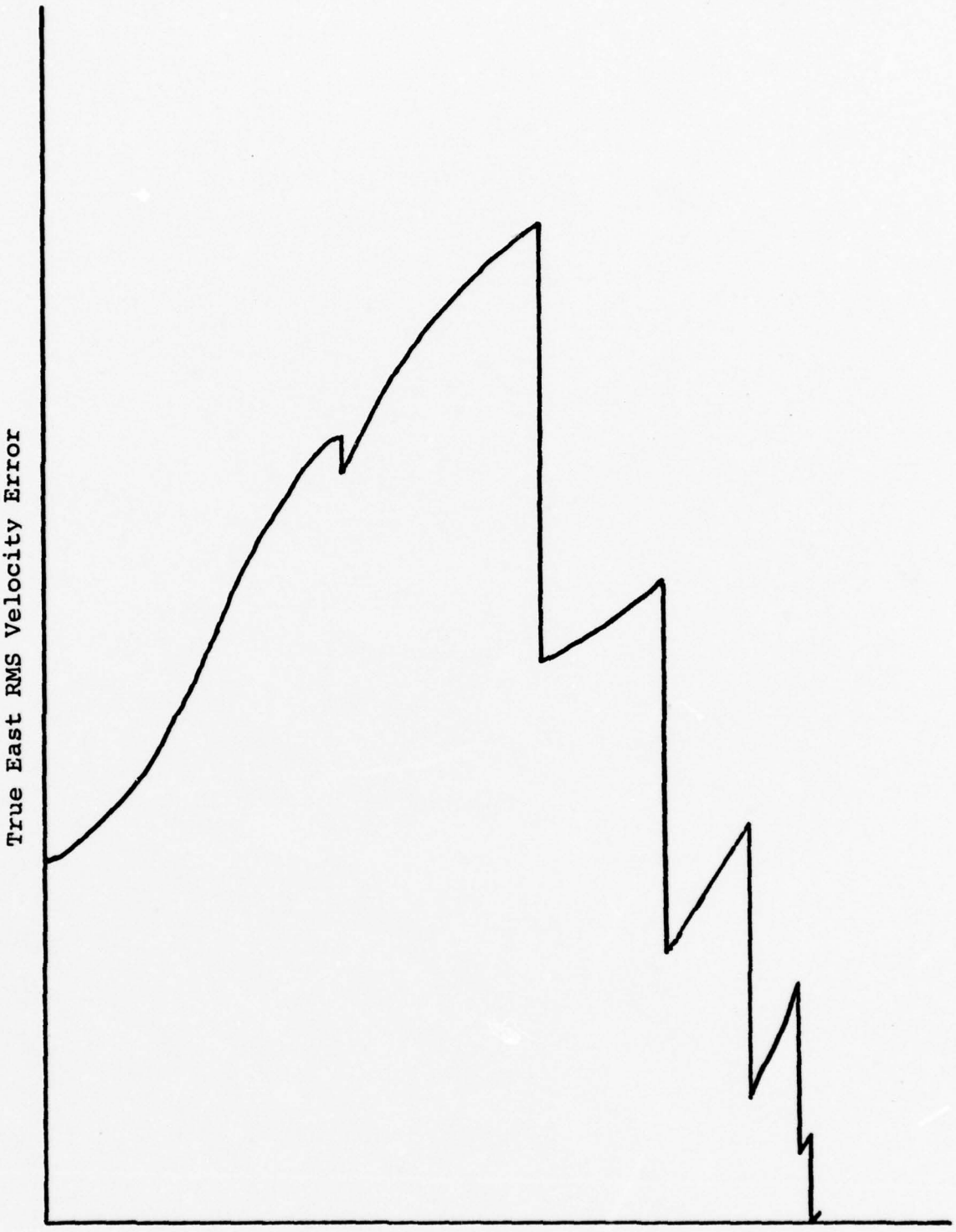

Figure 18. True East RMS Velocity Error Using Standard Propagation Filter and Sperry INS

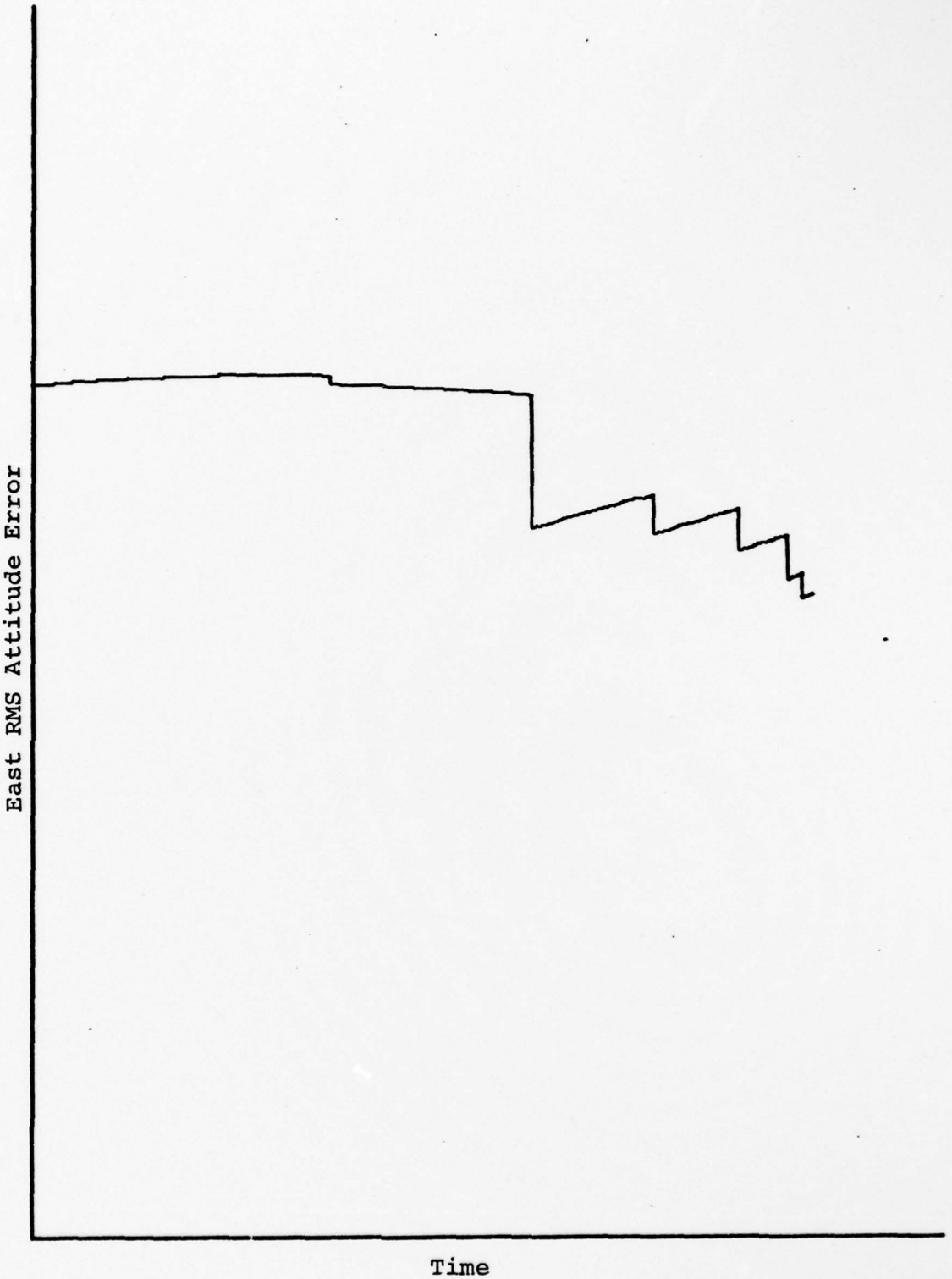

Figure 19. Standard Propagation Filter, East RMS Attitude Error Using Sperry INS

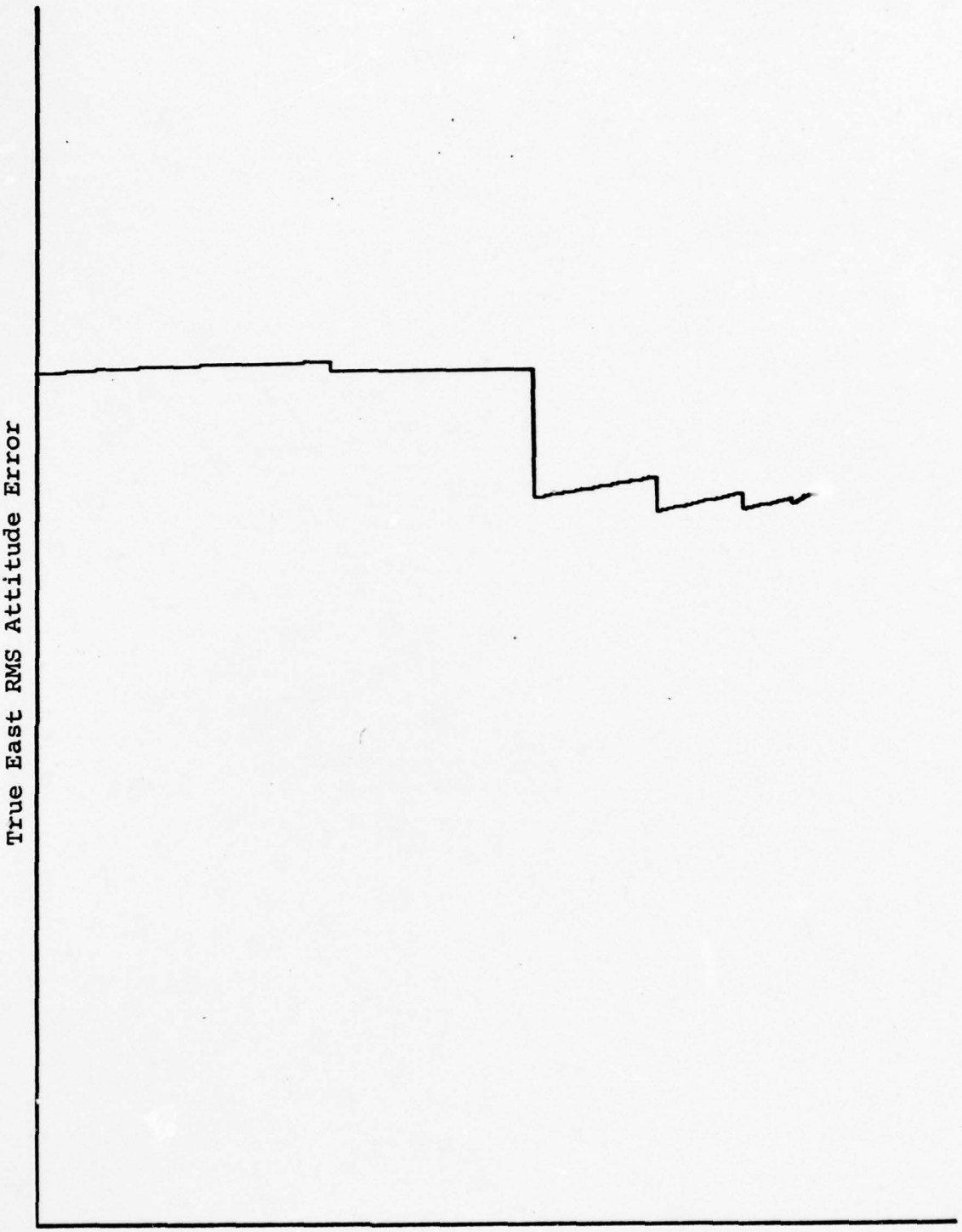

Figure 20. True East RMS Attitude Error Using Standard Propagation Filter and Sperry INS

made. The plots do indicate however that the sub-optimal filter is accurately estimating system RMS navigation errors, and that these errors are significantly lessened after each RAC position update. The filters estimating navigation errors for the Hamilton-Standard system are similarly well-tuned. The plots are not shown however because the benefits of many unscaled figures are doubtful. Comparisons between the two systems will be made through percentages depicted in tabular form.

Filter Performance: Sperry INS Versus Hamilton-Standard INS. The Sperry system significantly out-performed the Hamilton-Standard system on all three information channels. This can be attributed to the higher quality accelerometers and gyroscopes of that INS as indicated in Table III, Chapter IV. A percentage comparison between terminal RMS errors for the two systems is made in Table VII. The Sperry system is used as a baseline, and its errors arbitrarily labeled 100%.

Filter Performance: Benign Trajectory Versus Dynamic Trajectory. The errors committed by the sub-optimal filter in this work when the system is flown along the dynamic trajectory using either INS are significantly greater than similar errors committed along the relatively benign trajectory of Professor Maybeck's studies. Table VIII compares the terminal RMS errors when either INS is implemented into the system for the two trajectories.

Table VII

Terminal Navigation Error: Sperry System vs. Hamilton-Standard System

System with	Sperry INS	Hamilton-Standard INS
RMS Position Error	100%	116%
RMS Velocity Error	100%	185%
RMS Attitude Error	100%	357%

Table VIII

System Performance: Dynamic Trajectory vs. Benign Trajectory

System with	Sperry INS		Hamilton-Standard INS	
Trajectory	Benign	Dynamic	Benign	Dynamic
RMS Position Error	100%	226%	100%	241%
RMS Velocity Error	100%	105%	100%	96%
RMS Attitude Error	100%	94%	100%	95%

A logical conclusion that can be drawn from Table VIII is that if the navigation errors committed by the filters of this work are greater than final specification will allow, damping the dynamics of the vehicles trajectory with better autopilots will reduce terminal navigation errors.

Lockheed Filter Performance. Using the initial covariance matrices and white noise strengths of the standard propagation filter for the RAC guidance system with either INS implemented and the Lockheed filter performing the

estimation, the systems were flown over the dynamic trajectory. Figures 21 through 26 illustrate the RMS values of the errors produced by the Lockheed filter. The Lockheed filter provides fairly accurate position error information, but its estimates of velocity and attitude RMS errors are considerably higher than the true errors. Table IX compares the Lockheed and standard propagation filter terminal RMS error estimates.

Table IX

Terminal Navigation System Error: Standard Propagation Filters vs. Lockheed Filters

INS	Sperry		Hamilton-Standard	
Filter	Standard Propagation	Lockheed	Standard Propagation	Lockheed
RMS Position Error	100%	105%	100%	109%
RMS Velocity Error	100%	129%	100%	134%
RMS Attitude Error	100%	156%	100%	158%

Power Series Approximation of Standard Propagation Filter. The RMS navigation errors committed by the system when the power series approximation is substituted for the standard propagation filter are essentially the same as reflected in Figures 15 through 20. The difference in estimates is less than one-half percent for any of the information channels. Whether the additional memory required to implement the three additional off-diagonal variance

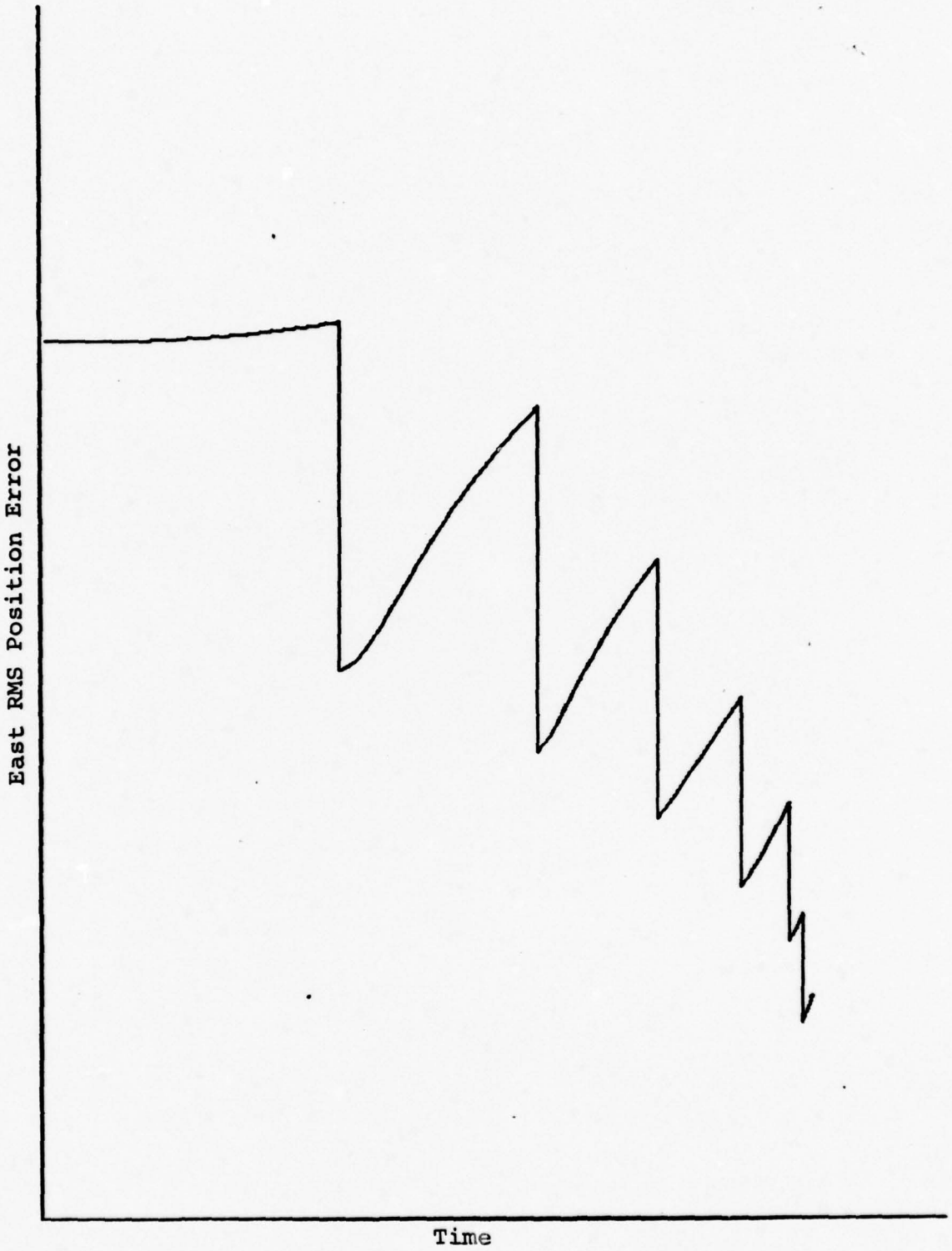

Figure 21. Lockheed Filter, East RMS Position Error Using Sperry INS

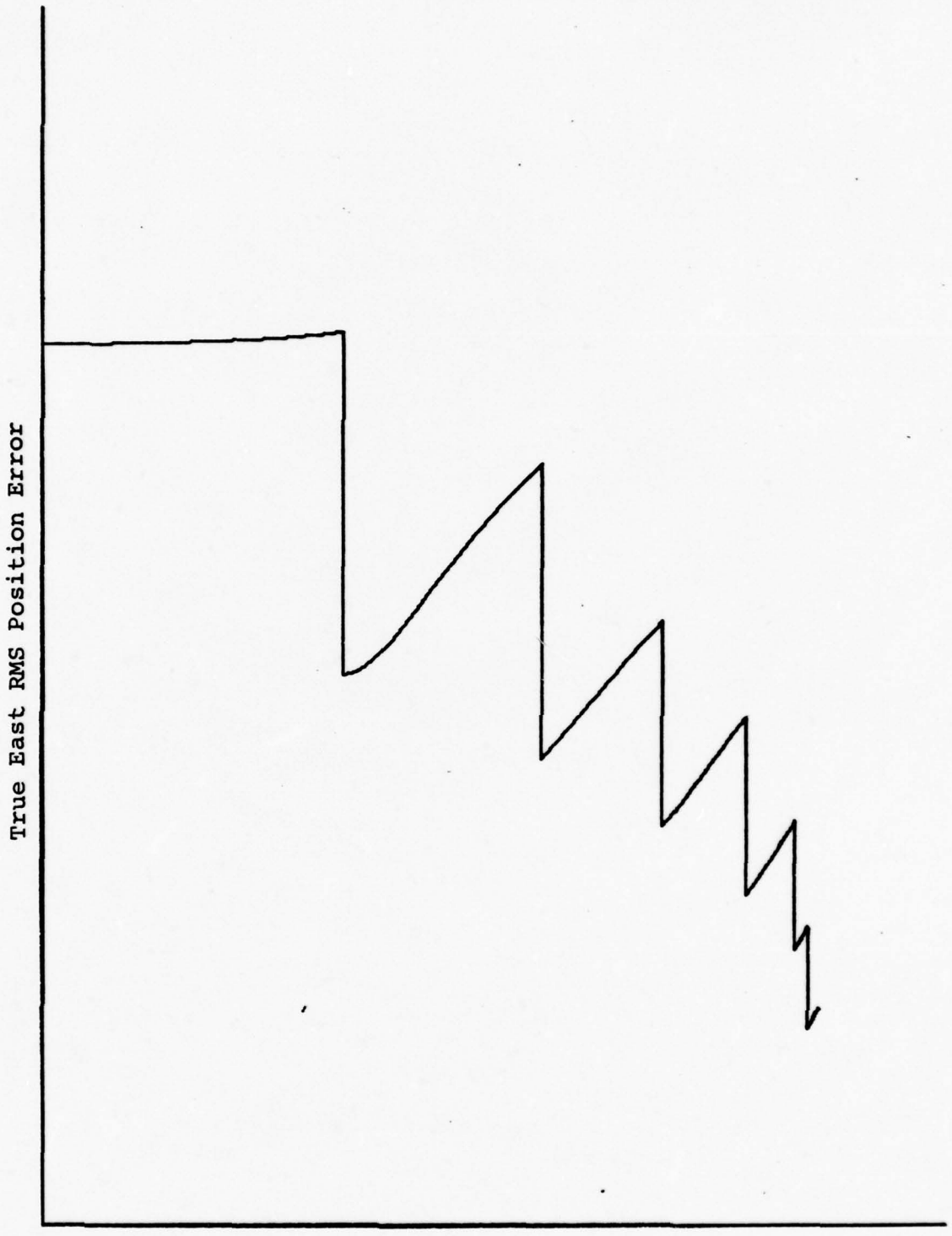

Figure 22. True East RMS Position Error Using Lockheed Filter and Sperry INS

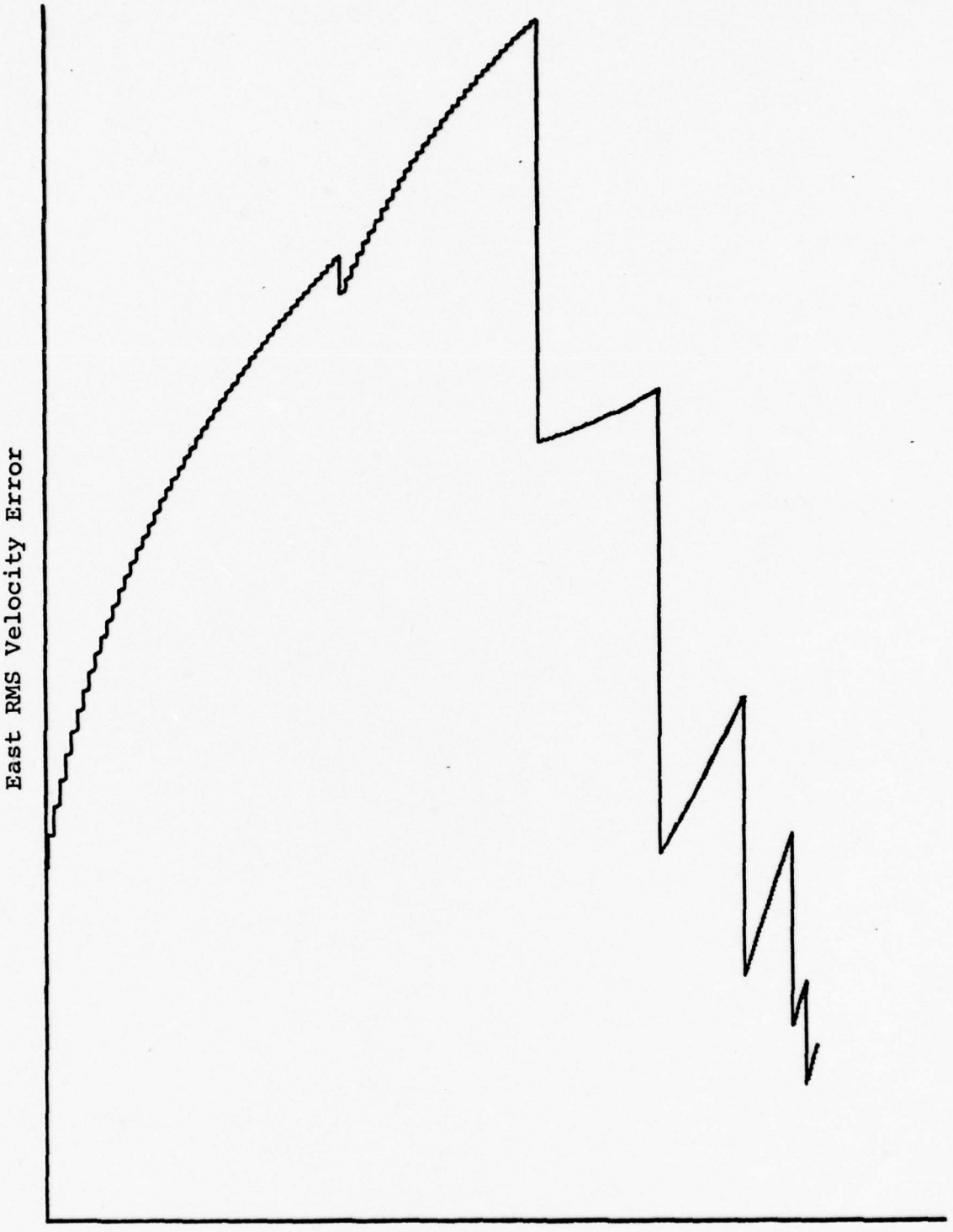

Figure 23. Lockheed Filter, East RMS Velocity Error Using Sperry INS

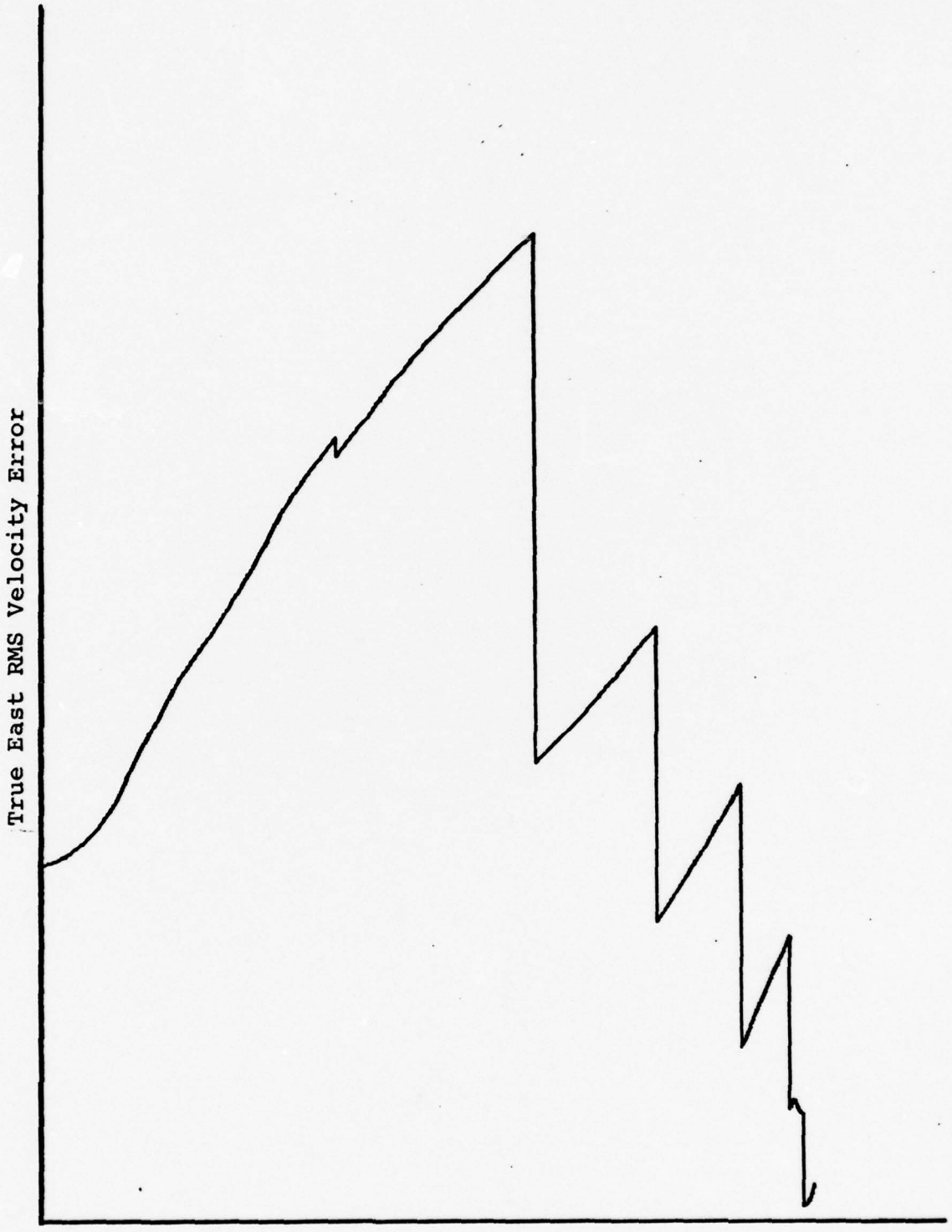

Figure 24. True East RMS Velocity Error Using Lockheed Filter and Sperry INS

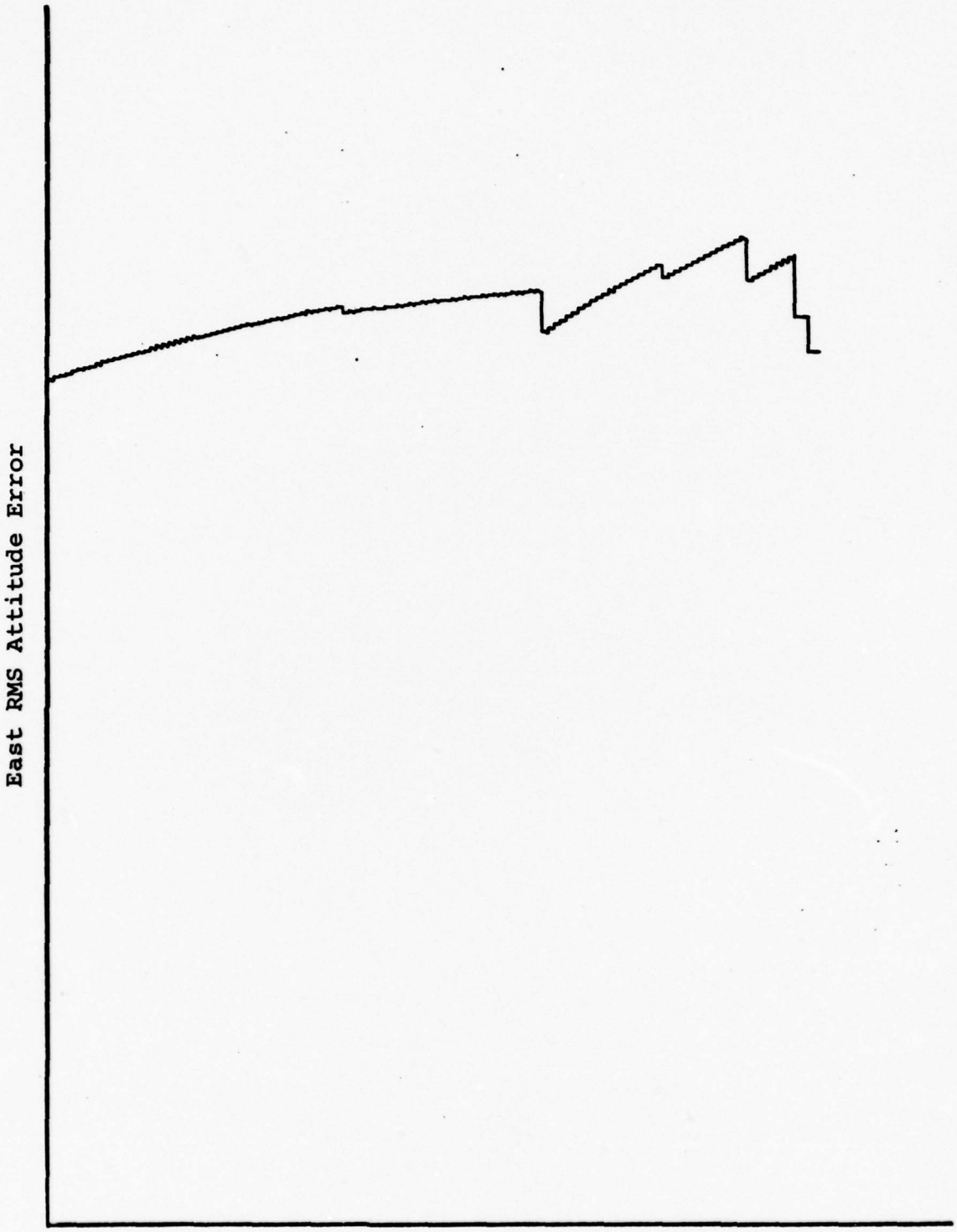

Figure 25. Lockheed Filter, East RMS Attitude Error Using Sperry INS

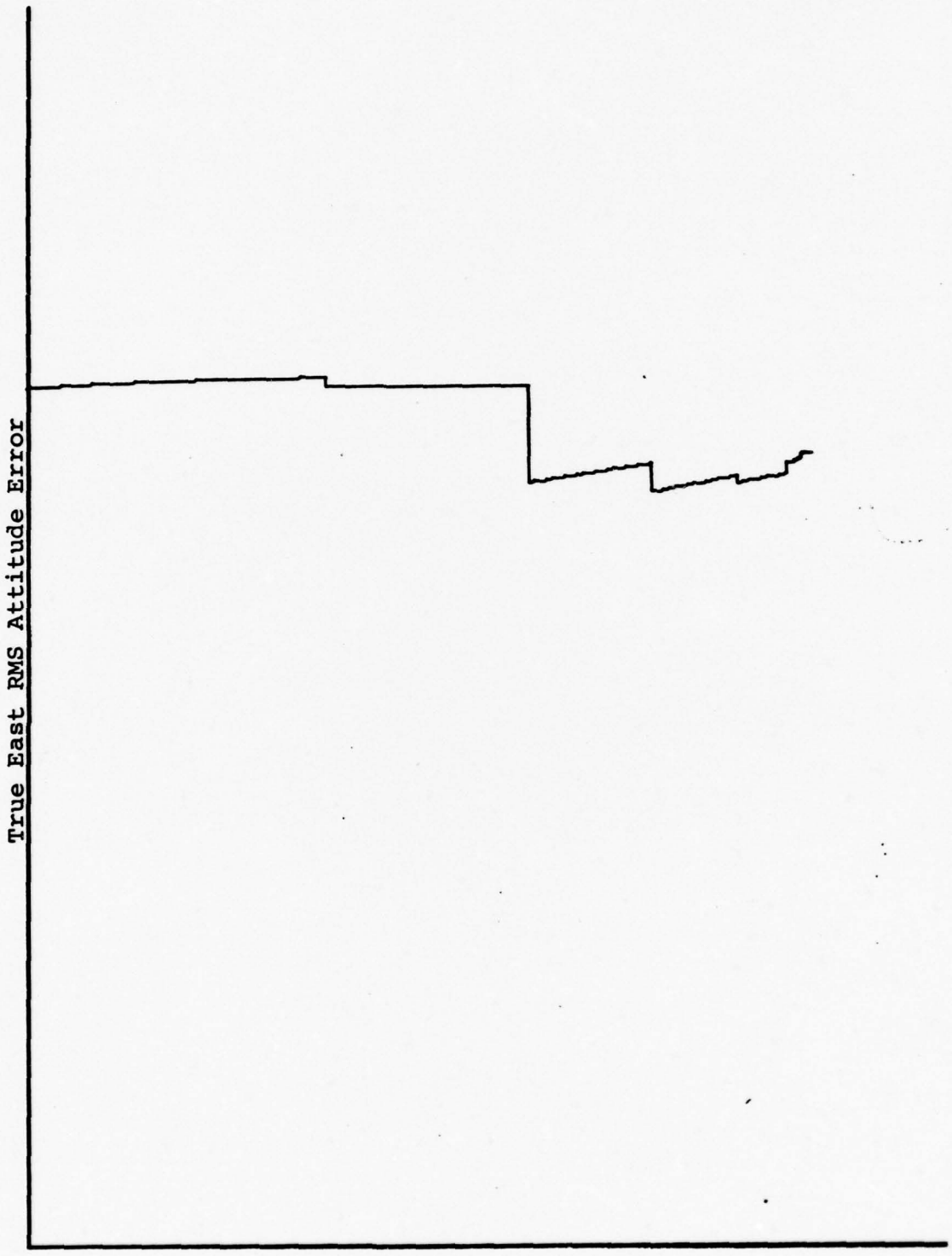

Figure 26. True East RMS Attitude Error Using Lockheed Filter and Sperry INS

equations of the approximation as compared to the Lockheed design should be allotted is dependent on the adequacy of the Lockheed filter to meet system specifications. In the remaining discussion, the power series approximation will be considered to perform identically to the standard propagation filter.

Error Budget

If overall system navigation error is considered to be too large for weapon system effectiveness, it may be decided to replace certain system components with more accurate ones. To aid in determining which components offer the most cost effective means for reducing system RMS navigation error, an error budget has been made. This error budget reflects the increase in RMS navigation accuracy attained if the effects of various error sources were eliminated. The budget was obtained by setting the noise strengths and initial variances of various error sources to zero in the system model. Table X is the error budget for the system employing the Sperry INS, and Table XI reflects the increase in navigation accuracy attained by zeroing these error sources for the system using the Hamilton-Standard INS. In both cases, the terminal navigation errors of the systems using the standard propagation filters were used as a 100% baseline.

From these tables it can be seen that the most dramatic reduction in RMS navigation error occurs when the RAC is

Table X

Error Budget Sperry System

Condition	Baseline	No Gyro Errors	No Accelerometer Errors	No Initial Condition Errors	No RAC Bias Errors	No RAC Errors
RMS Position Error	100%	98.8%	99.97%	98.6%	99.0%	25%
RMS Velocity Error	100%	93.5%	99.80%	93.0%	99.9%	60%
RMS Attitude Error	100%	89.0%	97.30%	94.6%	99.9%	93%

Table XI

Error Budget Hamilton-Standard System

Condition	Baseline	No Gyro Errors	No Accelerometer Errors	No Initial Condition Errors	No RAC Bias Errors	No RAC Errors
RMS Position Error	100%	96.5%	99.9%	99.9%	99.3%	26.3%
RMS Velocity Error	100%	89.0%	99.8%	99.9%	99.9%	45.7%
RMS Attitude Error	100%	57.0%	97.0%	99.9%	99.9%	85.0%

providing perfect position fixes. In this case, position errors are only approximately one-fourth as great as when the RAC's position fixes are corrupted by the bias and white Gaussian measurement noise. Velocity and attitude errors are also substantially reduced when the RAC is error-free.

Perfect gyroscopes also increase system accuracy significantly, especially for the Hamilton-Standard INS. The G and G^2 errors introduced by the dry-tuned gyros of that system seem to contribute heavily to RMS attitude errors. The only other significant reduction in RMS navigation error occurs when the Sperry system is initiated with perfect knowledge of vehicle position, velocity, and attitude.

Filter Performance With Fixed Q_F

The results presented thus far were obtained by supplying the sub-optimal filters with the initial conditions and time-varying white Gaussian noise strengths depicted in Tables V and VI. Again due to computer memory restraints, it may not be practical to implement the three sets of Q_F that tune the filters over fixed time periods. A simulation was made using the Q_F values that tuned the filters after the initial transient period was complete and the results are discussed in Appendix A.

VIII. Changes to the Trajectory and RAC Update Schedule Optimization

Introduction

In this chapter, the performance of the tuned standard propagation filters of Chapter VII will be evaluated for the cases in which changes to the trajectory are necessitated by mission objectives. Two alterations will be investigated: first, changes in vehicle heading toward the target from the original 45°, and secondly, lowering the pitchover altitude of the present trajectory to simulate an extension of the vehicle flight time to adjust for adverse headwinds.

In addition, the six RAC position fixes will be optimized in time so that terminal RMS navigation errors are minimized. The fix schedules will be optimized for both the Sperry and Hamilton-Standard system models, along the standard and lowered pitchover trajectories to include the possibility that a post-pitchover fix cannot be made. As a final consideration, the performance of the filters will be evaluated allowing two fixes per stored reference map while the vehicle is at relatively high altitude. Again, due to security considerations, performance of the filters will be expressed in tabular form as a percentage of the tuned standard propagation filter errors of Chapter VII. These errors are referred to in the tables as baseline.

Changes to the Trajectory

Heading Changes. The 45° vehicle heading angle used in the simulations of Chapter VII was selected to subject the vehicle to equal angular velocity and acceleration vector components in the east and north axes of the ENU frame. It was feared that the unequal force and rate vector components in the ENU frame that would be experienced by the vehicle flying headings other than 45° along the dynamic trajectory would make the accuracy of the sub-optimal filters "heading dependent." This heading dependence would arise if the difference between true navigation errors in the east and north directions grew large as a function of heading, because the filter, as presently tuned, would not detect this difference.

To determine if the accuracy of the standard propagation filters for the two system configurations was indeed heading dependent, computer simulations were conducted in which the four cardinal directions, north, east, south, and west, were used as heading angles for the vehicle. Although there was a slight deviation between corresponding true position, velocity, and attitude variances in the east and north directions for each heading simulated, the difference was so small, especially in position errors, that the filters retained their estimation precision. The largest deviation was 14% between the true δ_{Φ_N} and δ_{Φ_E} attitude error variances for the Hamilton-Standard system with a 180°

heading angle. The results of these simulations indicate that the tuned filters are good error estimators regardless of vehicle heading angle.

Lowered Pitchover Altitude. The second change to the trajectory is a lowering of the altitude at which vehicle pitchover is initiated. This extends the glide period of the vehicle before pitchover, resulting in a greater range and flight time for the weapon system in no-wind conditions. Due to the security classification of the trajectory, the distance the pitchover altitude is lowered cannot be specified.

Because the actual dynamics of the extended glide period from the present pitchover altitude to the lowered one were not exactly known, an approximation was used to implement the new pitchover altitude into the existing trajectory. The approximation was a linear extension in altitude versus time of the flight path from the present pitchover altitude to the lowered one. Along this linear extension, the vehicle total velocity, forward velocity, vertical velocity, and glide path angle were kept constant at the values they had last assumed. The dynamics of the pitchover are incorporated at the termination of the linear flight path extension. With this trajectory change, the time from completion of pitchover until vehicle impact is lessened considerably. System performance utilizing this lowered

trajectory will be evaluated in this chapter, after the conditions for update schedule optimality are set forth.

Update Schedule Optimization

Because navigation RMS errors are so dramatically reduced when each RAC position fix is taken, an optimal RAC position fix schedule is sought to reduce the errors committed by the tuned filters of Chapter VII. Using six fixes as the maximum practical number set by storage requirements, it was found that by taking as many fixes as possible toward the end of the trajectory, terminal navigation errors for the systems are the lowest. This is due to the altitude dependence of the white Gaussian noise strength corrupting the RAC position measurement. It is impractical however to take all six fixes at the end of the flight profile for two reasons:

1. Since the navigation information provided by the INS is inherently divergent unless updated by external aids, relying totally on the INS to guide the vehicle for the extended period from weapon release to near the end of the flight profile invites the danger of totally missing the area covered by the first stored reference map.

2. Even if a successful first fix were made it is possible that the controller's capabilities would be insufficient, in so short a time, to incorporate the fix, correct the flight path, and impact the target.

To insure a successful first fix, yet still incorporate the RAC's low altitude accuracy by taking as many fixes toward the end of the trajectory as possible, the following guidance, from Mr. P. Richter, AFATL, was used: if the 3σ value of the position errors reaches one fourth of the vehicle altitude, a fix must be taken. This criterion suggests that the area encompassed by the stored reference maps is dependent on the anticipated vehicle altitude at update time, and that by using the 3σ value of position errors, in approximately 99% of the cases the vehicle will be somewhere above this area at update time, assuring a successful fix.

Optimal Update Schedule Along the Standard Trajectory Incorporating a Post-Pitchover Fix. Implementing the above criterion, the Hamilton-Standard system required three RAC fixes along the standard trajectory before pitchover, and the more accurate Sperry system required two fixes. Allowing for a post-pitchover position fix, this left two low altitude fixes for the Hamilton-Standard system and three for the Sperry system to be taken just prior to vehicle pitchover. A time interval approximating the RAC's processing time was used between these low altitude fixes. The improvement in accuracy for the two systems using this optimized update schedule is displayed in Tables XII and XIII.

Table XII

Sperry System Performance

Update Schedule	Baseline	Optimized (With Post-Pitchover Fix)
RMS Position Error	100%	74%
RMS Velocity Error	100%	109%
RMS Attitude Error	100%	100%

Table XIII

Hamilton-Standard System Performance

Update Schedule	Baseline	Optimized (With Post-Pitchover Fix)
RMS Position Error	100%	75.4%
RMS Velocity Error	100%	104.0%
RMS Attitude Error	100%	100.3%

From these tables, it can be seen that terminal position errors are reduced by approximately 25% for the two systems while utilizing the optimum fix schedule.

Optimal Update Schedule Without a Post-Pitchover Fix: Standard Trajectory. It is of design interest to know the degree of freedom that must be allowed the RAC's gimbaled platform. Since the steepest vehicle glide path angle

occurs after pitchover, by eliminating a post-pitchover position fix the freedom of movement designed into the platform would not have to be as great. To provide terminal navigation error information about the RAC/INS guidance system's performance without a post-pitchover fix, a simulation was conducted in which the $3\sigma = 1/4$ altitude criterion for an update was implemented, with the sixth position fix taken just prior to pitchover. System performance is reflected in Tables XIV and XV.

Table XIV

Sperry System Performance

Update Schedule	Baseline	Optimized (Without A Post-Pitchover Fix)
RMS Position Errors	100%	124%
RMS Velocity Errors	100%	126%
RMS Attitude Errors	100%	101%

Table XV

Hamilton-Standard System Performance

Update Schedule	Baseline	Optimized (Without A Post-Pitchover Fix)
RMS Position Errors	100%	157%
RMS Velocity Errors	100%	137%
RMS Attitude Errors	100%	113%

These tables indicate that position errors are severely increased when either system is subjected to the relatively violent pitchover without the benefit of a low-altitude post-pitchover RAC fix. The Hamilton-Standard system especially suffers a performance degradation, seemingly due to the excitation of the G and G^2 gyro error sources during pitchover.

Optimal Update Schedule Without a Post-Pitchover Fix: Lowered Pitchover Altitude. Implementing the lowered pitchover altitude into the trajectory and using the $3\sigma = 1/4$ altitude fix criterion, a position update fix schedule was found for both systems with all six fixes occurring before vehicle pitchover. A comparison between the terminal navigation errors of the system using the lowered pitchover altitude with an optimum fix schedule and the baseline system errors is made in Tables XVI and XVII.

Table XVI

Sperry System Performance

Trajectory	Baseline	Lowered Pitchover Altitude
Update Schedule	Baseline	Optimized (Without A Post-Pitchover Fix)
RMS Position Errors	100%	87%
RMS Velocity Errors	100%	115%
RMS Attitude Errors	100%	102%

Table XVII

Hamilton-Standard System Performance

Trajectory	Baseline	Lowered Pitchover Altitude
Update Schedule	Baseline	Optimized (Without A Post-Pitchover Fix)
RMS Position Errors	100%	105%
RMS Velocity Errors	100%	130%
RMS Attitude Errors	100%	110%

The results reflected in these tables are significant. If cost prohibits incorporating a gimbaled platform for the RAC into the system with a freedom of movement sufficient to allow a post-pitchover fix, lowering the planned pitchover altitude can result in system performance that parallels the baseline cases. If the pitchover altitude were lowered, the reduced capability of the system to extend its flight time if adverse winds were encountered would have to be considered.

System Performance Along the Lowered Pitchover Trajectory Allowing More Than One Fix Per Reference Map. Because the size of a reference map is proportional to the vehicle's anticipated altitude at fix time, it may be possible to generate two position updates from the first few maps. A simulation was conducted, using the lowered pitchover trajectory, in which eight fixes were allotted to the

Sperry system and nine to the Hamilton-Standard system. Six of these fixes correspond to the optimal update schedule outlined above for the lowered pitchover altitude, and the additional updates simulate a second fix taken on the largest reference maps. One less fix was allocated to the Sperry system because using the $3\sigma = 1/4$ altitude criterion, the third RAC update for this system occurs at an altitude that was judged to be too low to ensure two successful fixes from the same relatively small reference map. The less accurate Hamilton-Standard system builds up RMS position error faster than the Sperry system, thus requiring updates earlier in time. The third fix was judged to occur when the vehicle is at an altitude sufficiently high to make the probability of two successful updates from the same reference map good.

Tables XVIII and XIX reflect the results of this simulation.

Table XVIII

Sperry System Performance

Trajectory	Standard	Lowered Pitchover Altitude
Fix Schedule	Baseline	Optimized With Two Updates on Each of the First Two Reference Maps (No Post-Pitchover Fix)
RMS Position Errors	100%	82%
RMS Velocity Errors	100%	98%
RMS Attitude Errors	100%	101%

Table XIX

Hamilton-Standard System Performance

Trajectory	Standard	Lowered Pitchover Altitude
Fix Schedule	Baseline	Optimized With Two Updates on Each of the First Three Reference Maps (No Post-Pitchover Fix)
RMS Position Errors	100%	97%
RMS Velocity Errors	100%	113%
RMS Attitude Errors	100%	103%

A comparison of these results with those reflected in Tables XVI and XVII indicates that the additional high altitude fixes do enhance system performance. RMS position error in the Sperry system was decreased approximately 5% with the two additional position updates, while the Hamilton-Standard's RMS position error estimation capability was enhanced by 8% incorporating three additional position updates.

IX. Results and Conclusions

Based on the material presented in this thesis, the results and conclusions are summarized as follows:

1. The Sperry INS provided more accurate navigation information than the Hamilton-Standard INS in every simulation conducted. The better accuracy of the Sperry INS is attributed to the higher precision accelerometers and gyroscopes of that INS as compared to those of the Hamilton-Standard INS, and also to the fact that its laser gyroscopes are not subject to G and G^2 error excitation as are the dry-tuned gyros of the Hamilton-Standard system.

2. System performance is severely degraded along a realistic dynamic trajectory as compared to a benign trajectory. Performance degradation is due to the relatively high pitch rates and accelerations encountered by the inertial navigation systems, especially during and after pitchover. If terminal navigation error is larger than final specifications will allow, two steps can be taken to limit error due to the trajectory. First, better autopilots can be designed to damp the dynamics inherent in the glide vehicle, and secondly, a more gradual pitchover maneuver could be planned.

3. The standard propagation filter, whose additive noise contributions can be accurately calculated using six

equations, outperforms the Lockheed filter, which uses three equations to approximate the noise dynamics. Performance for the Standard propagation filter is only slightly better in the position error channel at impact than the Lockheed filter's; however, in the velocity and attitude error channels it performs significantly better. If either of these filters is to be implemented into the RAC/INS weapon system, the tradeoff in storage space versus accuracy will be a significant factor in the decision process.

4. The low altitude accuracy of the RAC position fixes can be used to significantly decrease system navigation errors. High altitude position fixes should be taken only when necessary, and if possible, two fixes taken on each high altitude reference map to enhance filter estimation precision.

5. Without the benefit of a post-pitchover position fix, system terminal navigation errors are significantly higher than when one is utilized. This performance degradation can be totally offset, however, by lowering the vehicle pitchover altitude sufficiently. This is due to the shorter time span the vehicle is subjected to the relatively high dynamic inputs of post-pitchover flight. This shorter time span also limits the propagation of the velocity and attitude error sources excited during pitchover which aids in the reduction of position error.

It is emphasized that the results of the covariance analysis performed on the filters of this study are valid only to the extent that the mathematical models used do in fact provide an adequate representation of system behavior.

Bibliography

1. Maybeck, Peter S. "Covariance Analysis of a Laser Gyro INS/Radiometric Area Correlation Guidance (RACG) System Kalman Filter Design." Unpublished Technical Memorandum. Wright-Patterson Air Force Base: Air Force Institute of Technology, 1975.

2. Maybeck, Peter S. "Covariance Analysis of a Kalman Filter for a Conventional-Gyro Strapdown INS/Radiometric Area Correlator Guidance System." Unpublished Technical Memorandum. Wright-Patterson Air Force Base: Air Force Institute of Technology, 1975.

3. Britting, Kenneth R. Inertial Navigation Systems Analysis. New York: Wiley-Interscience, 1971.

4. Maybeck, Peter S. "Stochastic Estimation and Control Systems: Part I." Unpublished Class Notes. Wright-Patterson Air Force Base: Air Force Institute of Technology, 1975.

5. Hamilton, Edward L. The General Covariance Analysis Program (GCAP). An Efficient Implementation of the Covariance Analysis Equations. Unpublished Computer Program Guide. Wright-Patterson Air Force Base: Air Force Avionics Laboratory, 1976.

6. Broxmeyer, Charles. Inertial Navigation Systems. New York: McGraw-Hill, 1964.

7. Pitman, George R., ed. Inertial Guidance. New York: Wiley, 1962.

8. Widnall, W. S. and P. A. Grundy. Inertial Navigation System Error Models. Cambridge: Intermetrics Incorporated, 1973.

9. D'Azzo, J. J. and C. H. Houpis. Linear Control System Analysis and Design. New York: McGraw-Hill, 1975.

10. Selby, Samuel M., ed. Standard Mathematical Tables. Cleveland: Chemical Rubber Company, 1971.

11. "Subroutine ICSFKU." IMSL Library 3, Edition 5, 1975.

12. "Subroutine ICSVKU." IMSL Library 3, Edition 5, 1975.

13. "Subroutine LSQUAR." IMSL Library 3, Edition 5, 1975.

Appendix A

The tables below compare the terminal performance of the filters for each system model using a fixed Q_F for the entire simulation. The noise strengths used for both the standard propagation and Lockheed filters are as follows:

1. Sperry system - Q_{22} = .1E-6, Q_{33} = .3E-9
2. Hamilton-Standard system - Q_{22} = .1E-4, Q_{33} = .16E-7

Table XX

Standard Propagation Filter: Fixed Q_F vs. Variable Q_F

System with	Sperry INS		Hamilton-Standard INS	
Q_F	Variable	Fixed	Variable	Fixed
RMS Position Errors	100%	99%	100%	101%
RMS Velocity Errors	100%	94%	100%	100%
RMS Attitude Errors	100%	111%	100%	99%

Table XXI

Lockheed Filter: Fixed Q_F vs. Variable Q_F

System with	Sperry INS		Hamilton-Standard INS	
Q_F	Variable	Fixed	Variable	Fixed
RMS Position Errors	100%	98%	100%	100%
RMS Velocity Errors	100%	94%	100%	99%
RMS Attitude Errors	100%	109%	100%	99%

These tables indicate that terminal navigation errors are approximately the same using a fixed or variable Q_F. The loss in filter estimation precision lost by implementing a fixed Q_F is encountered early in the simulation when the difference between filter RMS position errors and the true RMS position errors was as large as 43%.

Vita

Charles Keith Fitschen was born on 12 September 1946 in Eugene, Oregon. When he was five years old, his family moved to the State of New York where he attended Archbishop Stepinac High School and Manhattan College. Upon college graduation, he received a Bachelor of Electrical Engineering degree, and a commission in the United States Air Force. He completed pilot training in July 1969. After a Vietnam tour of duty, during which he flew the AC-119G and C-47 aircraft, he served in the Strategic Air Command as a KC-135 pilot. He entered the School of Engineering, Air Force Institute of Technology, in June 1975.

Permanent address: 35 Dexter Road
Yonkers, N.Y. 10710

UNCLASSIFIED
SECURITY CLASSIFICATION OF THIS PAGE (When Data Entered)

(14) **REPORT DOCUMENTATION PAGE**

READ INSTRUCTIONS BEFORE COMPLETING FORM

1. REPORT NUMBER: GE/EE/76D-23
2. GOVT ACCESSION NO.
3. RECIPIENT'S CATALOG NUMBER

4. TITLE (and Subtitle) (6): COVARIANCE ANALYSIS OF KALMAN FILTERS PROPOSED FOR A RADIOMETRIC AREA CORRELATOR/INERTIAL NAVIGATION GUIDANCE SYSTEM

5. TYPE OF REPORT & PERIOD COVERED: M.S. Thesis

6. PERFORMING ORG. REPORT NUMBER

7. AUTHOR(S): Charles Kenneth Fitschen, Capt (10) USAF

8. CONTRACT OR GRANT NUMBER(s): (9) Master's thesis,

9. PERFORMING ORGANIZATION NAME AND ADDRESS: Air Force Institute of Technology (AFIT-EN), Wright-Patterson AFB, Ohio 45433

10. PROGRAM ELEMENT, PROJECT, TASK AREA & WORK UNIT NUMBERS

11. CONTROLLING OFFICE NAME AND ADDRESS: AF Armament Test Laboratory, Eglin AFB, Florida 32542

12. REPORT DATE: December 1976 (11)

13. NUMBER OF PAGES: 141 (12) 156 p.

14. MONITORING AGENCY NAME & ADDRESS (if different from Controlling Office)

15. SECURITY CLASS. (of this report): UNCLASSIFIED

15a. DECLASSIFICATION/DOWNGRADING SCHEDULE

16. DISTRIBUTION STATEMENT (of this Report)

Approved for public release; distribution unlimited

17. DISTRIBUTION STATEMENT (of the abstract entered in Block 20, if different from Report)

18. SUPPLEMENTARY NOTES

Approved for public release; IAW AFR 190-17

Jerral F. Guess, Captain, USAF
Director of Information

19. KEY WORDS (Continue on reverse side if necessary and identify by block number)

Kalman Filter
Inertial Navigation System
Radiometric Area Correlator
Covariance Analysis

20. ABSTRACT (Continue on reverse side if necessary and identify by block number)

In this report, a covariance analysis is performed on two Kalman filters proposed for use in a weapon system utilizing a strapdown inertial navigation system (INS), updated by position data from a radiometric area correlator (RAC), for guidance. Filter performance is analyzed when primary navigation information is provided by a Sperry INS, which uses laser gyroscopes, and when an INS employing conventional dry-tuned gyroscopes, manufactured

DD FORM 1 JAN 73 1473 EDITION OF 1 NOV 65 IS OBSOLETE

012225

UNCLASSIFIED
SECURITY CLASSIFICATION OF THIS PAGE (When Data Entered)

by Hamilton-Standard, is incorporated into the weapon system. For the covariance analysis, truth models in the form of linear state equations are presented which reflect the best description of the weapon system when either the Sperry or Hamilton-Standard INS is used. The Sperry system model is composed of 46 states and the Hamilton-Standard system model 61 states. Primary emphasis in this investigation is placed on minimizing system terminal navigation error. This is done through a filter tuning process, and an optimization of six highly accurate RAC position fixes along a simulated trajectory which reflects the actual system dynamics. The two filters analyzed each employ a linear six state mathematical model. Due to the security classification of the trajectory and RAC characteristics, filter performance is conveyed through unscaled graphs and percentages.